

**Generation and characterization of murine
(*Mus musculus* L.1758) L-arginine:glycine
amidinotransferase and guanidinoacetate N-methyl
transferase knockout models to study human creatine
deficiency syndromes**

Dissertation

Zur Erlangung des Doktorgrades
des Departments Biologie der Fakultät für Mathematik, Informatik und
Naturwissenschaften
der Universität Hamburg

Vorgelegt von
Rubén Peco Navío

Hamburg 2007

Abbreviations

Cr	creatine
GAA	guanidinoacetate
AGAT	L-arginine:glycine amidinotransferase
GAMT	<i>S</i> -adenosyl-L-methionine: <i>N</i> -guanidinoacetate methyltransferase
SAH	<i>S</i> -adenosyl-L-homocysteine
SAM	<i>S</i> -adenosyl-L-methionine
CDS	creatine deficiency syndromes
PCr	phosphorylcreatine
P-GAA	phosphoguanidinoacetate
Arg	arginine
CrT	creatine transporter
Crn	creatinine
ubMiCK	ubiquitous creatine kinase isoenzyme
sarMiCK	sarcomeric creatine kinase isoenzyme
B-CK	brain type creatine kinase isoenzyme
M-CK	muscle type creatine kinase isoenzyme
OAT	ornithine:2-oxo-acid aminotransferase
BAT	brown adipose tissue
ATP/ADP	adenosine triphosphate/adenosine diphosphate
AMP	adenosine monophosphate
TCA	tricarboxilic acid
Pi	inorganic phosphate
Gly	glycine
Met	methionine
Cit	citrulline
Orn	ornithine
Pro	proline
Glu	glutamic acid
Gln	glutamine
β -GPA	guanidinopropionate
GBA	guanidinobutyrate
SGK	glucocorticoid inducible kinase
mTOR	mammalian target for rapamycin
MRS	magnetic resonance spectroscopy
CSF	cerebrospinal fluid
CNS	central nervous system
SSADH	succinate semialdehyde dehydrogenase
ES	embryonic stem cells
MEF	mouse embryonic fibroblasts

Abbreviations

PME	phosphomonoesters
DIO	diet induced obesity
MMC	mitomycin C
PFA	paraformaldehyde
cDNA	complementary deoxyribonucleic acid
MG	methylguanidine
G	guanidine
AVA	aminovaleric acid
GSA	guanidinosuccinic acid
NAA	N-acetylarginine
GVA	guanidinovaleric acid
PAS	periodic acid shiff
Cre	cre recombinase
HPLC	high performance liquid chromatography
HE	hematoxilin-eosin
2,3 DPG	2,3 diphosphoglycerate
Iso	myo-inositol

Index

1 Introduction	1
1.1 Guanidino compounds and their biosynthesis	1
1.1.1 Cr tissue distribution and CrT-AGAT expression.....	3
1.2 Guanidino compounds as phosphagens	4
1.2.1 The temporal-energy buffer model	4
1.2.2 The spatial-transport buffer model.....	6
1.2.3 Intracellular phosphate trapping.....	7
1.3 Cr biosynthesis regulation	8
1.3.1- Arginine biosynthesis	8
1.3.2 AGAT activity and Cr feedback inhibition	10
1.3.3 GAMT activity.....	11
1.3.4 Cr transport	11
1.4 Creatine deficiency syndromes	12
1.4.1 AGAT deficiency.....	13
1.4.2 GAMT deficiency	13
1.4.3 CrT deficiency	14
1.4.4 Diagnostic of CDS	14
1.5 Treatment and comparative consideration of CDS	14
1.6 CDS pathophysiology	17
2 Materials and methods	19
2.1 Chemicals, buffers and media	19
2.2 Molecular biology	22
2.2.1 Bacterial transformation.....	23
2.2.2 DNA preparation.....	23
2.2.3 DNA-Electrophoresis gel.....	23
2.2.4 DNA-Isolation from agarose gel.....	24
2.2.5 Restriction enzyme digestion of DNA	24
2.2.6 DNA-dephosphorylation.....	24
2.2.7 DNA-Ligation	24
2.2.8 DNA-Sequencing.....	24
2.2.9 Polymerase chain reaction (PCR)	25
2.2.10 GAMT and AGAT genotyping	25
2.2.11 Screening of genomic clones and cloning of the AGAT targeting construct.....	25
2.2.12 AGAT gene targeting.....	26
2.2.13 Screening of genomic clones and cloning of the GAMT targeting construct.	26
2.2.14 GAMT Gene targeting	26
2.2.15 Western blots.	27
2.3 ES cells gene targeting	27
2.3.1 Primary Mouse Embryonic Fibroblast (MEF) Culture	27
2.3.2 ES Cell Culture	28
2.4 Determination of guanidino compounds	31
2.5 Analysis of body composition	31
2.6 Glucose tolerance test	31
2.7 Determination of metabolic hormones	31
2.8 Cage activity	31
2.9 Muscle performance analysis	32
2.10 Perfused Heart Experiments	33

Index

2.11 Cardiac 31P-MRS	34
2.12 Isolated Heart Protocols	34
2.13 Biochemical and Molecular Measurements.....	34
2.14 Animal groups and care	34
2.15 Statistical Analysis	35
3 <i>GAMT knockout model generation and phenotyping</i>	36
3.1 Generation of GAMT deficient mice	36
3.2 Biochemical abnormalities	37
3.3 Physiological abnormalities	38
3.3.1 Behavioral abnormalities	38
3.3.2 Skeletal muscle	39
3.3.3 Cardiac muscle.....	42
3.3.4 Growth and body weight.....	43
3.3.5 Male and female fertility.....	46
3.3.5.1 Testicles	46
3.3.5.2 Female fertility	47
4 <i>AGAT Knockout model generation and phenotyping</i>	49
4.1 Generation of AGAT deficient mice	49
4.2 Physiological abnormalities	51
4.2.1 MRS	51
4.2.2 Skeletal muscle	52
4.2.3 Cardiac muscle.....	54
4.2.4 Body growth and creatine supplementation	54
4.2.5 Testicles	56
4.2.6 Glucose and lipid homeostasis	56
4.2.7 Bone	58
5 <i>Discussion</i>	59
6 <i>Summary</i>	66
7 <i>References</i>	67

1 Introduction

1.1 Guanidino compounds and their biosynthesis

Creatine (Cr) was first described by Chevreul in 1835 (1) and Von Liebig in 1847 (2), thus being the second organic molecule ever discovered after urea. It was thereafter realized that Cr belongs to a broader family of molecules named guanidino compounds or phosphagens (Fig.1A), ubiquitously distributed among metazoans (Fig. 1C). Despite exhibiting remarkable heterogeneity regarding chemical structure they share a guanidino group as part of the chemical moiety (Fig.1A), a common biosynthesis pathway (Fig.1B) and a guanidino kinase that phosphorylates/dephosphorylates each of the guanidino compounds by using ATP/ADP (3).

The first step in the biosynthesis pathway includes the amidino-transfer from the amino acid arginine (Arg) to different acceptors such as glycine (generating Cr), hypotaurine (generating taurocyamine) and (D- or L-) serine ethanolamine (generating lombricine, thalassemine and opheline); in the second and final step the guanidinated derivatives are further subjected to methylation (4, Fig.1B). Amidino-transfers are odd enzymatic reactions constrained to guanidino compound production in metazoans but also detectable in the biosynthesis of antibiotics and toxic chemical species in microorganisms and plants (5-7).

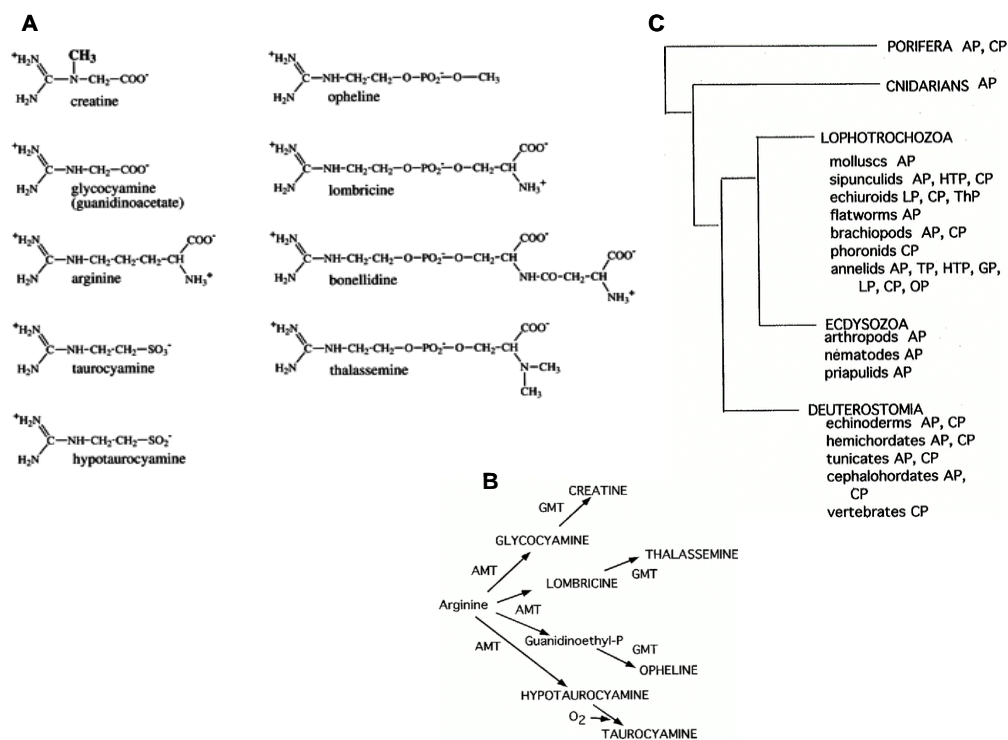
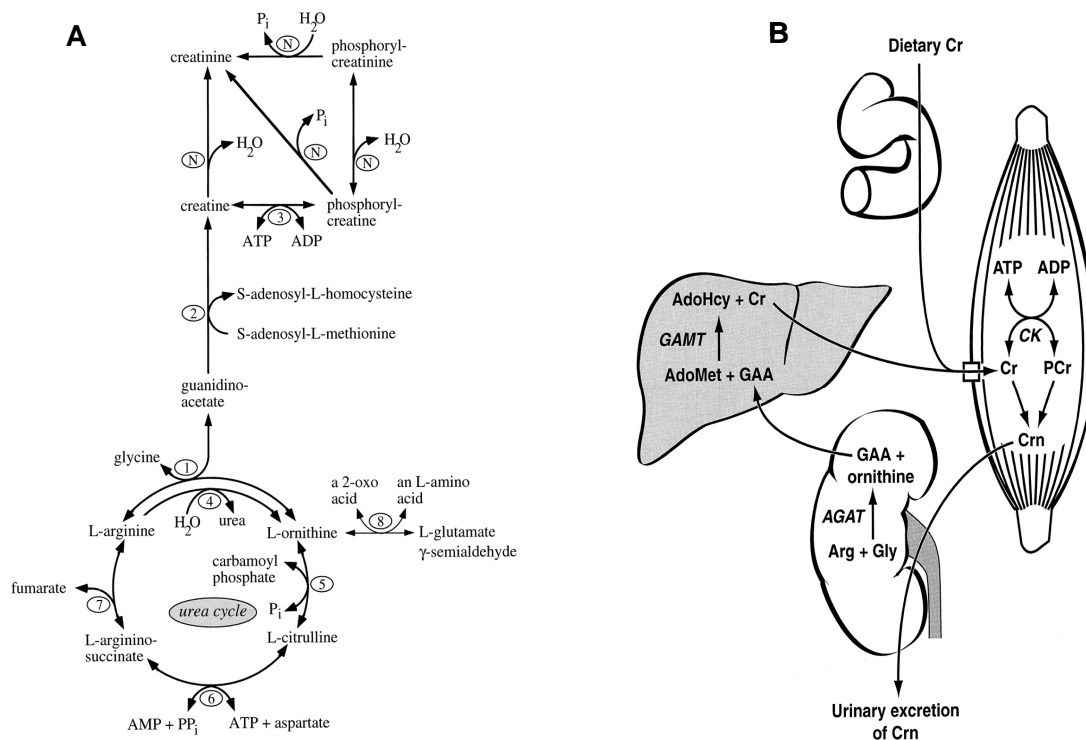


Figure 1A: The natural "phosphagen precursors" are as follows: creatine (Cr), guanidinoacetate = glycoyamine (Gc), arginine (Arg), taurocyamine (Tc), hypotaurocyamine, opheline, lombricine (L), bonellidine, and thalassemine. Note that they all share a guanidino group (drawn on the *left* of the chemical formulas) but differ substantially in terms of other chemical features. Cr is unique in having a disubstituted guanidino group (the additional methyl group is shown in bold), with this feature explaining some of the distinctive chemical properties of phosphorylcreatine (PCr). In the corresponding phosphagens, a phosphate group is covalently attached to the guanidino moiety of the molecule. LP is unique in that contains a D-serine moiety in annelids and an L-serine moiety in echiuroids (adapted from 11). **Figure 1B:** Biosynthetic pathways for the guanidino acceptors (adapted from 37). **Figure 1C:** Distribution of phosphagen systems mapped on a well-accepted phylogenetic tree for the major metazoan groups (adapted from 37).

Introduction

In mammals, L-arginine:glycine amidinotransferase (AGAT) catalyzes the first step by transferring the amidino group from Arg to the amino acid glycine (Gly), thus generating guanidinoacetate (GAA). *S*-adenosyl-L-methionine: *N*-guanidinoacetate methyltransferase (GAMT) subsequently transfers a methyl group from the coenzyme *S*-adenosyl-L-methionine (SAM) to GAA to produce Cr and *S*-adenosyl-L-homocysteine (SAH) (Fig.2A). The pathway is long known to physiology, providing the second instance of end-product feedback repression (8) and the first example of transcriptional co-regulation by two hormones (9,10).

It is classically accepted that the main route of Cr biosynthesis in mammals involves formation of GAA in the kidney and pancreas, its transport through the blood, and its methylation to Cr in the liver. Cr exported from the liver and transported through the blood may then be taken up by the Cr-requiring tissues through a specific, saturable, Na^+ and Cl^- dependent Cr transporter (CrT) (12, Fig.2B). Cr is nonenzymatically converted at an almost steady rate (~2% of total Cr per day) to creatinine (Crn), which diffuses out of the cells and is eventually excreted by the kidneys into the urine. As about 2% is broken down and excreted as Crn this loss entails a daily Cr requirement in order to replenish the actual Cr pool, which is met either by intestinal absorption of ingested Cr or from endogenous biosynthesis. Importantly, under high dietary Cr ingestion the pathway for de novo Cr production was neglected as superfluous and unimportant (11).



Introduction

The classical view however should be revisited for several reasons. First, the expression pattern of Cr biosynthesis enzymes and transport is wider than previously described, tissue-specific and developmentally regulated, making the detailed contribution of different tissues to total Cr synthesis not clear. Second, Cr transport is not only operative in an interorgan manner as, within a given tissue, different cell types may function as Cr-synthesizing and Cr-requiring cells thus establishing an intraorgan Cr shuttling (14). For example, glial and Sertoli cells are capable of Cr biosynthesis, whereas neurons and germ cells accumulate locally produced Cr. Third, Cr is found in feces of animals kept in a Cr-free diet: excreted from liver and pancreas to the small intestine, Cr might be reabsorbed through hepatic portal circulation to eventually reach the bloodstream before targeting Cr-requiring tissues (see discussion). Lastly, the severe clinical phenotype of human inherited Cr-related disorders evidenced that Cr biosynthesis and transport are indeed physiologically relevant.

1.1.1 Cr tissue distribution and CrT-AGAT expression

Tissues with high [Cr], such as skeletal muscle, heart, spermatozoa and photoreceptor cells of the retina display high levels of CrT mRNA but low levels of biosynthetic enzymes; kidney is the sole exception due to its additional role on Cr resorption from the primary urine. Intermediate [Cr] are found in brain, brush border epithelial cells, stomach parietal cells, brown adipose tissue, intestine, seminal vesicles, seminal vesicle fluid, endothelial cells, and macrophages, and only low [Cr] are found in lung, spleen, kidney, liver, pancreas, white adipose tissue, blood cells, and serum (14-24).

The highest amounts of CrT mRNA seem to be expressed in kidney, heart, and skeletal muscle; lower amounts in brain, small and large intestine, vas deferens, seminal vesicles, epididymis, testis, ovary, oviduct, uterus, prostate, and adrenal gland, and only very low amounts or no CrT mRNA at all in placenta, liver, lung, spleen, pancreas, astrocytes and thymus (25-30). On the contrary, high AGAT expression should be correlated with low tissue [Cr] and low CrT mRNA levels and be considered as a distinctive hallmark for a Cr-biosynthetic tissue; exceptions to this rule can be found where the mentioned intraorgan Cr shuttling is effective: brain and testicles for example have high tissue [Cr] and high AGAT and CrT expression (Fig.3). AGAT activity was detected, in addition to kidney and pancreas, in heart, lung, spleen, muscle, brain, testis, and thymus (13, 31). Although AGAT is absent from human placenta due to imprinting of the paternal allele (32), the decidua of pregnant females displayed the highest specific AGAT activity of all rat tissues examined (8), implying a major involvement of this tissue in Cr biosynthesis during early stages of development; maternofetal transport of Cr was also demonstrated in the rat (33).

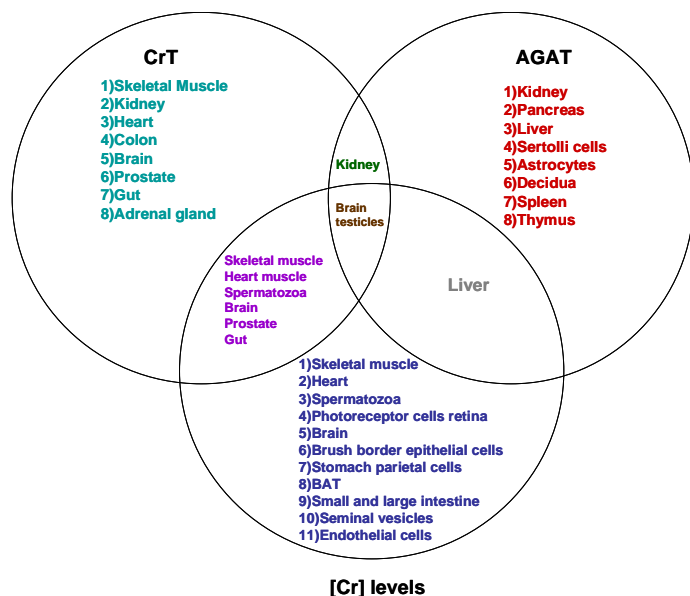


Figure 3: The figure suggests that tissues producing Cr are not the ones that need creatine for their functioning because tissues with Cr biosynthetic activity (Cr-synthesizing tissues) do not contain high [Cr] nor high CrT expression levels. Conversely, tissues accumulating Cr (Cr-requiring tissues) do express high levels of the CrT and display lower or no AGAT activity. Exceptions are kidney, which expresses AGAT and the CrT, due to the resorption of Cr performed by this organ, liver, due to its high Cr biosynthetic activity as well as testicles and brain, as the intraorgan Cr shuttle phenomenon is operative between Sertoli cells-germ cells and astrocytes-neurons.

1.2 Guanidino compounds as phosphagens

Each of the guanidino compounds is subjected to phosphorylation/dephosphorylation by a respective guanidine kinase, being alternatively termed phosphagens for this reason. Ever since the discovery of phosphorylcreatine (PCr) in 1927 and of the creatine kinase (CK) reaction in 1934 (34, 35) research efforts focused mainly on biochemical, physiological, and pathological aspects of the CK reaction itself and on its involvement in "high-energy phosphate" metabolism (11). The energy buffer and transport models developed since postulate that phosphagens serve as temporal and spatial ATP buffers, based on their intrinsic physicochemical properties such as higher Gibbs free energy of phosphorylation/dephosphorylation as well as higher diffusion coefficient compared to ATP-ADP (Fig.4).

1.2.1 The temporal-energy buffer model

Concerning the energy buffer model, the relative thermodynamic poise (ΔG°) for the hydrolysis of PCr is -45.0 kJ/mol compared with -31.8 kJ/mol for ATP, implying that in tissues with an active CK system the phosphorylation potential can be buffered at a higher level (36). In addition, the energy "content" of ATP is not fixed but is rather related to the extent of displacement of the hydrolysis reaction from thermodynamic equilibrium, as the actual free energy of ATP hydrolysis is a function of the physiological [ATP]/[ADP] ratio. Therefore, small changes in the extent of hydrolysis of ATP produce dramatic decreases in the ΔG_{ATP} that could impact the functioning of ATP-requiring processes (37, Fig.4A). PCr and Cr, relative to ATP and ADP, are smaller and less negatively charged molecules and can build up to much higher concentrations (over 10 fold higher in anaerobic type II muscle) allowing for a higher intracellular flux of high-energy phosphates and buffering of ATP levels.

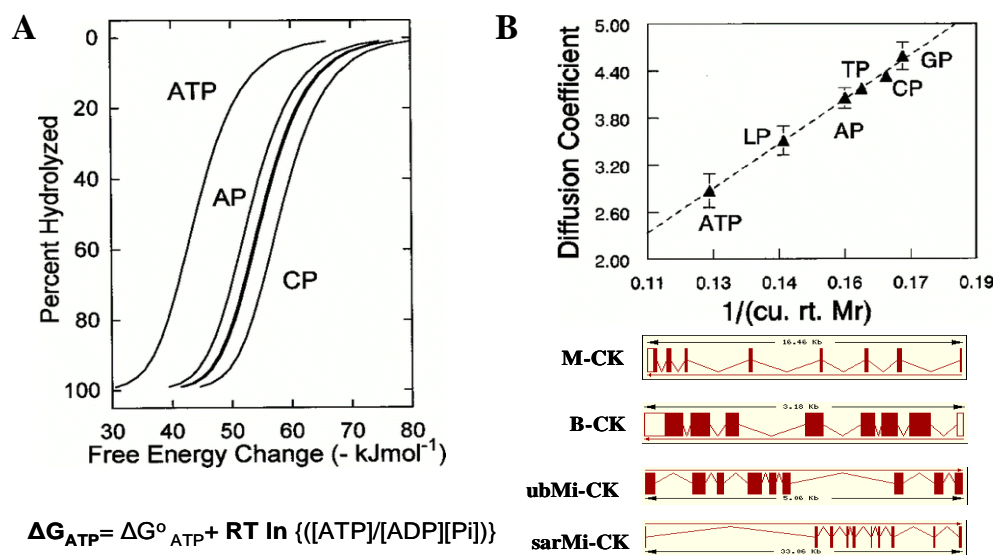


Figure 4A: Major physiological roles proposed for phosphagens. (A) temporal ATP buffering: the change in free energy (G°) (pH 7.0) for the hydrolysis of PCr is -45.0 kJ/mol compared with -31.8 kJ/mol for ATP, thus the cell phosphorylation potential can be buffered at a higher level. Plotted is the relationship between the effective free energy change of hydrolysis and the extent of hydrolysis of the total pool size of ATP, AP, CP, TP, GP, and LP. Curves for TP, GP, and LP nearly superimpose on each other and fall intermediate between AP and CP. **Figure 4B:** the bulk of cellular high-energy phosphate is transported in the form of PCr rather than ATP. Plotted is the relationship between the diffusion coefficient ($\times 10^{-6}$ cm^2/s) and the cubed root of the relative molecular mass for the various phosphagens and ATP. The genomic structures for the different CK isoenzymes are also displayed to note that CK isoenzymes are encoded by four distinct genomic loci (adapted from 37).

Introduction

Importantly, by keeping [ADP] low, the CK/PCr/Cr system also protects the cell from a net loss of adenine nucleotides via adenylate kinase, AMP deaminase, and 5'-nucleotidase (38, Fig.5). For example fructose loading, a challenging condition for hepatocytes resulting in a marked catabolism of ATP through this pathway, owing to uncontrolled uptake and phosphorylation of the sugar by the fructose transporter GLUT-5, was in fact prevented by liver-specific ectopic expression of rat brain type creatine kinase (B-CK) in the mouse (39, Fig.5B and 5C). Similar ATP catabolism occurs when the hepatocyte is subjected to ischemia or anoxia, and the effect could be prevented by the same transgenic approach (40, Fig.5D and 5E).

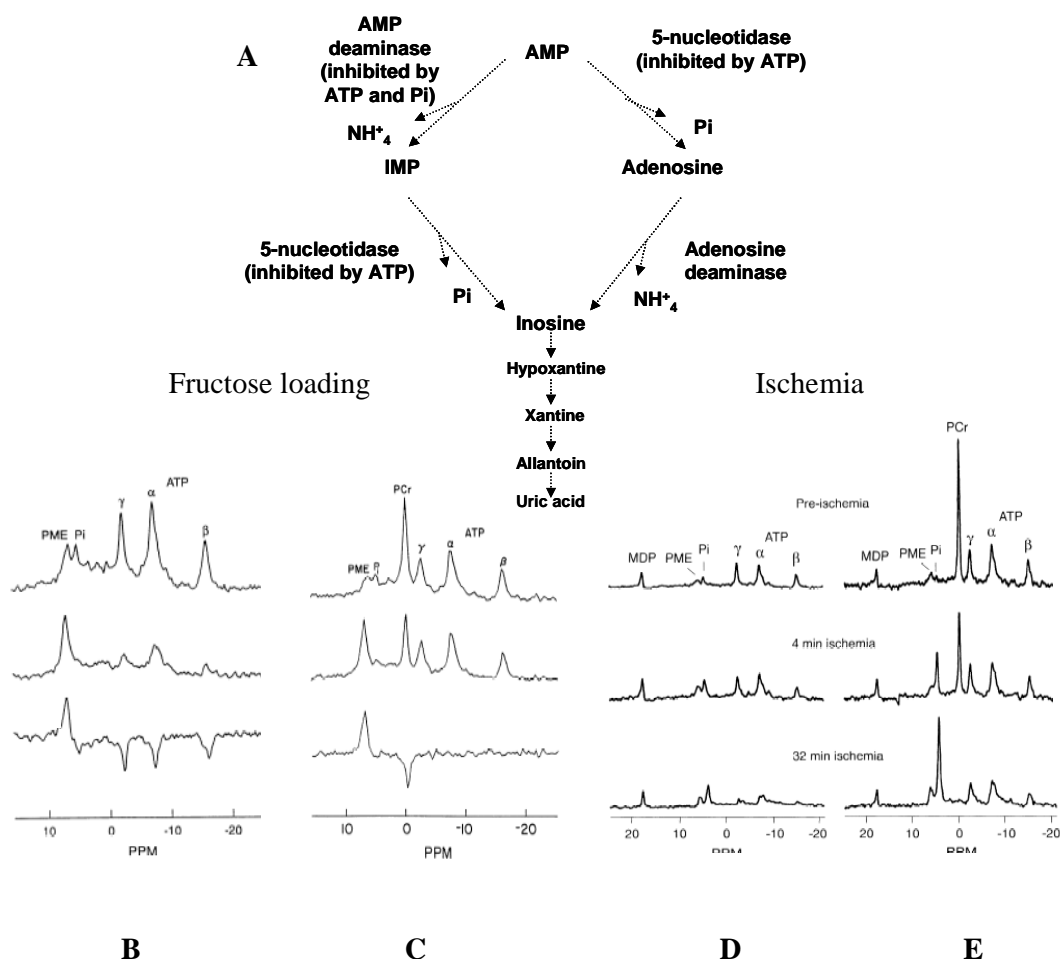


Figure 5: Proposed additional advantage of the energy buffer system, namely, the protection from net loss of nucleotides. (A) Metabolic pathway for nucleotide catabolism. Since ATP is an inhibitor of 5-nucleotidase and Pi an inhibitor of AMP deaminase, the decrease in the concentration of ATP and Pi upon fructose loading results in an increased rate of the reactions that cause an irreversible degradation of AMP. Below, liver ^{31}P MR spectra of wildtype (B and D) and transgenic (C and E) mice overexpressing B-CK specifically in liver. Note how the peaks corresponding to the three phosphates of ATP (α , β , γ) were reduced after fructose loading (B). On the right (D) the same phenomenon occurred after ischemia. Both effects were prevented by liver specific B-CK ectopic expression (C and E). The lower spectrum in B and C is a difference spectrum of the two upper spectra (adapted from 39 and 40).

Introduction

Tissues with high and fluctuating ATP requirements are also equipped with mechanisms to salvage AMP molecules from the deamination-catabolic pathway such as the purine nucleotide cycle, reciprocally regulating ATP content in addition to the CK/PCr/Cr system; the purine nucleotide cycle has been proposed to play a role in the liberation of ammonia from amino acids in kidney and brain (164, 167) and for the adjustment of citric acid intermediates in muscle (165, 166): in essence the activity of this pathway replenishes the tricarboxylic acid (TCA) cycle with anapleurotic substrates, fumarate by using aspartate, in tissues with limited anapleurotic mechanisms such as muscle or neurons (41, Fig.6). The mentioned transgenic mice expressing B-CK in their livers suggested that the CK/PCr/Cr system is functionally linked to the ATP catabolic pathway; however, a relationship with the opposite process, the purine nucleotide cycle with Cr phosphorylation/dephosphorylation or its biosynthesis has never been found

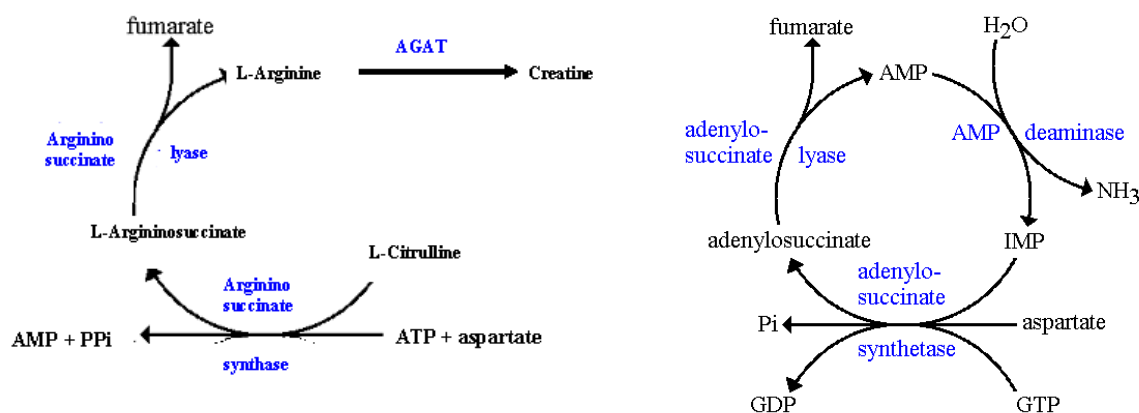


Figure 6: Similarities between Arg biosynthesis (left) and the purine nucleotide cycle (right). Both cycles consume aspartate and produce fumarate. The purine nucleotide cycle is also active in brain, muscle and kidney where it is thought to assist in the generation of TCA cycle intermediates due to the limited anapleurotic capacity of myocytes and neurons. In kidney it is supposed to support ammonia formation.

1.2.2 The spatial-transport buffer model

The transport hypothesis accounts for the isoenzyme-specific subcellular localization of CK isoenzymes. In vertebrates four distinct types of CK are encoded by different loci, with a complex subcellular distribution as well as tissue specific pattern of expression (Fig.4B). An ubiquitous mitochondrial CK isoenzyme (ubMiCK) exists targeted to the mitochondrial intermembrane space of virtually all cells; muscle sarcomeric mitochondria contains yet another isoenzyme termed sarcomeric CK (sarMiCK). Neurons express the cytoplasmic CK-B isoenzyme whereas muscle contains the cytoplasmic CK-M isoform. Heart for example contains a mixture of both. With such an intracellular arrangement, the transport hypothesis postulates that the γ -phosphate group of ATP, synthesized within the mitochondrial matrix, is transferred by ubMi-CK or sarMiCK at the mitochondrial intermembrane space to Cr to yield ADP plus PCr, which leaves the mitochondria and diffuses through the cytosol to the sites of ATP consumption, where cytosolic M-CK or B-CK isoenzymes locally regenerate ATP (43). Once liberated Cr diffuses back to the mitochondria thereby closing the cycle (11). Being smaller molecules, phosphagens have a higher diffusion coefficient than ATP nucleotides and thus display higher intrinsic diffusivity, better accomplishing the function of a "transport device" for high-energy phosphates than ATP molecules (37, Fig.4B); thus, in energy

Introduction

demanding tissues, high-energy phosphate transport between sites of ATP production (mitochondria, glycolysis) and ATP consumption (all sorts of cellular ATPases) relies on diffusion of PCr rather than on diffusion of ATP (11).

Both models are best illustrated considering the differences in mitochondrial versus cytoplasmic CK isoenzyme levels as well as tissue [Cr] between fast-twitch skeletal muscles, those displaying higher levels of cytoplasmic CK and a larger pool of PCr (~32 mM PCr and 7 mM Cr) compared to heart, slow-twitch skeletal muscles or spermatozoa with higher mitochondrial CK levels and lower [Cr]. The former, anaerobic type II glycolytic muscle conforms better to the buffer hypothesis in that PCr is available for immediate regeneration of ATP hydrolyzed during short periods of intense work. The second, aerobic fat-based type I muscle depends on a more continuous delivery of high-energy phosphates to the sites of ATP utilization, exhibiting larger mitochondrial CK isoenzyme levels as well as lower [Cr] (~16 mM PCr and 7 mM Cr).

A good correlation can be found between the CrT mRNA level and total CK activity which, in turn, also correlates with the tissue concentration of Cr. There may be only two exceptions. 1) Kidney displays a much higher Cr transporter content than expected from its CK activity, again due to an involvement of the Cr transporter in the resorption of Cr from the primary urine. 2) Liver has a considerably lower CK activity than expected from its Cr content (11, Fig.7).

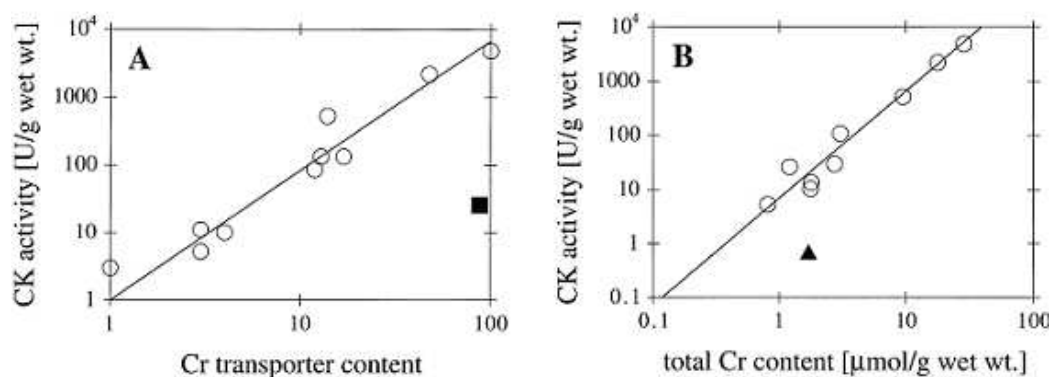


Figure 7: Correlations between Cr transporter level, CK activity, and total Cr content in different mammalian (rat, human, cat, dog, rabbit, mouse, and guinea pig) tissues. The respective tissues are, from *left to right*, as follows: **A:** pancreas, spleen, ovary, lung, small intestine, prostate, brain, colon, heart, kidney (■), and skeletal muscle. **B:** spleen, kidney, liver (▲), smooth muscle (carotid artery), macrophages, brown adipose tissue, uterus, brain, heart, and skeletal muscle (adapted from 11).

1.2.3 Intracellular phosphate trapping

Phosphagens have been also implicated in regulating intracellular inorganic phosphate (Pi) levels as they trap considerable amounts of Pi which is liberated upon net phosphagen hydrolysis (37). Since Pi is the actual substrate of the glycogen phosphorylase reaction, it has been hypothesized that liberation of Pi upon net PCr hydrolysis may be critical in promoting glycogen breakdown during muscle contraction (43).

Introduction

1.3 Cr biosynthesis regulation

Cr biosynthesis regulation is achieved at the pre-transcriptional level by end-product feedback repression of AGAT by Cr, whereas hormones like thyroxin and growth hormone act as positive transcriptional regulators; in addition, ornithine is a potent inhibitor of the protein (8, 44). The suspected effects of an elevated serum [Cr], to downregulate AGAT expression, would therefore help to spare precursors of Cr (Arg, Gly and Met). In addition, changes in the transport capacity or permeability of biological membranes for the intermediary metabolites, Arg, Cr, Crn and GAA are also expected to have an impact on Cr metabolism (11).

1.3.1 Arginine biosynthesis

Arg is a semiessential or conditionally essential amino acid, depending on the developmental stage and health status of the individual, synthesized from citrulline (Cit) by the sequential action of the cytosolic ubiquitous enzymes argininosuccinate synthetase (ASS) and argininosuccinate lyase (ASL) (45). The synthesis of each molecule of Arg consumes one molecule of aspartic acid and produces one molecule of fumarate, similarly to the purine nucleotide cycle (Fig.6).

In turn Cit can be derived from different sources: from Arg via nitric oxide synthase (NOS), from asymmetric dimethylarginine via dimethylarginine dimethylaminohydrolase (DDAH) or most importantly from ornithine (Orn) via catabolism of proline (Pro) or glutamine/glutamate (Gln/Glu); carbamoyl phosphate synthetase should be present if Cit is to be derived from Orn (Fig.8). The pathways linking Arg, Gln and Pro are bidirectional, making the utilization or production of these amino acids highly inter-dependent (47). It seems reasonable that Cr synthesizing cells should be equipped with a mechanism to provide with Arg, either through an active Arg uptake, mediated by the cationic transporter system y^+ (48), or via an active de novo biosynthesis from Arg intermediates.

On a whole body basis, synthesis of Arg occurs principally via the intestinal-renal axis, wherein the brush-border of epithelial cells of the small intestine, which produce Arg primarily from Gln/Glu, collaborate with the proximal tubule cells of the kidney, which extract Cit from the circulation and convert it to Arg (Fig.8). At birth, the small intestine is the major site of net Arg synthesis from Gln/Glu, but gradually becomes the major site of net Cit production as intestinal arginase expression increases. This transition is compensated for by the gradually increasing capacity of the kidney to synthesize Arg from Cit (47). Exactly at the site where Arg is being produced, the basal membrane of the proximal convoluted tubules of the kidney, AGAT activity is maximal. Arg once produced engages in a variety of catabolic reactions such as production of nitric oxide, agmatine, putrescine, spermidine, Cr, Cit and Orn as well as ureagenesis (Fig.9); Cr synthesis represents the second major fraction of total-body Arg utilization, after ureagenesis, accounting for approximately 10% of the total plasma Arg flux (49, 50).

Transgenic mice overexpressing arginase specifically in enterocytes displayed reduced Cr, GAA, guanidinopropionate (β -GPA), guanidinobutyrate (GBA) and homoarginine but less than one third in brain, muscle, kidney and serum and failed to thrive during the suckling period; afterwards, a catch-up growth of the wild type littermates was observed; the mice also had abnormalities in hair and muscle growth and B-cell maturation (158, 159). Their biochemical and physiological changes suggested a direct relationship between Arg and Cr biosynthesis during lactation, a time at which GAA levels in brain, liver and kidney reached maximum levels (157). We can also surmise from these results that the subcellular localization of Cr biosynthesis should not overlap with that of ureagenesis, namely, AGAT and arginase expression should not coexist in the same physiological compartment, in view of the fact that both enzymatic reactions would compete for the same substrate. Proximal

Introduction

convoluted tubes of the nephron and astrocytes, for example, contain AGAT and Arg synthesizing enzymes, but do not express arginase (193).

Gyrate atrophy is an autosomal recessive tapetoretinal dystrophy. The clinical phenotype is mainly limited to the eye, beginning at 5-9 years of age with night blindness, myopia, and progressive constriction of the visual fields. By age 20-40 years the patients are practically blind. In addition to the retinal degeneration, type II muscle fiber atrophy, an increase in the proportion of type I muscle fibers with age, as well as the formation of tubular aggregates in affected type II fibers were observed in vastus lateralis muscle of gyrate atrophy patients (188).

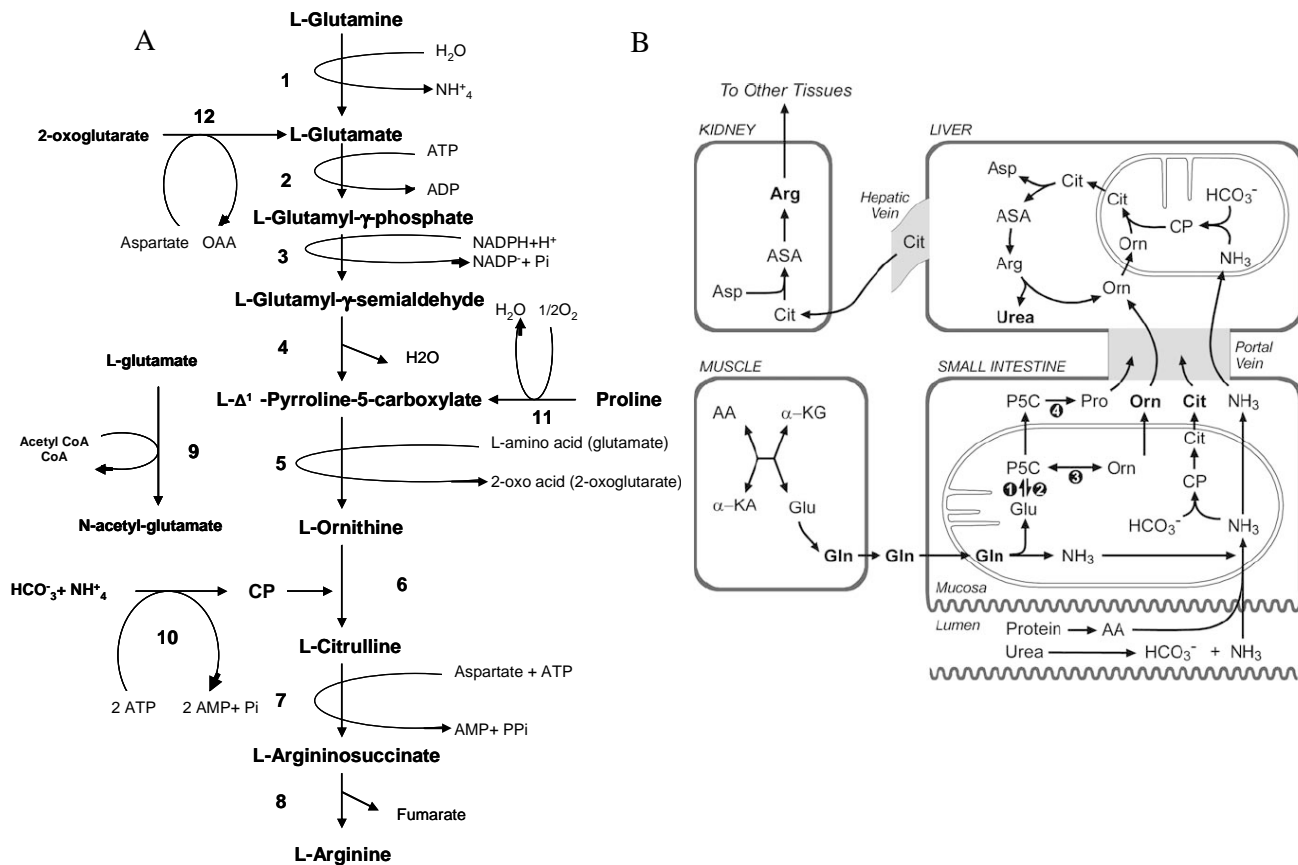


Figure 8A: The metabolic pathways involved in the synthesis of ornithine, arginine and proline from glutamate. The enzymes indicated are (left): 1) phosphate-dependent glutaminase; 2) and 3) Delta 1-pyrroline-5-carboxylate synthetase (P5CS); 5) ornithine aminotransferase (OAT); 6) ornithine carbamoyltransferase; 7) argininosuccinate synthase; 8) argininosuccinate lyase; 9) N-acetylglutamate synthase; 10) carbamoyl-phosphate synthase I; 11) proline oxidase; 12) aspartate aminotransferase. Step 4 is spontaneous non-enzymatic process. Glutamyl-γ-semialdehyde is in chemical equilibrium with Delta 1-pyrroline-5-carboxylate (P5C). The chemical equilibrium favours P5C formation. Reactions 1-6 occurs in mitochondria, reactions 7 and 8 take place in cytosol and reaction 12 occurs in both. **Figure 8B:** Organs involved in the synthesis of ornithine, arginine and proline from glutamate. 1) P5CS; 2) P5C dehydrogenase; 3) OAT; ornithine:2-oxo-acid aminotransferase; 4) P5C reductase. (AA: aminoacids, Arg: arginine, ASA: arginino succinnic acid, Asp: aspartate, Cit: citrulline, CP: carbamoylphosphate, Gln: glutamine, Glu: glutamate, α-KG: α-ketoglutarate, Orn: ornithine, Pro: proline)

The underlying primary defect is a deficiency in the mitochondrial matrix enzyme L-ornithine:2-oxo-acid aminotransferase (OAT; EC 2.6.1.13), the major enzyme catabolizing ornithine. Because of this deficiency, ornithine accumulates in the body, with the plasma

Introduction

concentration being raised 10- to 20-fold (450-1,200 μM vs. \sim 40-60 μM in controls) (189). Ornithine, in turn, inhibits AGAT ($K_i = 253 \mu\text{M}$), the rate-limiting enzyme for Cr biosynthesis, and therefore it was suggested that Orn accumulation might slow production of both GAA and Cr. Accordingly, [GAA] is decreased in plasma and urine by a factor of 5 and 20, respectively. Similarly, [Cr] is reduced in plasma, urine, cerebrospinal fluid (CSF), erythrocytes, and vastus lateralis muscle by a factor of 2-6 (189). Cr supplementation caused the disappearance of tubular aggregates in type II muscle fibers as well as an increase in the diameter of type II muscle fibers (11, 190). In the few patients that discontinued Cr supplementation, the pathological muscle changes promptly reappeared.

Surprisingly, OAT-deficient mice exhibited paradoxical neonatal hypoornithinaemia and lethality, rescuable by short-term arginine supplementation. Post-weaning, these mice developed hyperornithinaemia similar to human gyrate atrophy patients. Subsequent studies in one human gyrate atrophy infant also showed transient hypoornithinaemia (192). Thus, the OAT reaction play opposite roles in neonatal and adult mammals, suggesting that intestinal Arg synthesis from Gln/Glu is important just during the early postnatal period. Hence, Arg biosynthesis from Glu might be curtailed under OAT deficiency and thus lead to reduced Cr biosynthesis during this period. The finding of other hyperornithinemas and also AGAT patients that are not accompanied by gyrate atrophy casts doubt on a potential causal link between AGAT inhibition by Orn and muscle and eye pathology in gyrate atrophy, but the lowered GAA and Cr levels demonstrate the relevance of Gln and Pro as nitrogen donors for Orn production by transamination during early neonatal development, and how the biochemical route is ultimately orchestrated with Cr biosynthesis.

1.3.2 AGAT activity and Cr feedback inhibition

The formation of GAA is normally the rate-limiting step of Cr biosynthesis; thus, the AGAT reaction is the most likely committed stage. Most important in this respect is the feedback repression of AGAT by Cr, the end-product of the pathway, which may serve to conserve the dietary essential amino acids Arg and Met (8, 11). Although the mitochondrial localization has been corroborated by amino acid and cDNA sequencing, showing that AGAT is synthesized as a precursor protein containing an N-terminal presequence typical for matrix/inner membrane proteins (51), an additional cytoplasmic localization due to alternative splicing cannot be excluded. Immunological studies suggested the presence of multiple forms (or isoenzymes) of AGAT in rat kidney, of which only some are repressible by Cr, whereas others are not (52). Feedback repression of AGAT by Cr is most pronounced in kidney and pancreas, but is also observed in the decidua of pregnant rats (8).

In addition to Cr, the expression of AGAT may be modulated by hormonal factors. Thyroidectomy or hypophysectomy of rats decreased AGAT activity in the kidney. The original AGAT activity could be restored by injection of thyroxine or growth hormone, respectively. In contrast, injections of growth hormone into thyroidectomized rats and of thyroxine into hypophysectomized rats were without effect, indicating that both hormones are necessary for maintaining proper levels of AGAT in rat kidney (9, 10). Because enzyme activity, protein and mRNA contents are always affected to the same extent, regulation of AGAT expression by thyroxine and growth hormone occurs at a pretranslational level, similar to the feedback repression by Cr (54).

An important point to add regarding AGAT activity is its broad specificity, as in addition to the physiological substrates (Arg, Gly, Orn and GAA), canavanine, hydroxyguanidine, guanidinobutyrate (GBA), guanidinopropionate (β -GPA), and homoarginine act as amidine donors (13), and canaline, hydroxylamine, glycylglycine, 1,4-diaminobutylphosphonate, 4-aminobutyrate (GABA), 3-aminopropionate, and β -alanine as amidine acceptors (55).

Introduction

1.3.3 GAMT activity

Methylation of GAA by GAMT is the second and last step in Cr biosynthesis and occurs mainly in liver and pancreas. Interestingly, upon lowering of the Met and choline levels in the diet, the deficit in labile methyl groups is compensated for by increased de novo Met biosynthesis, indicating that the delivery of labile methyl groups should normally not become limiting for Cr biosynthesis (56). It was estimated that the GAMT reaction consumes ~70% of the total utilization of labile methyl groups in the body but the conclusion is not consistent with recent studies in which the phosphatidylethanolamine methyltransferase gene was deleted in mice (57). Loss of this hepatic enzyme resulted in a 50% decrease in plasma homocysteine, which suggests that it accounts for a major component of whole-body SAM utilization. A subsequent re-examination of human Cr metabolism deemed that Cr biosynthesis can account for as much as 50% of daily Cr requirements; therefore, estimates on the amount of methyl groups used for Cr synthesis need to be reduced (58). Nevertheless, it remains to be recognized how homocysteine remethylation and transsulfuration metabolism is interrelated to the methylation demand imposed by Cr biosynthesis (Fig.9A). In fact, rats fed with GAA increased SAH levels in blood, suggesting that the mentioned functional link exists (59, Fig.9B). Interestingly, GAA-mediated increase of serum SAH through oral supplementation of GAA has been shown to underlie the paradoxical increase in atherosclerotic lesion size phenotype of apoE^{-/-}/iNOS^{-/-} double knockout mice (60-62, Fig.10), implying that Cr biosynthesis and nitric oxide production may compete for Arg. ApoE^{-/-}/iNOS^{-/-} double knockout mice exhibited exacerbated atherosclerosis upon Arg feeding, the opposite phenotype of the single ApoE^{-/-} and non Arg treated apoE^{-/-}/iNOS^{-/-} double knockout mice. J. Loscalzo speculated, and subsequently showed, that a non-existing NOS pathway would leave increased Arg concentrations for Cr biosynthesis and thus boost production of SAH, causing atherosclerosis.

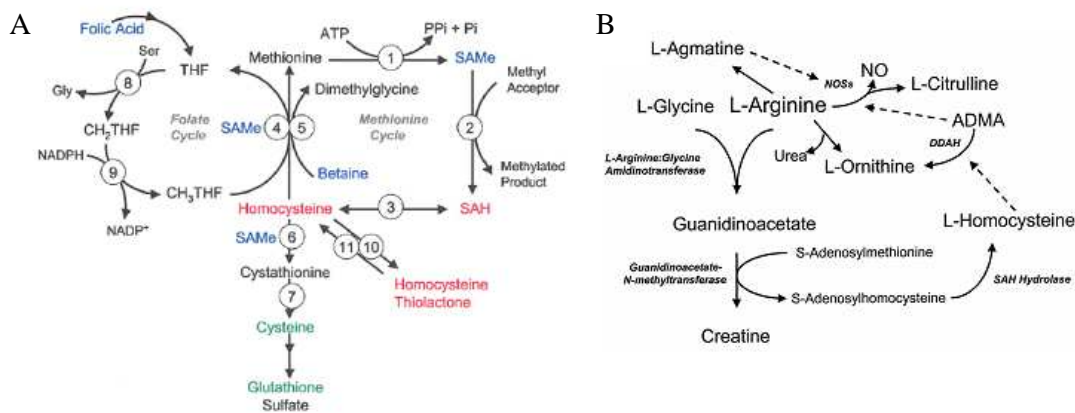


Figure 9: possible relationships across methylation metabolism and Cr biosynthesis (adapted from 60)

1.3.4 Cr transport

Transport of intermediary metabolites across biological membranes represents an integral part of Cr metabolism. Arg has to be taken up into mitochondria for GAA biosynthesis; GAA is released from pancreas and kidney cells and taken up by the liver. Likewise, Cr is exported from the liver and accumulated in CK-containing tissues (11). For example, in chicken kidney and liver, penetration of Arg through the inner mitochondrial membrane was found to occur only in respiring mitochondria and in the presence of anions such as acetate or phosphate (63).

Introduction

1.3.4.1 The CrT

The creatine transporter (CrT) is a member of the Na⁺-dependent "neurotransmitter" transporter family, being most closely related to the GABA/taurine/betaine transporter subfamily (46-53% amino acid sequence identity), while the homology to Gly, Pro, catecholamine, and serotonin transporters is less pronounced (38-44% amino acid sequence identity). Regarding its regulation, the expression and/or specific activity of the CrT seems to be influenced by dietary and hormonal factors as a fasting for 24-h slightly increased [Cr] in the plasma but decreases Cr uptake into tibialis anterior and cardiac muscle of the mouse by ~50% (64). Because the downregulation of the Cr transporter activity by extracellular Cr is slowed by cycloheximide, an inhibitor of protein synthesis, it was hypothesized that Cr transport is controlled by regulatory proteins (65). It remains to be clarified however how extracellular [Cr] is transformed into an intracellular signal. Simultaneous ingestion of relatively large amounts of carbohydrates (glucose and simple sugars) also augmented Cr retention in muscle (66, 67). This effect seems to be mediated indirectly by insulin, which increased in plasma almost 20-fold within 20 min of carbohydrate ingestion (68).

Recently, the glucocorticoid inducible kinases SGK1 and SGK3 (69), two kinases upregulated during ischemia, and the mammalian target for rapamycin (mTOR) (70), a kinase which stimulates cellular nutrient uptake, have been implicated in regulating the activity of the CrT by increasing the maximal transport rate of the carrier when coexpressed in heterologous expression systems. The SGK1-mTOR system is also responsible for activating intestinal Pi absorption, accomplished by the Na⁺-Pi cotransporter NaPi IIb (SLC34A2) (71). Interestingly, an alternative isoform of the same transporter (NaPi IIa) mediates Pi resorption in the proximal convoluted tubules of the nephron (160), where GAA is generated. Because approximately two thirds of the Cr accumulated in CK-containing tissues is converted to PCr, it might be anticipated that Cr and Pi uptake influence each other. In fact, in mouse myoblasts exposed to extracellular Cr, Pi uptake is transiently stimulated (72).

In cultured mouse G8 myoblasts Cr uptake is also stimulated by isoproterenol, norepinephrine, the cAMP analog *N*⁶,2'-*O*-dibutyryl adenosine, 3',5'-cyclic monophosphate, and the β₂-agonist clenbuterol, but not by the α₁-adrenergic receptor agonist methoxamin (28). Thus CrT activity may be controlled predominantly by β₂-adrenergic receptors that have cAMP as their intracellular signal. In fact, analysis of the CrT cDNA sequence revealed consensus phosphorylation sites for cAMP-dependent protein kinase (PKA) and for protein kinase C (PKC) (73, 74).

An important issue to add regarding CrT activity is that Cr uptake by the CrT is inhibited most efficiently and in a competitive manner by β-GPA and GBA, whereas GAA, Ala, *p*-guanidinobenzoate, and succinamic acid are less inhibitory (75). In addition to simply inhibiting Cr uptake, β-GPA, GAA and other Cr analogs are likely to be transported themselves by the Cr transporter (76).

1.4 Creatine deficiency syndromes

Since the initial description on the clinical symptoms of patients harboring mutations in the GAMT gene (77-79), the subsequent discovery of individuals with mutations in the CrT gene (80, 81), and the eventual finding of patients carrying mutations in the AGAT gene (82, 83), it appears that Cr and/or its biosynthesis-transport have an unforeseen relevance in brain function. The three diseases invariably show different degrees of mental retardation, seizures, and speech delay as a common clinical denominator. GAMT (MIM601240), AGAT (MIM602360) and CrT (MIM300036) deficiencies are collectively termed creatine deficiency syndromes (CDS) (84, 85); they are characterized by an absence of Cr in central nervous system (CNS) as measured *in vivo* by magnetic resonance spectroscopy (MRS) techniques.

Introduction

Their comparative consideration may, in light of the observed clinical phenotypes, uncover new physiological functions of Cr.

The overall comparison among diseases is not trivial however, as each condition presents with particular complications: extra-pyramidal syndrome, self aggressive behavior and intractable seizures in GAMT patients, for instance, are not found in AGAT or CrT deficiencies. Also heterogeneous clinical manifestations and differential penetrance within each of the diseases add to the complexity: GAMT patients again display several degrees of severity and can be subdivided in three different groups accounting for severe to mild presentations (84).

1.4.1 AGAT deficiency

In 2001 AGAT deficiency was identified as a new genetic defect in Cr metabolism in two female siblings with mental retardation who had brain Cr deficiency that could be reversed with oral Cr supplementation (82, 83). The two sisters, 4 and 6 years of age, suffered from mild mental retardation and severe language delay. They started walking unaided at 24 months and started speaking the first words at 30 months. Besides one complicated febrile seizure in one girl, they had no further seizures. In AGAT patients, Cr supplementation led to a rapid progress in the acquisition of visual perceptual and fine motor skills. Language disabilities also improved, but more slowly than nonverbal skills.

1.4.2 GAMT deficiency

“The index patient with GAMT deficiency was born after an uneventful pregnancy at 41 weeks of gestation. The neonatal period and early development were normal. At 4-6 months, dystonic postures were noticed. He was also hypotonic, although there was no severe muscular weakness. Over the next months, global developmental delay became more evident, with an abnormal dyskinetic movement pattern, failing head control, and irregular eye movements. The electroencephalogram showed a peculiar pattern of intermittent runs of high-voltage slow activity (1.5-3 s) intermingled with few spikes. At this time MRS of the brain showed a spectrum lacking a creatine signal and having an elevated guanidinoacetate peak. Such a spectrum had never been seen or described in the literature. The combination of high guanidinoacetate with deficient creatine suggested a block in creatine synthesis at the level of the transformation of guanidinoacetate to creatine. Oral supplementation with creatine monohydrate resulted in the appearance of a creatine signal and a decrease in guanidinoacetate. The patient’s condition improved with respect to muscle tone, dyskinetic movements and mental and motor development. Since the age of 5 years he has been able to walk without ataxia or dyskinetic movements. His muscle tonus is still low, and at the age of 6 years he still does not speak. Despite the marked progress in motor development, he shows some autistic features, with self-injurious behavior. Subsequent studies confirmed the postulated lack of GAMT activity in liver and identified the molecular defect”. The description is from (79) and represents the first realization that Cr biosynthesis is, directly or indirectly, important for brain function. As we have seen, MRS was essential to uncover the underlying molecular defect in GAMT deficiency, but it was also important in the disclosure of AGAT and CrT deficiencies; it is indeed routinely used in the diagnosis of CDS (87).

Since the first description of the index GAMT patient in 1994 (77), an increasing number of hemizygous carriers have been identified and the clinical manifestations refined. Currently, three subgroups are considered depending on the penetrance of the clinical phenotype. The severe phenotype includes intractable epilepsy, early global developmental delay, extra pyramidal movement disorder and abnormal signal intensities of the basal ganglia with aberrant EEGs consisting in intermittent runs of high-voltage slow activity (1.5-3s) overall showing multifocal spike wave change. Patients with the intermediate type exhibit a

Introduction

moderate to severe mental retardation, speech delay, behavioral changes (autistic, hyperkinetic behavior), and epilepsy (treatable with common anticonvulsive drugs) with minor or unspecific EEG changes. The few cases reported with the mild presentation abnormalities included mental retardation, autistic behavior and speech delay (84).

1.4.3 CrT deficiency

A molecular defect on the CrT was first identified in 2001; at this time, a metabolic screening revealed elevated Cr in the serum and urine of the index patient, with normal levels of GAA. The male index patient initially presented with mild mental retardation, mild epilepsy, but with severe delay both in speech and in expressive-language function. Although mild central hypotonia was observed, gross and fine motor functions were normal (80, 81). Interestingly, two old patients have been recently reported (87). Neurological examination at the age of 70 years in the first patient showed a myopathic face with ptosis, external ophthalmoplegia and open, hanging mouth. Case 2, the younger brother of case 1, attended special education and learned to write and read. In his fifties, he had urological problems (urethra stenosis) and gastrointestinal problems (chronic constipation and a bowel ileus). Spontaneous luxations of several digits had occurred since the age of 50. Neurological examination at the age of 67 showed parkinsonism (probably caused by medication), upward gaze paresis, expressionless face, hanging mouth and hanging shoulders. Although those symptoms cannot be considered truly pathognomonic of CrT deficiency, clinical features present in CrT adult patients are myopathic facies (including ptosis), hyperextensible joints, soft skin and gastrointestinal problems, such as megacolon, severe constipation and bowel ileus. The latter might be a consequence of (smooth) muscle problems or autonomic nerve dysfunction (87). Unlike the case with GAMT and AGAT deficiency, treatment with oral Cr monohydrate effected no observable increase of Cr in brain MRS and no improvement in clinical symptoms for none of the CrT patients described so far.

1.4.4 Diagnostic of CDS

The absence of a Cr/PCr signal in the patient's brain measured by means of MRS is the common finding and the diagnostic clue in the three diseases. In AGAT deficiency GAA is decreased, whereas Cr in blood was found to be normal. On the other hand the CrT defect is characterized by an increased concentration of Cr in blood and urine whereas GAA concentration is normal. GAMT deficiency is characterized by decreased Cr serum concentration and abnormally elevated GAA levels in blood. Thus, measurement of guanidinoacetate in body fluids (particularly 24 hours urine or GAA-to-Cr_n ratio) may discriminate between the GAMT (high concentration), AGAT (low concentration) and CrT (normal concentration) deficiencies. In general, GAA and Cr are reliable biochemical markers of CDS.

1.5 Treatment and comparative consideration of CDS

Systemic Cr deficiency caused by disorders of Cr synthesis (GAMT, AGAT) can be corrected with oral supplementation of creatine-monohydrate (90, 91). The different therapeutic outcome of CDS patients to Cr administration revealed unexpected features of Cr transport and biosynthesis. Following Cr oral supplementation the molecule entered the brain and accumulated to 100% of control levels during a period of 16 months in AGAT patients, and to only 50% during the first year and 80% during the second in GAMT patients, presumably due to GAA-mediated competitive inhibition of Cr uptake in the latter group (90, 91).

In sharp contrast, Cr supplementation was unsuccessful in CrT deficient patients. Importantly, CrT patients lacked Cr in their central nervous system (CNS) (81) implying that this organ is fully dependent on circulating Cr and suggesting that Cr biosynthesis does not

Introduction

occur in brain. Accordingly, CrT expression could be observed in CNS capillary endothelial cells (92) but it was not expressed in blood brain barrier forming astrocytes (92): therefore, Cr might enter the brain via CNS capillary endothelium that is free of astrocytic endings (93). The prompt increase in brain proton Cr/PCr signals in AGAT and GAMT patients upon Cr supplementation supports the hypothesis that the brain is dependent on circulating Cr.

On the other hand, brain spectra of AGAT patients lacked brain Cr signals as well. Considering that in AGAT patients the transport system is intact and that Cr biosynthesis enzymes are widely expressed in neural tissue, the lack of Cr in the spectra of AGAT patients paradoxically suggests that the brain is self-sufficient in terms of Cr biosynthesis.

The discrepancy is resolved when considering that an active release of metabolic intermediates (GAA and Cr) to extracellular cerebro spinal fluid (CSF) from glial cells is effective for its subsequent uptake by neurons, where PCr is produced, the mentioned intraorgan Cr shuttle (14). Astrocytes were shown to synthesize and export mainly Arg from radioactively labelled aspartate (168), and are able to form Cr from Arg and Gly in culture (169). Co-culturing of astrocytes and neurons increased Cr concentrations 10-fold compared to neuronal cultures alone (14).

If such a strict isolation of Cr biosynthesis and Cr phosphorylation is truly operative, accumulation of reactive metabolic intermediates in CSF might be of additional relevance for CrT deficiency as well, because neurotoxic guanidine compounds such as GAA may be accumulating in the interstitial CSF fluid. The hypothesis still leaves unexplained, however, the lack of Cr on AGAT patients brain spectra.

Accumulation of GAA, a distinct pathognomonic feature of GAMT patients can be further corrected by substrate deprivation of Arg combined with Orn supplementation, in order to limit substrate availability and inhibit AGAT activity, respectively (94). The distinct additional effect on the clinical course over the responses achieved with sole Cr supplementation is direct evidence of the meaning of GAA accumulation on GAMT clinical manifestations. Further lowering of GAA in body fluids following this approach led to an impressive clinical improvement compared to Cr substitution alone (95): therapy-refractory epileptic seizures disappeared almost completely, interpersonal and motor skills, general behaviour and extrapyramidal movement disorder improved significantly. Sodium benzoate and sodium phenylbutyrate are also useful in the treatment because they divert nitrogen from urea synthesis to alternatives routes of excretion. Arg absorption at the level of the tubules can be decreased in addition through Orn and lysine supplementation because they compete with Arg uptake at the level of the tubular dibasic amino acid transporter (98).

Remarkably, presymptomatic Cr treatment in GAMT and AGAT patients has been recently shown to prevent the development of the diseases (99, 100). The same parents of the only two siblings with AGAT deficiency had another child diagnosed during the neonatal period and treated while the infant still had no symptoms. Biochemical investigations found that blood GAA and Cr were both low from the first days of life; also severe brain Cr depletion measured by ^1H -MRS was already present at 2 weeks of life. The mother was supplemented with Cr during breastfeeding but Cr did not increase in the infant: thus the general delay of 4-6 months for the symptoms in CDS is not due to a component present in breast milk. The patient was treated after weaning (4 months) and did not develop any of the symptoms after 18 months, an age at which affected relatives already showed severe delay in somatic growth and psychomotor development, associated with hypotonia and autistic behaviour (99).

A sister of another GAMT patient was diagnosed during the neonatal period. Blood was taken from the umbilical cord and subsequently every 12 hours until day 5. GAA was already elevated in cord blood. A subsequent increase during the first 24 hours of life was

Introduction

followed by a decline thereafter. However, GAA remained permanently elevated until day 5. In the third week of life the GAA-to-Crn ratio reached higher diagnostic sensitivity owing to Crn decrease occurring after the first week of life. As result of treatment (initiated already at age of 22 days, Cr (400 mg/kg-d), high-dose Orn (increasing the dose over 3 days from 400 to 800 mg/kg-d), sodium benzoate (100 mg/kg-d), and an arginine restricted diet (0.6 g natural protein intake and 1.0 g essential amino acids/kg-d) GAA decreased immediately.

	GAMT deficiency	CrT1 deficiency	AGAT deficiency
Patients	10 (7 published, incl. 1 in abstr./3 unpublished) *1	6 (3 published, incl. 2 in abstr./3 unpublished)*2	2 (2 published)*3
Gender	1 female/8 male	3 male	2 female
Origin	Kurdish/German/Welsh/2 Turkish/Italian	Caucasian	2 Italian
Consanguinity	2 consang./4 unrelated	?	None
Age at onset	Developm. delay median 5 mo (3–7 mo) seizures median 2½ yrs (10 mo–4 yrs)	7 mo in 1/3	?
Age at diagnosis	Median 3 yrs 8 mo (19 mo–26 yrs)	6, 16, 20 yrs	4 yrs 4 mo/6 yrs 5 mo
Developmental delay/arrest	8/8	mild 3/3	2/2
Hypotonia	7/8	1/3	0/2
Dyskinesia	4/8	0/3	0/2
Reflexes, increased	2/7	0/3	0/2
Seizures	7/8 untractable seizures: 5/8	mild 3/3	None (only one febrile seizure)
Mental retardation	Severe 7/8, mild 1/8	mild 3/3	Severe 2/2
Autism/self-injurious behaviour	7/7	1/3	0/2
Active speech	None 7/8, single words 1/8	Single words, severe expressive dysphasia 3/3	Delayed 2/2
MRI	Myelination delay 3/8, T2 intens Pallidum 3/8 (1 pat. with both), no MRI changes 3/8	White matter lesion 2/3 Brain atrophica 2/3	Normal
EEG (pathol)	7/7	1/3	?
Treatment	Creatine 350–1250 (–2000) mg/kg/day 8/8 Arginine restrictive diet 3/8 Phenylbutyrate 1/8 Sodium benzoate 1/8	None	Creatine 400 mg/kg/day 2/2
Outcome	Unfavourable		Satisfying
Motor development	Improved		Improved 1/2
Active speech	None		Improved 1/2
Social contact/behaviour	Improved	No changes	Improved 1/2
Seizures	Improved (after GAA lowering)		
Mental retardation	Severe		

Comparative findings in creatine deficiency syndromes (adapted from 84)

Biochemical findings at the age of 3 weeks were similar to those found in older patients, except for the brain Cr content, which seemed not completely diminished, suggesting prenatal Cr supply. Therefore, slow postnatal release of Cr/PCr pools might explain a presymptomatic period of 3 to 6 months in GAMT patients. At the age of 14 months the patient was healthy and developing normally. Her psychomotor and psychosocial development was according to age. She uses at least five words correctly, understands simple verbal demands, and knows and shows several social gestures. She has been able to walk without support since the age of 11 months (100).

1.6 CDS pathophysiology

Two candidate pathophysiological mechanisms became evident once the first index GAMT patient was reported (79): the lack of Cr on the one hand, the accumulation of GAA on the other hand. Data from CK knockout mice (101-105) along with human CK mutation carriers for the M-CK isoenzyme (106, 107) both showing no overt abnormalities, together with the known neurotoxic actions of guanidino compounds (108-111) favoured the second hypothesis, which was shown to operate through GAA-mediated partial agonism upon GABA_A receptor subtypes (112). Electrophysiological recordings measuring neuron responses induced by GAA application in primary culture and acute murine brain slices evoked picrotoxin and bicuculline sensitive GABA_A receptor-mediated chloride currents with an EC₅₀ of 167 μ M. In addition, pathophysiological GAA concentrations hyperpolarized globus pallidus neurons and reduced their spontaneous spike frequency with an EC₅₀ of 15.1 μ M. Moreover, GAA acted as a partial agonist at heterologously expressed GABA_A but not GABA_B receptors (Fig.11). Alternative neurotoxic mechanisms for GAA have been proposed such as GABA-antagonistic (113), inhibition of Na⁺/K⁺-ATPase activity (114), inhibition of Cr uptake (115) and generation of reactive oxygen species (116).

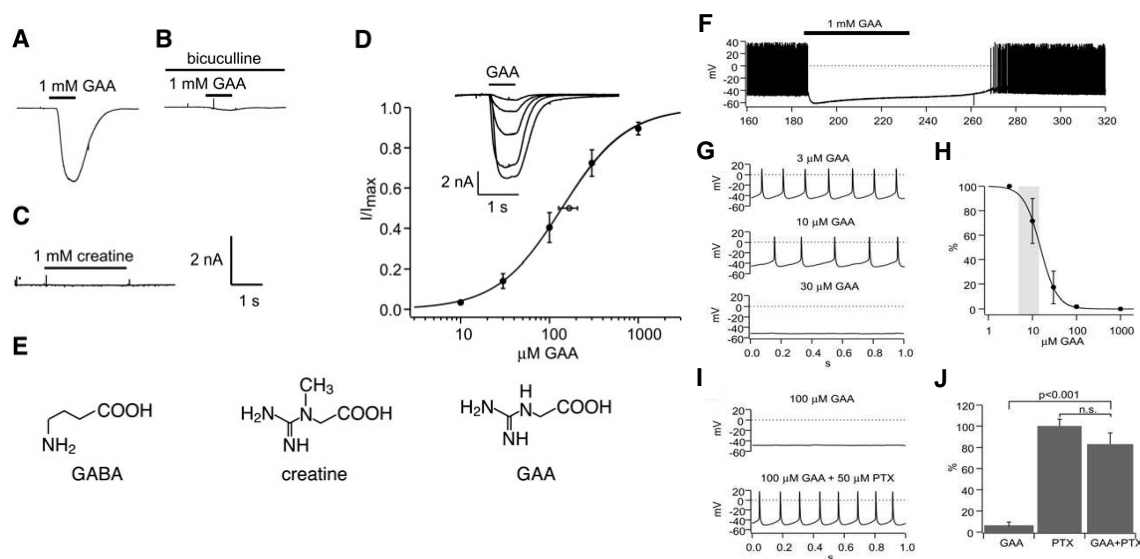


Figure 11: GAA is a partial agonist of GABA_A receptors and activates currents at pathophysiological concentrations. Rapid application of agonists on cultured neuron in TXX held at -60mV. **(A)** Application of GAA induced inward currents that quickly deactivated following GAA washout. **(B)** GAA-induced currents were blocked by coapplication of the GABA_A receptor antagonist bicuculline. **(C)** Application of Cr had no effect on membrane currents. **(D)** The GAA-induced currents were dose dependent and were fit by a Hill function with an IC₅₀ of 167 and a Hill coefficient of 1.4. **(E)** The chemical structures of GABA, creatine and GAA reveal a high degree of similarity. On the right, current clamp recordings of fast-spiking central neurons in acute brain slices containing the globus pallidus (GP) by the use of a low internal chloride concentration (4mM). **(F)** Application of GAA led to hyperpolarization of the GP neurons and inhibition of pacemaker activity. This effect was reversible after washout. **(G)** Current-clamp recording of a fast-spiking neuron, displaying intrinsic pacemaker activity under various GAA concentrations. 3 μ M GAA did not affect the spike frequency, whereas 10 or 30 μ M respectively, inhibited spiking to 71.7 and 17.4 of control conditions. **(H)** The relative change in spiking activity was dose dependent and fit a Hill function with an EC₅₀ of 15.1 μ M and a Hill coefficient of 2.3. The concentration range found in the CSF of GAMT patients is shown in gray. **(I)** application of GAA under control conditions inhibited neuronal activity (upper trace). In the presence of PTX the effect of GAA on the same cell was largely masked. **(J)** Statistical analysis of the results obtained in (I) expressed in percent of spike frequencies recorded in the presence of 50 μ M PTX. Application of 100 μ M GAA reduced spike frequency to 4.9 whereas co-application of 100 μ M GAA and 50 μ M PTX did not induce significant changes (adapted from 112).

Introduction

The subsequent finding of AGAT and CrT deficiencies prompted a view, however, in which the sole lack of Cr without accumulation of GAA leads to neurological dysfunction itself, and the conclusion can be predicated on the marked improvement of the symptoms evidenced in AGAT patients upon Cr supplementation as well as the unsuccessful treatment attempts in CrT patients. It is thus tempting to ascribe those abnormalities commonly present in all disorders, such as developmental delay/arrest, mental retardation and impairment of active speech to the systemic lack of Cr, whereas the mentioned more specific complications applying to GAMT patients (therapy-refractory epileptic seizures and extrapyramidal movement disorder) would be rather linked to the accumulation of GAA, or both (84, 85). In view of the elaborate tissue and developmental specific manner in which Cr exhibits its proposed roles, that of a temporal energy buffer (117-123), a spatial transport device of high-energy phosphates (63-69) and Pi trapping (124-129). The complex amino acid metabolic network to which Cr biosynthesis is anchored, involving the aminoacids Gly, Arg, and Met, as well as the required diffused-active transport of different intermediates between the tissues through the blood, altogether may indicate that multiple reasons can underlie CDS pathophysiology. Yet, lack of Cr and accumulation of GAA still remain the two most parsimonious hypotheses.

To conclude, CDS pathophysiology, in the form of lack of Cr, is being considered a candidate explanatory mechanism in other genetic disorders exhibiting neurological manifestations such those affecting leucine catabolism (130), cystinosis (131) or MCAD deficiency (132). Furthermore, combined methylmalonic aciduria and homocystinuria appeared to accumulate GAA due to secondary depletion of labile methyl groups (133), and the neurological phenotype in these patients was hypothesized to be mediated by the neurotoxic effects of GAA. Mutations on the GABA-degradative enzyme succinate semialdehyde dehydrogenase (SSADH) manifested with elevations of GAA and GBA in urine, as well as GBA levels in CSF, implying additional pathways of pathophysiology for SSADH deficiency and identifying a third instance of elevated GAA and GBA in a human inborn error of metabolism (134). It is thus necessary to understand what is the underlying mechanism leading to encephalopathy and brain dysfunction when the Cr/PCr system is disturbed.

Knockout mice technology provides a means to study CDS pathophysiology. For example littermates born from deficient mothers may clarify the issue as to what extent Cr is essential during development, as there will be a complete absence of Cr during pregnancy. Organic abnormalities requiring invasive methods to be realized, such subtle signs of myopathy as well as detailed biochemical and morphological analysis can be conducted; also alternative treatments for the diseases can be tested in mice. Additional advantages of analysing murine models compared to working with human patients are as follows: it is difficult to assess how important is the lack of Cr/PCr on the development of the symptoms, since it is not possible to achieve complete absence of Cr in adult humans due to dietary intake, or during development due to maternofetal transport. By using mouse deficient mothers as a model, a complete absence of Cr can be achieved and we will be able to learn how important Cr is for general development and to what extent the symptomatology depends on perinatal damage. Cr supplementation at different time points during pregnancy and neonates may identify the particular developmental stage at which irreversible brain damage occurs. Second, comparison of AGAT and GAMT deficient mice should clarify as to what extent GAA phosphorylation is rescuing the phenotype of GAMT mice as well as how important GAA accumulation is for CDS pathophysiology. Towards this end we generated and phenotyped GAMT ($GAMT^{-/-}$) and AGAT ($AGAT^{-/-}$) knockout mouse models to study human CDS.

2 Materials and methods

2.1 Chemicals, buffers and media

Chemicals

All the chemicals used were mainly from Sigma (www.sigma-aldrich.com), Merck (www.merck.com), Gibco/BRL (www.invitrogen.com), Roth (www.carl-roth.de), and Fermentas (www.fermentas.de).

Buffers and medium

All buffers and medium were made with deionised water (ddH₂O, membranePure GmbH, www.membranePure.de), autoclaved (20 min, 121°C, 2x10⁵ Pa) or filtered by 0,22 µm Millex-GP-Filter (Millipore, www.millipore.com).

Bacterial medium

Luria Broth

1. Dissolve 25 g Luria broth powder in 750 ml of distilled water.
2. Add 800 ml distilled water.
3. Adjust to pH 7.0 with either HCl or NaOH as appropriate.
4. Make up volume to 1 liter with distilled water.
5. Sterilize next day (no longer) by autoclaving.

SOB: 20 g peptone 140, 5 g yeast extract, 0,5 g NaCl, 2,5 ml KCl (1M Stock), 1000ml H₂O.

Buffers

10M ammonium acetate

Dissolve 385.4 g ammonium acetate in 150 ml H₂O
Add H₂O to 500 ml

1M CaCl₂

147 g CaCl₂-2H₂O
H₂O to 1 Liter

0.5M EDTA (ethylenediamine tetraacetic acid)

Dissolve 186.1 g Na₂EDTA-2H₂O in 700 ml H₂O
Adjust pH to 8.0 with 10M NaOH (~50ml)
Add H₂O to 1 Liter

Materials and methods

10 mg/ml ethidium bromide

Dissolve 0.2 g ethidium bromide in 20 ml H₂O
Mix well and store at 4°C in dark
(ethidium bromide is a mutagen handle carefully)

1M HCl, 1 Liter

Mix in the following order:
913.8 ml H₂O
86.2 ml concentrated HCl

1M KCl

74.6 g KCl
Add H₂O to 1 Liter

1M MgCl₂

20.3 g MgCl₂·6H₂O
Add H₂O to 100 ml

5M NaCl

292 g NaCl
Add H₂O to 1 Liter

10M NaOH

Dissolve 400 g NaOH in 450 ml H₂O
Add H₂O to 1 Liter

3M Sodium Acetate

Dissolve 408 g sodium acetate·3H₂O in H₂O
Add H₂O to 1 Liter
Adjust pH to 5.2 with 3M Acetic Acid

1M Tris-Cl (Adjust pH with varying amounts of 0.1M HCl)

Dissolve 121 g Tris base in 800 ml H₂O
Adjust to desired pH with concentrated HCl
Mix and add H₂O to 1 Liter

Phosphate-buffered saline (PBS)

10X Stock Solution, 1 Liter

80 g NaCl
2 g KCl

Materials and methods

11.5 g Na₂HPO₄·7H₂O
2 g KH₂PO₄

Working stock, pH ~7.3

137mM NaCl
2.7mM KCl
4.3mM Na₂HPO₄·7H₂O
1.4mM KH₂PO₄

20X SSC

3M NaCl (175 g / Liter)
0.3M Na₃citrate·2H₂O (88 g / Liter)
Adjust pH to 7.0 with 1M HCl

STE Buffer

10mM Tris-Cl, pH7.5
10mM NaCl
1mM EDTA

TAE Buffer

50X stock solution, 1 Liter
242 g Tris base
57.1 ml glacial acetic acid
37.2 g Na₂EDTA·2H₂O (2mM)
pH ~8.5

TE Buffer, pH 7.4, 7.5, or 8.0

10mM Tris-Cl, pH 7.4, 7.5, or 8.0
1mM EDTA, pH 8.0

1M Tris-HCl, pH 6-8

12.1g Tris base (MW 121.14) in 100ml H₂O (adjust pH with concentrated HCl)

SDS- PAGE Running Buffer

25mM Tris/HCl pH 8,3
200mM glycine
1% SDS

SDS-PAGE Loading buffer 2x

125mM Tris/HCl,pH 6,8
4% SDS
10% β-mercaptoethanol
20% glycerol

Materials and methods

0,02% Bromphenolblue

TAE (Tris-acetate EDTA) 10x

400mM Tris/HCl, pH 7,9
100mM NaAc
10mM NaEDTA

PIM (Protease inhibitors mixture)

1mM PMSF (phenylmethylsulfonyl fluoride)
0,2µM Leupeptin
0,2µM Pepstatin

Western blocking buffer

25mM Tris/HCl pH 8,3
200mM glycine
0,1% SDS
10% methanol

10X Buffer G (green) 10mM Tris-HCl (pH 7.5 at 37°C), 10mM MgCl₂, 50mM NaCl, 0.1mg/ml BSA

10X Buffer O (orange) 50mM Tris-HCl (pH 7.5 at 37°C), 10mM MgCl₂, 100mM NaCl, 0.1mg/ml BSA

10X Buffer R (red) 10mM Tris-HCl (pH 8.5 at 37°C), 10mM MgCl₂, 100mM KCl, 0.1mg/ml BSA

10X Buffer Tango (yellow) 33mM Tris-acetate (pH 7.9 at 37°C), 10mM magnesiumacetate, 66mM potassium acetate,

1M LiCl

2.12g LiCl (MW 42.4) in 50ml H₂O, autoclave.

25mg/ml Ampicillin stock solution

Dissolve 1 g ampicillin (sodium salt) in 35 ml of distilled water. Make up volume to 40 ml with distilled water. Sterilize by filtration.

2.2 Molecular biology

Oligonucleotides

Materials and methods

All constructs made in this work were done by PCR using oligonucleotides from MWG-Biotech (www.mwg-biotech.com).

2.2.1 Bacterial transformation

For transformation of *E.coli* competent cells, 100 µl of –80°C stored cells were thawed on ice and 1,7 µl of β-mercaptoethanol was added. After 10 min, competent cells were incubated for 30 min on ice with 10-50 ng of DNA. A heat-pulse was then applied for 20 (BL21 DE3-RIL) or 40 seconds (XL-Blue, BL21-Gold DE3, BL21-GoldDE3 pLysS) at 42°C in a water bath. Reaction was incubated on ice for 2 min, 900 µl of prewarmed SOC medium was added and incubated for 1 hour at 37°C with shaking (250 rpm).

After transformation, 100 µl of the reaction volume were plated onto a single LB agar plate containing the appropriate antibiotic. Plates were incubated O.N. at 37°C.

2.2.2 DNA preparation

For mini-preparations the GFX Micro plasmid Prep Kit (*Amersham Biosciences*) was used. 3 ml of an O.N. culture (antibiotic + selected colony) were centrifuged at 6000 rpm for 2 min (2 x 1,5 ml in Eppendorf tubes using a micro centrifuge *Biofuges Pico, Heraeus Instruments*). Pellet was resuspended in 150 µl of buffer I, and suspension was mixed with 150 µl of buffer II. After 4 min incubation (RT), 600 µl of buffer III were added, gently mixed and incubated on ice for 10 min. Lysate was then cleared by centrifugation (13000 rpm, 5 min) and supernatant loaded onto the GFX column, incubated for 1 min and centrifuged (13000 rpm, 1 min). Columns were washed with 400 µl of washing buffer and centrifuged (13000 rpm, 1 min). DNA was eluted from the column with 30 µl of 10 mM Tris/HCl, pH8,0 by centrifugation (13.000 rpm, 1 min).

For midi-preparations a Plasmid DNA Purification Kit (*Macherey-Nagel*, www.macherey-nagel.com) was used. Bacteria from a 50 ml O.N. culture (antibiotic + selected colony) were centrifuged at 7000 rpm for 10 min at 4°C (*SIGMA 2K15* centrifuge). Pellet was resuspended in 4 ml of buffer S1 + Rnase A. 4 ml of buffer S2 were added and gently mixed. After 4 min at RT, 4 ml of buffer S3 were added to the reaction and incubated on ice for 10 min. Lysate was then cleared by centrifugation (8000 rpm for 25 min at 4°C). Supernatant was loaded into a NucleoBond AX 100 column pre-equilibrated with 2,5 ml of buffer N2. Column was washed 2 x 5 ml of buffer N3 and DNA eluted with 5 ml elution buffer N5. Plasmid DNA was precipitated with 3,5 ml isopropanol and centrifuged at 12000 rpm for 30 min (*RC5C Sorvall-Centrifuge, SS-34rotor*). DNA was then resuspended in 50 µl of 10 mM Tris/HCl, pH8,0.

DNA concentration was adjusted to 1 µg/µl by measuring UV-light absorption (O.D) at 260nm with Gene Quant II-Photometer (*Pharmacia*, www.Pharmacia.de). DNA preparation quality was judged from the O.D₂₆₀/O.D₂₈₀ ratio.

2.2.3 DNA-Electrophoresis gel

To analyze or separate DNA fragments, agarose gel electrophoresis was used. The gel was 1, 1,5 or 2 % agarose in Tris-acetate-EDTA (TAE) buffer with 1 µg/l ethidium bromide. 15 mV current per cm was applied to the agarose gel using a electrophoresis chamber (*Pharmacia, LKB GPS 200/400*). The distance DNA migrated in the gel could be judged by visually monitoring migration of the tracking dyes, bromophenol blue and xylene cyanol.

To estimate size and amount of the DNA fragments, a standard DNA-marker was used (*Smart Ladder, Eurogentec*, www.eurogentec.de). DNA migrated was visualized using a UV-Transilluminator (*BioDoc II, Biometra*).

Materials and methods

2.2.4 DNA-Isolation from agarose gel

To purify DNA from agarose gel, GFX PCR DNA and gel band Purification Kit (*Amersham Biosciences*) was used. The desired “band” from an ethidium-stained gel was viewed with a UV transilluminator (*DESAGA*, 254/366 nm) and excised using a scalpel blade. Because UV light can fragment DNA, it is best to work expeditiously and keep exposure time to a minimum. The agarose piece was placed in a 1,5 ml Eppendorf tube and dissolved in 300 µl capture buffer by heating at 60°C. Once the agarose gel was dissolved, the solution was loaded onto a GFX-column, incubated for 1 min and shortly centrifuged at 13000 rpm in a micro-centrifuge (*Biofuges Pico, Heraeus Instruments*). 500 µl of wash buffer were added and a short centrifugation was performed, 1 minute at 13000 rpm. DNA was eluted by incubation for 1 min at RT with 30 µl of 10 mM Tris/HCl, pH8, 0 and collected into a new 1,5 ml Eppendorf tube by short centrifugation at 13000 rpm.

2.2.5 Restriction enzyme digestion of DNA

Plasmid DNA and PCR products were digested by restriction enzymes (*Fermentas*, www.Fermentas.com) that recognized specific sequences of DNA. The digestion reaction was composed of DNA sample (volume should not be more than about 1/3 of the total digest volume if possible), 1/10 digest volume of 10X restriction buffer, the appropriate number of units of enzyme (one unit of enzyme activity is defined as the amount needed to digest 1 µg of a specific DNA in a 50 µl digest volume at the appropriate temperature, usually 37 C), and sufficient H₂O to bring the mix up to the digest volume (50µl). Digestion reactions were incubated for 90 min at 37°C and stopped by adding 0, 2 volume of the tracking dyes followed by the agarose gel electrophoresis.

2.2.6 DNA-dephosphorylation

To avoid self-ligation of linearized vectors with complementary ends, it is necessary to remove phosphate from protruding ends (3´ or 5´) of dsDNA generated by restriction endonucleases. In this work Calf Intestinal Alkaline Phosphatase (CIAP, from *Fermentas*) was used. 1 unit of enzyme was added to the restriction reaction and incubated for 30 min at 37°C. Reaction was stopped by adding 0,2 volume of the tracking dyes followed by the agarose gel eletrophoresis.

2.2.7 DNA-Ligation

40 ng of vector DNA was ligated with 150 ng of insert DNA in 20 µl ligation volume with 1 U of T4-DNA-Ligase (*Fermentas*) and T4-ligation buffer. Reaction was incubated over the weekend at 4 degrees, O.N. at 16°C or at RT for 3 hours.

2.2.8 DNA-Sequencing

DNA sequence analysis was made using the Sanger method (Sanger et al., 1977) by the service laboratory of the ZMNH using an ABI Prism 377 DNA sequencer (*Perkin Elmer*, www.perkin-elmer.de). Sequencing Kit was Prism Dye Terminator Cycle Sequencing Ready Reaction Kit (*Perkin Elmer*).

Materials and methods

2.2.9 Polymerase chain reaction (PCR)

To amplified DNA, pTaq (purified from natural sources; Fermentas) or pfx (Fermentas) was used. The reaction volume (50 μ l) was run in 0,5 ml Eppendorf tube. PCR took place in a thermal cycler (Peltier Thermal Cycler PTC-200, *MJ Research*, www.mjr.com). Cycle conditions were: 35 cycles of 95 °C/55–60 °C/60 °C (30–45 s each). Touchdown PCR programs were calculated and performed by decreasing the annealing temperature 2 degrees every cycle to a 'touchdown' annealing temperature which was then repeated for 25 cycles. When needed, target DNA was amplified by oligonucleotides containing appropriated restriction sites for the subsequent digestion and ligation of the PCR products. All PCR reactions carried out following standard protocols. PCR products were gel-purified when used for cloning or southern probes.

2.2.10 GAMT and AGAT genotyping

Ear biopsies were digested overnight in lysis buffer (10 mM Tris-HCl (pH 8.3) 2.5 mM MgCl₂- 6H₂O, 0.45% v/v Tween 20 and 1 μ l proteinase K (10mg/ml) per tube). The next morning 5 μ l of the lysate were added to the following PCR mixture:

Lysate	5 μ l
10X PCR buffer	5 μ l
MgCl ₂ (25mM)	4 μ l
Betaine (5M)	10 μ l
DMSO	2,5 μ l
Primers (50pM)	0,5 μ l
dNTPs (25mM)	0,5 μ l
pTaq	1 μ l
H ₂ O	to 50 μ l

Primers AGAT genotyping

AGAT_gen1f: AGCCCCTCTATTTCCCTTTTCATT

AGAT_gen2r: AGGCCTACCCGCTTCCATTGCTCA

AGAT_gen4r: TTCCACTGCGTCATTCTCCTGTAA

For animals containing the neo cassette all three primers were used together in a multiplex PCR (knockout band: 468bp; wiltype band: 523bp). When genotyping animals with the neo cassette excised just primers AGAT_gen1f and AGAT_gen4f were used (knockout band: 277bp; wiltype band: 523bp).

Primers GAMT genotyping:

mGAMT 59nc: GGTCTCCCAACGCTCCATCACT

mGAMT 60c: CCTCAGGCTCCCACCCACTTG

mGAMT 56nc: AGGCCTACCCGCTTCCATTG

All primers were used in a multiplex PCR (knockout band:430bp; wiltype band: 265bp)

2.2.11 Screening of genomic clones and cloning of the AGAT targeting construct

A 129/Sv cosmid genomic library (RZPD: German resource center for genomic research) was screened by PCR with primers AGAT_3 (CAGCACTGACCTGTAGACTCAAA),

Materials and methods

AGAT_4(CAGCTCAGAACTGCCTATAACTCC). One well was found to be positive and a second formatted 96-well cosmid library was obtained containing an array of the clones present in the positive well of the primary screening. In the second 96-well version cosmid clones are arranged in a way that three positives are to be detected across the 12 columns of the 96-well plate, leading to a single cosmid clone. Cosmid DNA was prepared following standard methods and digested with *Bam*HI. A 10kb band was gel purified and subcloned in pKO_901_DT digested with *Bam*HI and treated with *CIAP* to prevent self-ligation of the vector. The genomic subclone was further digested at two single sites (*Bst*XI and *Bsa*I) present in exon 3 and intron 4, removing 273 bp, refilled with *Klenow*, dephosphorylated with *CIAP* and ligated to a blunted fragment containing the neo cassette, retrieved by *Asc*I digestion and *Klenow* refilling from the plasmid *Asc*I_ploxPNEO.

2.2.12 AGAT gene targeting

The AGAT targeting construct was linearized with *Not*I and electroporated in R1 cells. The followed protocols for ES cells gene targeting are outlined below. A 3' external probe (680bp) was PCR amplified from a B57Bl/6 BAC DNA and used for Southern blot experiments to detect recombination at the 3' end. Genomic ES cells DNA (280 clones) was digested with *Spe*I overnight, separated in 0.7% agarose gels and stained with ethidium bromide. Gels were incubated in HCl 5M for 5-10 minutes, and NaOH for 15 minutes. Blotting to nitrocellulose membranes was carried out overnight in NaOH. Blots were hybridized with a radioactively labelled 3' probe. The wildtype *Spe*I fragment is 16kb and shortened in two smaller fragments of 8kb when correct homologous recombination occurred.

2.2.13 Screening of genomic clones and cloning of the GAMT targeting construct

A 129/SvJ mouse genomic library (Stratagene, La Jolla, CA, USA) was screened using the mGAMT cDNA as a probe and obtained one positive clone. Complete insert sequencing showed that this clone contained the complete mGAMT open reading frame. The 5.2 kb *Hind*III/*Bgl*II restriction fragment isolated by partial digestions of the phage DNA, which contained all six exons, was subcloned into pBluescriptKS (Stratagene). The 5' end of the fragment was shortened by 500 bp, yielding pBKS-mGAMT. The region deleted from the 5' end of the genomic clone was subcloned to pBluescript KS and used as 5' external probe in Southern blot experiments.

2.2.14 GAMT Gene targeting

pBKS-mGAMT DNA was cut with *Mlu*I, filled with *Klenow* polymerase and ligated with a blunt-ended restriction fragment containing the neomycin resistance gene (neo) under the control of the phosphoglycerate kinase (PGK) promoter yielding the targeting vector pmGAMT-KO. The linearized targeting vector was electroporated into 129 (R1) embryonic stem (ES) cells, which were subjected to selection by geneticin (G418, Invitrogen, Karlsruhe, Germany). Southern blotting was performed on 280 resistant ES cell clones, 10 of which were positive for the targeting event. Genomic ES cell DNA was digested with *Dra*I, separated on 0.8% agarose gels, transferred to nylon membranes and hybridized with the 3' external probe derived from DNA distal to the pBKS-mGAMT *Bgl*II site. The wild-type 6.8-kb *Dra*I restriction fragment was 1.5 kb shorter (5.3 kb) when homologous recombination occurred

Materials and methods

Homologous recombination at the 5' end was verified by Southern blot analysis of *HindIII*-digested genomic ES cell DNA as described above using the 5' external probe. In the case of homologous recombination, the wild-type 4.3-kb *HindIII* fragment was 1.5 kb longer (5.8 kb). One of the positive ES clones (#167) was expanded and microinjected into C57BL/6J mouse blastocysts, which were then transferred into pseudopregnant CBA/C57BL/6J females. Two of three chimeric mice that were mated gave rise to germ-line transmission of the disrupted allele. Males and females with different genotypes from different litters were randomly intercrossed to obtain mGAMT^{+/+}, mGAMT^{+/-} and mGAMT^{-/-} progeny. Genomic DNA from mouse-tail or ear biopsies was screened either by Southern analysis or multiplex polymerase chain reaction (PCR) following standard protocols.

2.2.15 Western blots.

GAMT polyclonal antibodies were generated in rabbit against recombinant N-terminally, six-histidine (His)-tagged mGAMT or hGAMT proteins purified from *E. coli* following standard procedures according to the manufacturer (Qiagen, Hilden, Germany). The antibodies used in this study were affinity purified against the respective antigen immobilized on NHS-activated Sepharose (Amersham, Freiburg, Germany). The specificity of the antibodies was first verified by western blot experiments using antigen-blocked and unblocked antibodies (not shown). Upon availability of GAMT^{-/-} mice, specificity of the antibodies was reconfirmed.

AGAT antibodies were generated by rabbit peptide injections and further affinity purification of the primary bleeding. The specificity was verified by pre-incubation of the blots with the peptides and further confirmed by lack of signal on AGAT^{-/-} tissues.

2. 3 ES cells gene targeting

2.3.1 Primary Mouse Embryonic Fibroblast (MEF) Culture

Thawing MEF Cells

A vial of primary embryonic fibroblast cells was thawed by holding at 37°C in a water bath. MEF media was prepared. 1mL of thawed fibroblasts was mixed onto MEF media. Cells were centrifuged at 850 rpm for 5 minutes and media was aspirated and discarded. The pellet was resuspended in 10mL MEF media, transferred to a 10 cm tissue culture plate and incubated at 37°C, 5% CO₂. When preparing MEF cells for subsequent culture of ES cells, MEF cells are to be inactivated by mytomicin C (MMC). To do that, 15cm plates with 15 ml MEF media were used. 150ml MMC was added and plates were swirled and incubated 2-3 h at 37°C. After that, MEF media was removed, cells were trypsinized with 3ml trypsin 3-5 minutes at 37°C, and eventually recovered in 7 ml MEF media and either dispensed in other three plates or frozen down in freezing media.

Passaging Cells

Once MEF cells were fully confluent (about 3 days) cells were passaged aspirating the media and discarding it (tilt plate to ensure complete removal). The plate was washed with 10mL PBS by pipetting onto the side of the plate, not the base so as not to dislodge cells and repeated once. 1mL Trypsin/EDTA was added, swirled to cover and incubated at 37°C for 2-5 minutes. Plates were monitored under a microscope to ensure that cells were fully trypsinized.

Materials and methods

Any adherent cells were dislodged by flicking the plate. Cells should be rounded and floating freely. 8mL MEF media was added to each plate, pipetted up and down 5 times, washing each plate thoroughly. 3mL of the cell suspension was added to a fresh plate containing 7mL media (3 plates in total), pipetted up and down 3-5 times to ensure cells are fully mixed and incubated. Fibroblasts were used until passaging reached P4.

2.3.2 ES Cell Culture

10 cm tissue culture plates were treated with sterile 0.1% gelatin. 2-3mL gelatin was swirled to fully cover the plate and left stand for 5-10 minutes. Gelatin was aspirated and discarded. 1×10^6 MEFs are needed for a feeder layer of this size plate. MEFs were thawed as usual. Cells were spun down and resuspended in 10mL MEF media. 5mL of suspension was added to each of two gelatin coated plates containing 5mL MEF media each. Plates were incubated overnight to allow the MEFs to attach and spread. Subsequently, a vial containing 1×10^7 ES cells was thawed into 4mL ES media, spun down, and cells were resuspended in 10mL ES media. MEF media was removed from a feeder plate and ES cells were plated onto the feeder layer and incubated as usual. Cells were checked next day to determine if fresh media was required (indicated by a change of media color to yellow). Once the plate was very crowded and colonies were large (may take 2-3 days but is variable), cells were passaged 1 in 2. To passage, 2x10 cm plates of feeder cells should be ready. ES media was removed, plates were washed with PBS twice and 1.2mL Trypsin was added and Incubated at 37°C for 2-5 minutes. 10mL ES media was added and pipetted vigorously to break up all the clumps (ES cells tend to stick together which can make counting difficult). 5mL of ES media was added to each of two feeder plates. ES cells should always be passaged the day before you intend to electroporate.

Electroporation of ES cells

On the morning of the electroporation, cells were fed with fresh media. Later that afternoon, ES cells were harvested as usual and the number of cells in counted. 1×10^7 cells is the minimum number required for electroporation. The volume of cells required for electroporation was spun down, media was removed and 25-40µg knockout construct DNA purified and already linearized (2X phenolyzed, ethanol precipitated and dried as a pellet; DNA was dissolved in 30µL PBS inside the hood). DNA was added to the ES cell pellet (no mixing needed) plus 600µL sterile PBS inside the hood. The mixture was transferred to a 0.4cm cuvette, placed on ice for 8 minutes and electroporated at 500µF, 0.24kV. After electroporation, cuvettes were incubated on ice for 10 minutes and cells were transferred to 40 mL ES media using a Pasteur pipette, mixed, and subsequently transferred 10 mL to each of 4 pre-prepared feeder plates. Electroporated cells were incubated for approximately 36 hours prior to selection. To select for transformants, ES media containing between 150-300µg/mL G148 (Geneticin) was added. After 48 hours cell death was obvious. Cells were fed every day if there were a lot of debris and media was yellowing, otherwise every second day is sufficient. If debris were sticking to the living cells, cells were washed gently with PBS before feeding with fresh media. Care should be taken not to dislodge the feeder layer. Cells were left growing for around 10 days post electroporation. Colonies were generally ready for picking 9-11 days after electroporation, depending upon the cell line and the media used.

The day before picking, 96 well plates were treated with gelatin (200µl per well). Approximately 5×10^5 MEFs should be used per plate (i.e. 1 vial can be used on 2x96 well plates). MEFs were resuspended in 48mL MEF media. 200µl of the mixture was added to each well and incubated as usual. When ready to pick colonies, wear gloves, gown and face

Materials and methods

mask. Wipe down the microscope, bench, tip boxes and pipette with ethanol. Keep dish closed as much as possible and keep traffic in the room to a minimum. Look at cells at 4x magnification. Any colonies picked should be spaced well enough apart to ensure no contamination from surrounding colonies. Once a desired colony was found lid was removed, and using a yellow tip and pipette set to 15 μ L the colony was circled with the tip to loosen the surrounding fibroblast layer (otherwise colony may stick). Scrape the colony with the tip to dislodge, then aspirate in 15 μ L. The colony can usually be seen inside tip. Clones were then transferred to an empty well in a 96 well plate. Transferring to a fresh well should be performed using a fresh tip each time, until a suitable number is picked (usually 192 clones). 96 well plates were transferred to the hood, 5 μ l of Trypsin added to each well and incubated at 37 degrees, 2-5 minutes. ES media was added after trypsinizing and, with a pipette set to 50 μ L, pipetted up and down to break up each colony, with careful not to cause too excessive foaming. The better the colony is dispersed the faster it will grow. A fresh tip was used for each well. Each well should ideally be evenly covered with colonies before harvesting. Continue feeding every second day or whenever the media turns yellow, until a good coverage of colonies in each well is achieved. This usually takes about 3-4 days.

Harvesting and DNA Preparation

Cells in the 96 wells plate were washed twice with PBS and incubated with 100 ul lysis buffer overnight at 55°C. The next morning 10ul LiCl (1M) and 100ul isopropanol per well were added and the 96-well plates incubated at 4 degrees for three days. Plates were then centrifuged for 10 minutes and washed with 200 μ L 70% ethanol twice. Pellets were air dried and redissolved in 100 μ L TE (less if pellet is very small). Pellets were allowed to completely dissolve for 2 hours at 65°C then overnight at 4°C. Before digesting, plates were heated up to 65°C for 10 minutes. If pipetting was very difficult, the solution was pipetted straight from 65°C. Depending upon the size of the original DNA pellet, between 10-30 μ L of DNA should be digested for Southern analysis.

Freezing Plates

When colonies have all regrown, media was removed from each well, washed with 200 μ l PBS and trypsinized with 40 μ l trypsin 3-5 minutes. 60 μ l ES medium was added and clones were gently resuspended. At this point, 96-well plates were transferred to ice. 100 μ l 2X freezing media was added to each well. Afterwards, 50 μ l mineral oil was added on the top of each well. Without mixing the contents, plates were isolated around with parafilm and transferred to -80°C to freeze. Plates can be kept for a number of months. To thaw, 0.5mL ES media was added. Plates were thawed quickly by holding in 37°C water bath, subsequently transferred to a hood and each well manually pipetted. The contents were transferred to a fresh 24 well plates with feeders. Next day, media was changed to remove DMSO. Grow was allowed for up to 2 weeks for colonies to form.

Media for ES cells culture

All media and reagents for ES and MEF cells culture were from Gibco unless otherwise specified.

MEF medium:

DMEM (high glucose, no pyruvate, with glutamax): 500ml; FCS (origin, South America): 50ml; MEM(non-essential aminoacids100X) 5,5 ml; Pen/Strep (5000IU, 5000 μ gStrep/ml, 100X) 5.5ml.

Materials and methods

ES-medium:

DMEM (high glucose, no pyruvate, 25mMHepes): 500ml; FCS(ES-qualified, 15%): 92ml; Glutamine (200mM, 100X): 6,2ml; MEM (NEAA non-essential aminoacids): 6,2ml; Pen/Strep (5000IU, 5000µg Strep/ml, 100X): 6.2ml; Nucleosid mix (100X): 6,2ml; Sodium Pyruvate: 6,2 ml; 2-Mercaptoethanol (50mM, 1000X, 100uM):1,24ml; LIF(107µ/ml, Esgro): 62µl.

Others

2,5% trypsin(10X solution): dissolve 1 ml in 8ml PBS/EDTA and 10% chicken serum.

Trypsin/EDTA for MEF cells: 0.05%

Trypsin/EDTA for ES cells:0,25 %

G418 (stock 50mg/ml): final concentration at plate 200-300µg/ml; add 4-6µl/ml

0.1% gelatine

Mineral oil

Freezing media: FCS: 50%; ES cells medium: 40%; DMSO:10%.

Mytomycin C (Sigma)

2.4 Morphology

Muscle.

To analyze muscle tissue, mice were perfused transcardially with 4% paraformaldehyde (PFA) and 2% glutaraldehyde (GA) in PBS. Tissues were postfixed in 1% OsO₄, dehydrated and embedded in Epon. Ultrathin sections were stained with uranylacetate and lead citrate and examined with a Zeiss EM902.

Testis.

Whole mouse testes were fixed in 3.5% glutaraldehyde in 0.05 M sodium phosphate buffer pH 7.1–7.4 for 3 h. Small pieces of the testes were then postfixed in 1% OsO₄, dehydrated in ascending alcoholic series and finally embedded in Epon 812. Semi-thin free-floating sections (1 µm thick) were stained with toluidine blue/pyronine G and covered with Caedax (Merck, Darmstadt, Germany).

Liver

Liver specimens were obtained without mouse perfusion and dehydrated overnight in 70% ethanol. Livers were subjected to ascending alcoholic series and embedded in Epon 812. 1µM slices were obtained and stained for periodic shiff acid staining (PAS) following standart protocols specified in the kit (sigma).

Materials and methods

2.5 Determination of guanidino compounds

The concentration of the guanidino compounds was determined using a Biotronic LC 5001 (Biotronik, Maintal, Germany) amino acid analyzer adapted for guanidino compound determination. The guanidino compounds were separated via a cation exchange column using sodium citrate buffers and were detected with the fluorescence ninhydrin method, which is described in detail elsewhere.

2.6 Analysis of body composition

Carcasses were weighed and oven dried at 60°C for at least 2 weeks until weight was constant. Total body water was calculated as the difference between the weights before and after drying. The carcass was then chloroform-extracted using a Soxhlet apparatus. The extracted carcass was dried and weighed to calculate fat mass and lean mass.

2.7 Glucose tolerance test

Mice were fasted for 16-18 hours (overnight) ensuring that they have access to drinking water all the time. On the following day, at 8 a.m., mice were placed individually in clean cages with water only (no food). Cages were identified with a mouse number. The weight of each mouse was recorded and the volume of glucose required was calculated as follows: volume of IP glucose injection (μl) = $10 \times \text{body weight (g)} \times (\text{glucose solution } 12.5\% \text{ (12.5g in 100ml distilled water)})$ sterilised. The Glucotrend (Roche diagnostics) was calibrated with the standard stick. The mouse was placed in a restraining device for blood collection. A small incision was made over the lateral tail vein (2 cm from the tail base) using a scalpel blade. 3 μl of blood with a 20 μl Micropipettor was collected and dropped the blood sample on the stick placed in the Glucotrend apparatus. The glucose level was recorded (= T0 result). Direct pressure was applied to the incision for 1-2 minutes to facilitate haemostasis.

The mouse was then injected intraperitoneally with the appropriate amount of glucose solution. Another 3 μl of blood from the tail of the mouse was collected 15 minutes after glucose IP injection and glucose was measured with the Glucotrend apparatus (=T15). Bleeding started again by removing the clot from the first incision and by massaging the tail if blood flow is inadequate. Similarly, 3 μl of blood was collected at the following time points (in minutes) after IP injection of glucose: T30, T60, T90, T120, T150 and eventually T180. At the end of the experiment, mice were returned to their cages making sure that a plentiful supply of water and food was available to the animals.

2.8 Determination of metabolic hormones

Leptin, insulin and adiponectin levels in serum were measured by ELISA assays according to the protocols provided by the manufacturers (leptin, insulin: Crystal Chemistry, Downers Grove, IL, USA; adiponectin: BioCat, Heidelberg, Germany).

2.9 Cage activity

The home cage activity was monitored for 3 consecutive days with an infrared motion detector with a sampling frequency of 1 Hz and a bin size of 4 min (INFRA-E-MOTION GmbH, Hamburg, Germany). Activity levels were calculated as the sum of activity values obtained during daylight and dark phases.

Materials and methods

2.10 Muscle performance analysis

Preparation. Before the experiment, animals were anesthetized with nembotal (80 mg/kg) and urethane (1.5 g/kg) and kept under anesthesia with regular doses of nembotal (20 mg/kg). Body temperature during the surgery and the experiment was maintained by placing the mouse on a heated pad.

For the surgical preparation of the *in situ* stimulation, the medial head of the gastrocnemius muscle was prepared free from the surrounding tissue, leaving the origin on the femur and the blood supply intact. Distally, the Achilles tendon was cut and attached to a measuring device as described before. The muscle-tendon complex was stimulated (0.3–0.4 mA, pulse width 50 μ s) via the severed sciatic nerve, with only the branch leading to the medial gastrocnemius muscle left intact.

Muscle optimal length (L_o) was first estimated using twitch contractions at different lengths of the muscle-tendon complex, and further assessed by applying tetani (stimulation frequency 250 Hz, stimulation duration 150 ms) with rest intervals of 3 min. Muscle temperature during the experiment was kept at 33°C by a water-saturated airflow around the muscle.

Contractions. In all three groups (Con, $n = 10$; $GAMT^{-/-}$, $n = 10$; $GAMT_{Cr}^{-/-}$, $n = 5$) L_o was determined as described in (135) and subsequently force-frequency relations were measured at several stimulation frequencies, varying from 60 to 250 Hz (stimulation duration 250 ms). The stimulation frequencies were applied in a random order, and contractions were separated by 3-min rest intervals.

Thereafter, in all three groups (Con, $n = 9$; $GAMT^{-/-}$, $n = 9$; $GAMT_{Cr}^{-/-}$, $n = 5$) resistance to fatigue during dynamic contractions was examined by applying a series of 30 repeated dynamic contractions within 7.5 s (stimulation duration 55 ms, stimulation frequency 150 Hz, shortening velocity 20 mm/s, one contraction every 250 ms).

In a separate experiment (Con, $n = 10$; $GAMT^{-/-}$, $n = 10$; $GAMT_{Cr}^{-/-}$, $n = 6$), determination of L_o was followed by a series of 30 repeated isometric contractions (at L_o , stimulation duration 50 ms, stimulation frequency 150 Hz, one contraction every 250 ms) within 7.5 s to test the resistance to fatigue during isometric contractions. Immediately after the last contraction, the muscle was freeze clamped, weighted, and stored in liquid nitrogen until further analysis.

All force signals of the muscle were digitized (1,000 Hz) and analyzed for peak force, maximal rate of force rise (RFR_{max}), and half-time of relaxation (HRT) (time for force to fall from one-half to one-fourth at the end of stimulation). Because force signals were hardly fused at a stimulation frequency of 60 Hz, the force of the first pulse at this stimulation frequency was used to estimate twitch force.

In vivo 1H and ^{31}P magnetic resonance spectroscopy (MRS) of brain and skeletal muscle

The MR experiments have been described in detail elsewhere and are briefly summarized here. During the *in vivo* magnetic resonance (MR) experiments, all animals were anesthetized using 1.2% isoflurane in a gas mixture of 50% O_2 and 50% N_2O delivered through a facemask. Breathing frequency was monitored and a warm waterbed (37°C) was used to keep

Materials and methods

the animals at body temperature. *In vivo* MR was performed on a 7.0 T horizontal bore magnet. Metabolic profiles of brain and hind leg were assessed *in vivo* both by ^1H and ^{31}P MRS. For the ^1H MR studies on the mouse brain, localized spectroscopy was performed of a $3\times 3\times 3\text{ mm}^3$ (27 μl) voxel using a STEAM sequence (TE=10 ms, TM=15 ms) in 10 $\text{GAMT}^{-/-}$ and seven control animals. The voxel was positioned in the center of the brain guided by gradient echo MR images. Phosphorous compounds were measured in the brain of seven $\text{GAMT}^{-/-}$ and seven control animals. Two ^{31}P surface coils working in quadrature mode were used together with an ISIS pulse sequence to measure a spectrum from an image-guided voxel of $6.5\times 6.5\times 4.5\text{ mm}^3$ (volume 190 μl).

Proton measurements on the mouse hind leg were done using an Alderman–Grant type of coil. The STEAM sequence used was the same as that employed for ^1H brain measurements (voxel size $1.8\times 1.8\times 3.4\text{ mm}^3$). Seven $\text{GAMT}^{-/-}$ and seven control animals were measured. ^{31}P spectra of the hind leg were obtained by a pulse acquire experiment in seven $\text{GAMT}^{-/-}$ animals and seven control animals.

Three groups of $\text{GAMT}^{-/-}$ animals were supplemented with 2 g (kg body weight) $^{-1}$ day $^{-1}$ Cr monohydrate (Sigma C0780) dissolved in the drinking water. Saccharose (1.6 g (kg body weight) $^{-1}$ day $^{-1}$) was added to the drinking water of the supplemented animals to mask the bitter taste of the Cr monohydrate. One group ($n = 4$, 3 females, 1 male) was supplemented for 1 day (24 h), the second group ($n = 6$, 5 females, 1 male) was supplemented for 2 days (48 h) and finally a third group ($n = 4$, 3 females, 1 male) was supplemented for 1 month. In the group that was supplemented for 48 h ischaemia measurements were carried out as described in (155).

In Vivo Hemodynamics at Baseline and During Inotropic Stimulation

Measurements were made in closed-chest, spontaneously breathing mice (as described in Nemoto et al). $\text{GAMT}^{-/-}$ and WT littermates ($n=12$; 5 males, 7 females in each group) were anesthetized with 2% isoflurane in oxygen on a homeothermic blanket. A 1.4F microtipped conductance cannula (SPR-839, Millar Instruments) was advanced retrogradely into the LV via the right carotid artery under echocardiographic guidance. The right jugular vein was cannulated with stretched polythene tubing for infusion of dobutamine. Preload conditions were altered by occlusion of the inferior vena cava. A small incision was made in the abdominal wall at the level of the xiphisternum, and a cotton swab was used to apply transient compression. Isoflurane was reduced to 1.25% to 1.5%, followed by equilibration until hemodynamic indices were stable for >15 minutes. Measurements were taken under steady state and inferior vena cava occlusion, at baseline and during infusion of low- and high-dose dobutamine (4 and 16 ng/g body wt per minute). Recordings were analyzed with the use of PVAN software version 3.0 (Millar Instruments). The cannula was calibrated to relative volume units with a cuvette system, and parallel conductance was measured by saline bolus method. No correction for the electrical field inhomogeneity (α) was made; therefore, the only occlusion parameter reported is preload recruitable stroke work (PRSW) because this is α and chamber size independent. Systolic and diastolic blood pressures were measured invasively in separate groups of anesthetized mice ($n=4$ WT; $n=5$ $\text{GAMT}^{-/-}$).

2.12 Perfused Heart Experiments

Male mice were heparinized (5000 U/kg body wt) and anesthetized (pentobarbitone 140 mg/kg body wt IP). Hearts were excised, cannulated, and perfused in Langendorff mode at 80 mm Hg and 37°C with Krebs-Henseleit buffer gassed with 95% O_2 /5% CO_2 (pH 7.4)

Materials and methods

containing the following (in mmol/L): 149 Na⁺, 5.9 K⁺, 1.2 Mg²⁺, 2.25 Ca²⁺, 1.2 SO₄²⁻, 126.2 Cl⁻, 0.5 EDTA²⁻, 25 HCO₃⁻, 1.2 H₂PO₄⁻, 11 D-glucose, 4.5 pyruvate, and 0.5 lactate. Contractility was assessed with a fluid-filled intraventricular balloon connected to a pressure transducer (AD Instruments Ltd). The end-diastolic pressure (EDP) was set to 5 to 15 mm Hg.

2.13 Cardiac 31P-MRS

Five-minute ³¹P-nuclear MR spectra of perfused mouse hearts were acquired on a Bruker Avance 500 spectrometer equipped with a 11.7-T magnet and a 20-mm ¹H-/³¹P-cross-cage resonator with a pulse-and-collect sequence (repetition time=100 ms, α=29°, number of scans=3000) and corrected for partial saturation. Metabolites were quantified with respect to the signal intensity of a known amount of phenylphosphonic acid in the intraventricular balloon with the use of the AMARES algorithm and MRUI software. Baseline concentrations were calculated with the use of 20-minute spectra. Baseline [Pi] was too low for quantification, and therefore [Pi] is only shown from ischemia onward. Intracellular volume was assumed to be 0.5 mL/g wet wt. pH_i was determined from the chemical shift between Pi and PCr with the use of $\text{pH} = 6.72 - \log(\delta - 5.72) / (3.17 - \delta)$. In the absence of PCr, phenylphosphonic acid (18 ppm) was used as a frequency reference. GAMT^{-/-} mice show an additional resonance at -0.5 ppm, which previously has been assigned to P-GAA' as also described in a human patient with GAMT deficiency. In addition, this resonance has been shown to appear to the right of PCr in ³¹P-MR spectra of porcine coronary arteries perfused with GA. Finally, we detected GA in cardiac tissue from GAMT^{-/-} mice with high-performance liquid chromatography (data not shown). Altogether this demonstrates that the resonance at -0.5 ppm originates from P-GAA.

2.14 Isolated Heart Protocols

To test utilization of P-GAA in the CK reaction during increased workload, hearts (n=5 per group) were perfused for 20 minutes with the β-agonist isoproterenol (20 nmol/L) in the buffer. ³¹P-spectra from the last 10 minutes were used to quantify PCr/P-GAA. Susceptibility to ischemia/reperfusion was tested in other hearts (n=5 WT, n=4 GAMT^{-/-}) subjected to 10 minutes of total, global, and normothermic ischemia, followed by 30 minutes of reperfusion.

2.15 Biochemical and molecular measurements

Total creatine kinase and citrate synthase activities were determined by spectrophotometry as previously described. To measure relative quantities of atrial natriuretic factor (ANF) and β-myosin heavy chain (MHC) mRNA, total RNA was extracted from frozen LV heart tissue (n=8 per group) with the use of the RNeasy Kit (Qiagen), involving treatment with proteinase K and DNase I and used in real time-polymerase chain reaction (Qiagen Quantitect SYBR Green RTPCR kit, Qiagen) with the use of previously described primers for ANF and β-MHC and the Rotor-Gene system (Corbett Research Ltd). Results were normalized to the expression levels of the housekeeping gene MLN51 and related to 100% in WT mice.

2.16 Animal groups and care

If not otherwise stated, the control group (control) consisted of wild-type (GAMT^{+/+}) and heterozygous (GAMT^{+/-}) littermates. The knockout group consisted of homozygous GAMT-deficient mice (GAMT^{-/-}). The same applies for AGAT animals.

Materials and methods

Mixed genotype groups of not more than five animals were housed in standard mouse cages under conventional laboratory conditions (12/12 h dark–light cycle, constant temperature, constant humidity, and food and water *ad libitum*). According to the manufacturer, the food did not contain animal ingredients (rodent maintenance chow R/M-H; ssniff, Soest, Germany) and should therefore be free of creatine. Our own analysis of random food samples showed only trace amounts of creatine close to the detection limit. Generation, care and use of the animals were in accordance with institutional guidelines. All experimental procedures were in accordance with the German Law for the Protection of Experimental Animals and complied with the regulations of the National Institutes of Health and those of the Society for Neuroscience (USA). In addition, all experiments were approved by the respective local animal ethics committees.

2.17 Statistical Analysis

Statistical significance was assessed by ANOVA or Student *t* test where appropriate. Data are mean±SD or mean±SEM. Differences were considered significant at $P<0.05$.

3 GAMT knockout model generation and phenotyping

3.1 Generation of GAMT deficient mice

A 129Sv lambda phage genomic library was screened by classic filter hybridization with a cDNA probe. A targeting construct was engineered by subcloning a neomycin selection cassette in exon one frameshifting the translation and creating a premature stop codon. The endogenous transcription of the GAMT gen is therefore expected to stop within the polyadenylation signal present in the neomycin cassette, thus creating a hypomorphic allele. The targeting proved to be successful at the genomic, RNA and protein levels as shown by Southern, Northern and Western blot analysis (135, Fig.12).

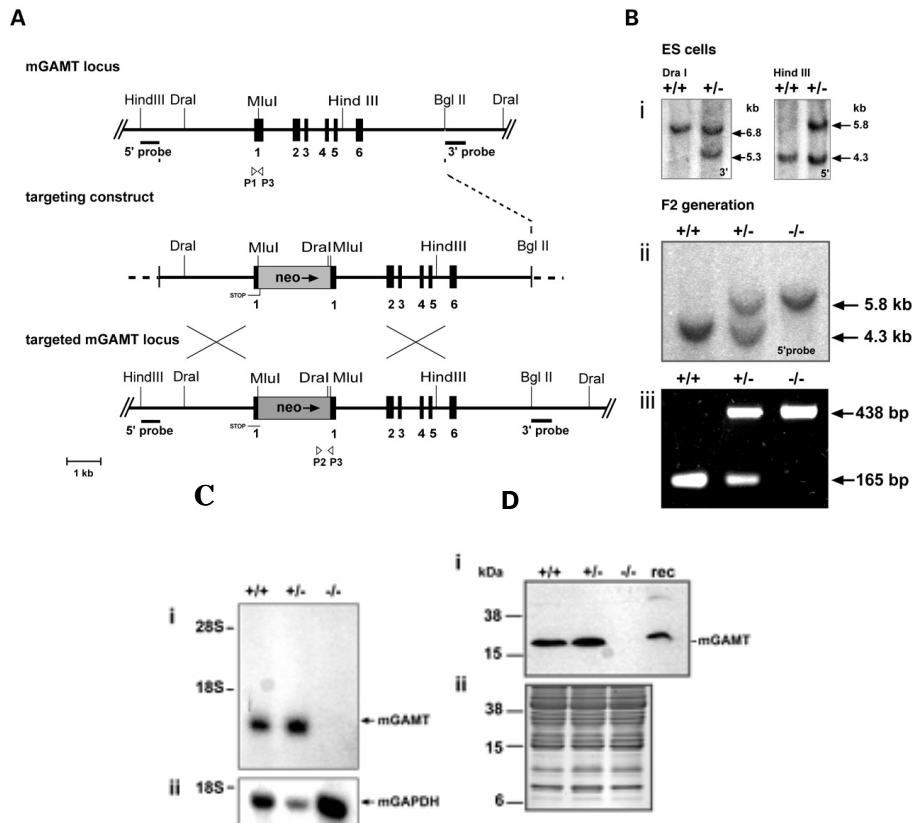
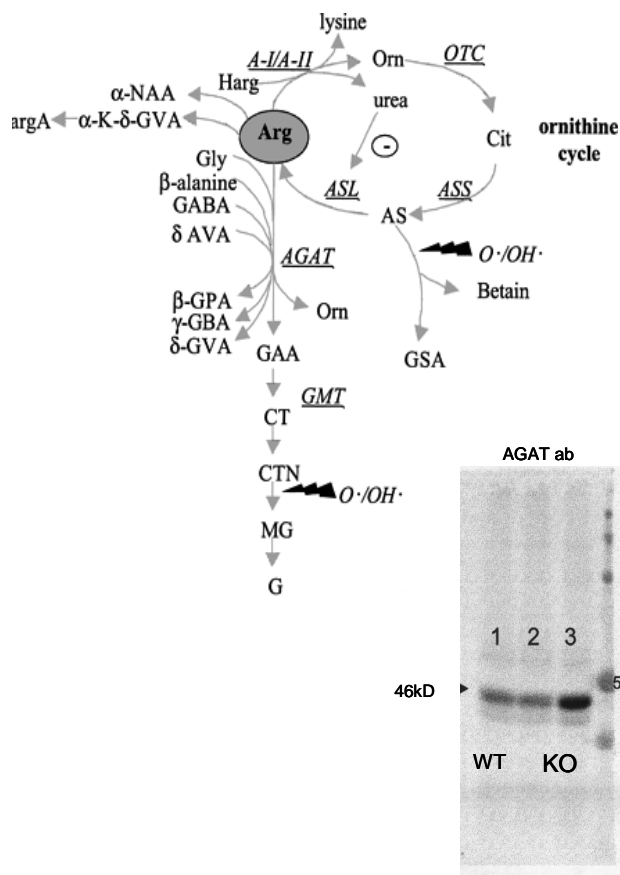


Figure 12: Targeting of the mGAMT gene locus by homologous recombination in ES cells. (A) Schematic representation of mGAMT gene locus (top), targeting vector (middle) and mGAMT gene locus after the homologous recombination event (bottom). Lines below top and bottom panels give the locations of 5' and 3' external probes used for Southern blot genotyping. PCR primer sites are indicated with open arrows. (B) Southern blots of *DraI* or *HindIII*-digested genomic DNA were performed to detect homologous recombination at the mGAMT gene locus in ES cells (Bi) and the presence of knockout alleles in mice (Bii). Blots were hybridized with (α - 32 P)-labeled 5' and 3' external DNA probes homologous to sequences outside the genomic fragment present in the targeting construct. The knockout allele caused distinct 1.5-kb size shifts of the respective restriction fragment (Bi, left) and an increase for the *HindIII* digest (Bi, right and ii). PCR analyses with internal primers P1, P2 and P3 (see A) were used for genotyping of genomic DNA isolated from mouse ear biopsies (Biii). (C) Northern blot containing total liver RNA with the genotypes indicated at the top of each lane was hybridized with an (α - 32 P)-labelled cDNA probe. (ii) After the detection of mGAMT-specific RNA, the northern blot was hybridized with an (α - 32 P)-labelled cDNA probe for mouse GAPDH. Size markers on the left indicate 28S and 18S RNAs. (D) (i) Western blot with liver lysates was probed with affinity-purified polyclonal anti-mGAMT antibodies. (ii) Coomassie blue-stained SDS polyacrylamide gel loaded with 20 μ g of the same liver homogenates used for the western blot in (Bi). Adapted from (135).

GAMT knockout model generation and phenotyping

3.2 Biochemical abnormalities

GAMT^{-/-} animals had biochemical abnormalities comparable to those found in GAMT patients: Cr was decreased 14 to 122 fold and Crn levels were reduced 7 to 27 fold in blood, CSF and urine (135). GAA accumulation was also detectable in urine, plasma and CSF as 10, 53 and 142 fold increases. In addition, other guanidino compounds were increased in brain and muscle (136, Fig.13). Brain showed 10 fold increased concentrations of GSA, β-GPA, GBA, 2 fold increase in ArgA and a tendency to increased homoarginine, whereas muscle presented a 10 fold accumulation of GBA, increased homoarginine and a tendency to hyperargininemia. Western blots of GAMT^{-/-} kidney tissue showed that AGAT was upregulated in this tissue (Fig.13). GAMT patients consistently had increased homoarginine levels in blood (137) although this was not observed in GAMT^{-/-} mice.



Concentrations of guanidino compounds in brain of GAMT wild type (WT), heterozygous (HZ) and knockout (KO) mice

Brain (nmol/g tiss.)	Mice		
Compound	WT (n=5)	HZ (n=7)	KO (n=11)
α-keto-δ-GVA	0.80±0.08	0.60±0.08	0.73±0.05
GSA	0.17±0.02	0.22±0.03	2.36±0.19***
CT	11,277±422	10,336±465	466±86***
GAA	12.2±1.3	12.8±1.02	1852±61***
α-N-AA	0.86±0.14	1.30±0.11	1.14±0.14
ArgA	2.10±0.25	2.33±0.20	4.47±0.19***
β-GPA	0.15±0.03	0.21±0.03	1.05±0.08***
CTN	323±48	246±38	<DL-2.0.2°
γ-GBA	1.59±0.12	1.73±0.07	11.2±0.84***
Arg	174±6.4	219±51	174±9.31
Harg	<DL-0.69	<DL-1.04	<DL-2.18°
G	2.24±0.12	6.14±2.95	5.03±1.07
MG	1.16±0.34	<DL-1.51	<DL-0.41

Concentrations of guanidino compounds in muscle of GAMT wild type (WT), heterozygous (HZ) and knockout (KO) mice

Muscle (nmol/g tiss.)	Mice		
Compound	WT (n=4)	HZ (n=6)	KO (n=6)
α-keto-δ-GVA	<DL	<DL	<DL-0.496
GSA	<DL	<DL	<DL
CT	16,508±278	18,788±2157	1501±301***
GAA	1.88±0.43	4.47±1.0	14,450±2088***
α-N-AA	<DL	<DL	<DL
ArgA	<DL	<DL-0.95	<DL-0.541
β-GPA	<DL-0.4	<DL-0.6	22±4.3°
CTN	176±20	331±94	<DL°
γ-GBA	0.53±0.11	0.54±0.11	17±3.3***
Arg	121±25	265±115	623±162 _{BS}
Harg	<DL-0.711	<DL-1.13	4.0±0.8°
G	3.31±0.84	3.42±0.79	3.0±0.89
MG	<DL	<DL	<DL

Figure 13: Guanidino compounds (GCs) concentration in brain and muscle of WT, HZ and KO mice are presented as mean±S.E.M. Harg, homoarginine; ArgA, argininic acid; GAA, guanidinoacetic acid; CT, creatine; CTN, creatinine; MG, methylguanidine; G, guanidine; GABA, -aminobutyric acid; AVA, -aminovaleric acid; -GBA, -guanidinobutyric acid; β-GPA, β-guanidinopropionic acid; -GVA, -guanidinovaleric acid; -K--GVA, -keto--guanidinovaleric acid; GSA, guanidinosuccinic acid; -NAA, -N-acetylarginine. In addition to the biochemical proof for AGAT upregulation, Western blots of kidney homogenates also evidenced that AGAT was upregulated at the protein level. The so-called ornithine cycle illustrates the origin of the guanidino compounds. AGAT has broad substrate specificity and is able to transfer the guanidino group to different acceptors such as β-alanine, GABA and aminovaleric acid. Guanidinosuccinic acid, increased 10-fold in GAMT^{-/-} brain, and guanidine are form by free radical assault of arginiosuccinate and creatinine, respectively. *P<0.05; ***P<0.001 (adapted from 136).

3.3 Physiological abnormalities

3.3.1 Behavioral abnormalities

GAMT^{-/-} mice had no neurological symptoms such as ataxia or seizures, but showed differences in performance of hippocampal dependent memory tasks such as Morris water maze (MWM). Although mutant and control animals learned equally well during learning trials, the percent of time spent in each quadrant during probe trials revealed that GAMT^{-/-} mice experienced impaired retrieval of learned information, as the latency time in each quadrant was not above chance (25% is the statistical probability expected for the animals to spend in each quadrant by chance; Fig.14C). GAMT^{-/-} mice also exhibited a significantly different search pattern and swimming velocity. Open field exploration showed that GAMT^{-/-} mice entered less often the corners of the arena (136, Fig.14).

GAMT^{-/-} mice did not score abnormally in passive avoidance test indicating that not all forms of learning and memory are affected, nor showed abnormalities in activity, exploration or neuromotor assessments performed by rotarod, activity, social exploration, dark-light transition or open field exploration tests. Thus GAMT^{-/-} mice showed a mild cognitive defect. Importantly, GAMT^{-/-} mice practice coprophagia and thus ingest modest amounts of Cr when animals from different genotypes are housed together (135), and the behavioural analyses were performed in mice housed in mixed genotypes. Thus, the neurological phenotype is expected to be more pronounced in coprophagia-free animals.

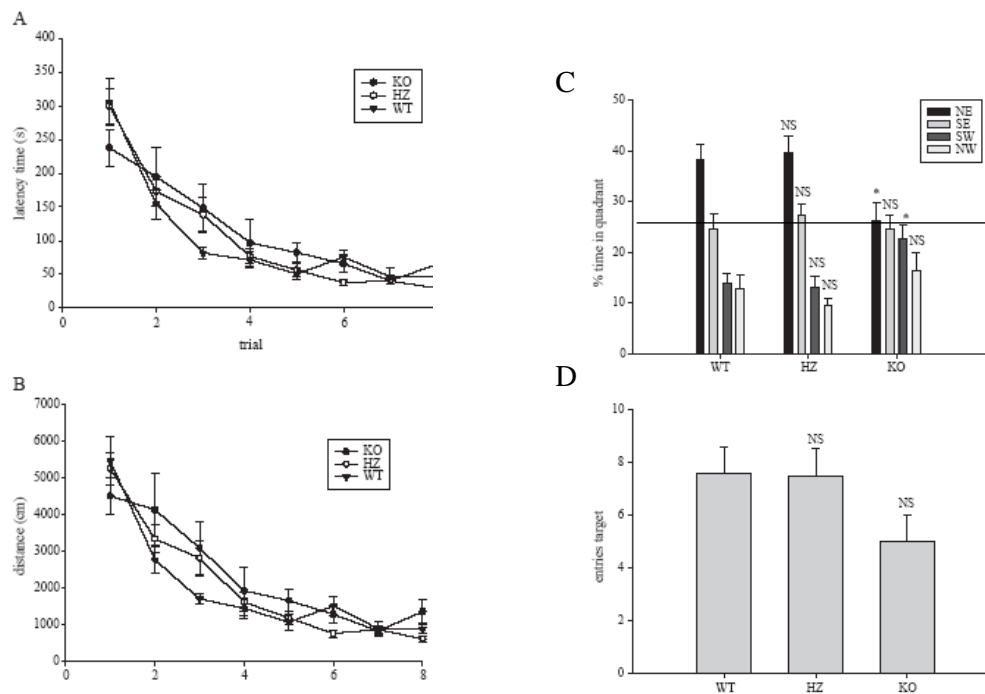


Figure 14: (A) Latency time of GAMT wild type (WT), heterozygous (HZ) and knockout (KO) mice during acquisition trial blocks in the MWM test. (B) Path length of GAMT WT, HZ and KO mice during acquisition trial blocks in the MWM test. Each data point represents mean (\pm S.E.M.) of summed results of four daily trials. (C) % time spent in each quadrant (northeast (NE), southeast (SE), southwest (SW), northwest (NW)) during probe trial by GAMT wild type (WT), heterozygous (HZ) and knock out (KO) mice. (D) Entries of GAMT WT, HZ and KO mice in target quadrant (NE) during probe trial. Presented as mean \pm S.E.M.; asterisks indicate significance of difference with WT group (Student's *t*-test: * p <0.05); when no significant difference with WT group was observed, this was indicated as NS (not significant). The line drawn on (C) indicates the % time expected to be spent in a given quadrant by chance (25%) (adapted from 136).

GAMT knockout model generation and phenotyping

3.3.2 Skeletal muscle

GAMT^{-/-} muscle tissue and performance has been analysed in great detail by Kan HE et al (153,154). GAMT^{-/-} mice displayed signs of hypotonia when lifted by tail. Also maximum grip force showed muscular weakness. Although no cytoarchitectural abnormalities were found under EM microscopy (135, Fig.15), a subsequent re-examination of coprophagia-free GAMT^{-/-} mice detected cytoarchitectural abnormalities (see Fig.34)

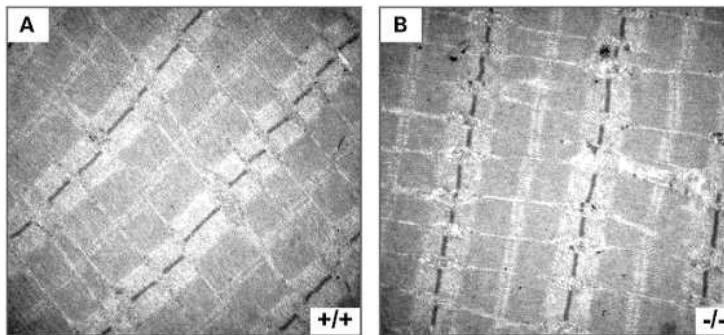


Figure 15: Electron microscopy of skeletal muscle sections from control and GAMT^{-/-} mice. Electron micrographs of longitudinal sections from gastrocnemius muscle from a control (A) or a GAMT-deficient (B) mouse. Magnification: 12 000x (adapted from 135).

Detailed analysis of muscle performance uncovered unique abnormalities differing from the muscle phenotype previously reported in CK isoenzyme knockout models. During single contractions of intact muscles, twitch force and absolute force at all studied stimulation frequencies were significantly lower than controls (Fig.16); this phenotype was not observed in mice lacking one or two CK isoenzymes (101). The fatigue protocol, both dynamically and isometrically, showed that GAMT^{-/-} animals had a reduced capacity to maintain force during high-intensity exercise (Fig.17), an effect shared with some of the CK isoenzyme knockout models and guanidinopropionate fed animals (101). Cr supplementation for two days resulted in an increased total muscle Cr content and alleviated some of the consequences of GAMT deficiency: twitch-force production returned to normal levels and fatigue resistance protocols showed a normalization to wild type controls (153, Fig.18).

It was the first time that those parameters were measured in the virtual absence of Cr/PCr, because CK isoenzyme knockout models still contained Cr/PCr in their muscles (103). Although it was assumed from a previous study that GAA is being used as a high energy compound and thus partially rescue PCr functions (see 3.1.4), the data clearly demonstrated the relevance of high-energy compounds in muscle performance. It is still arguable that GAA accumulation-related abnormalities mediate the phenotype.

GAMT knockout model generation and phenotyping

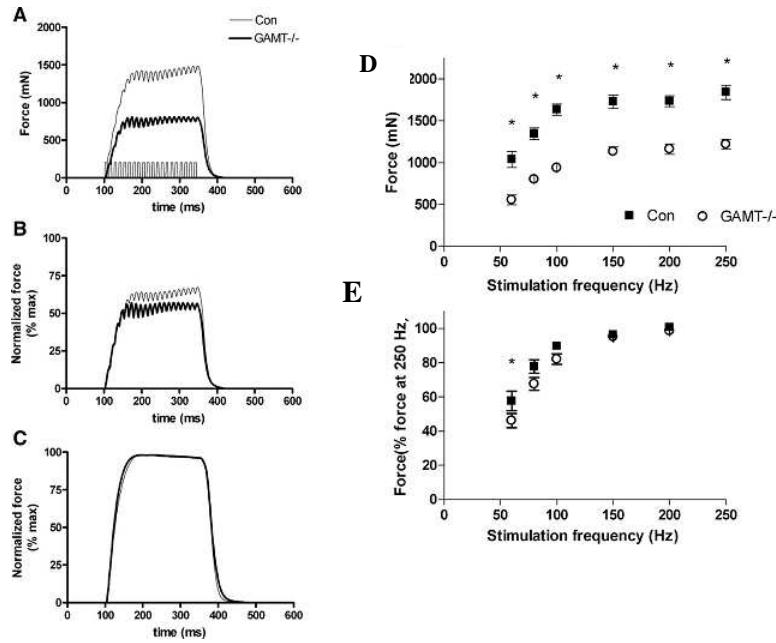


Figure 16: Typical example traces from digitized force signals of medial gastrocnemius muscle of control (Con) and $GAMT^{-/-}$ mice. Signals from Con and $GAMT^{-/-}$ are shown as absolute values (A) and normalized to the force of the same muscle at 250 Hz (B and C). Force traces shown are single contractions at 80 Hz (A and B) and 200 Hz (C). In A, stimulation pulses are shown with arbitrary height for clarity. Influence of stimulation frequency on force characteristics of Con and $GAMT^{-/-}$ medial gastrocnemius muscles. Force in Con and $GAMT^{-/-}$ ($n = 10$ in both groups) is expressed in absolute values (D) and normalized to the force at maximal stimulation frequency (E). Data are shown as means \pm SE. * $P < 0.05$, significant difference between Con and $GAMT^{-/-}$ mice (adapted from 153).

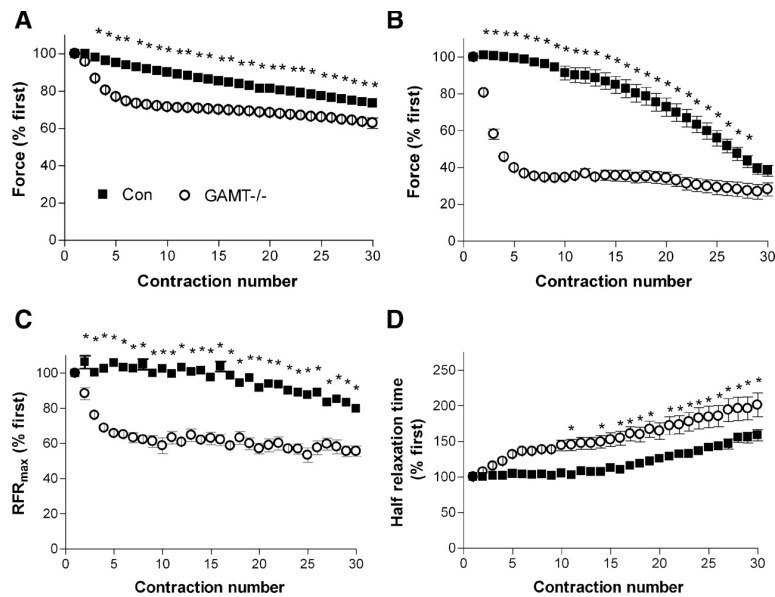


Figure 17: Force characteristics during the isometric and dynamic high-intensity stimulation protocol. Changes in relative force in Con and $GAMT^{-/-}$ during the isometric protocol (A) ($n = 10$ in both groups) and the dynamic protocol (B) ($n = 9$ in both groups). Maximal rate of force rise (RFR_{max}) (C) and relaxation rate (D) during the isometric protocol are shown. Data are shown as means \pm SE. * $P < 0.05$ indicates a significant difference between Con and $GAMT^{-/-}$ mice (adapted from 154).

GAMT knockout model generation and phenotyping

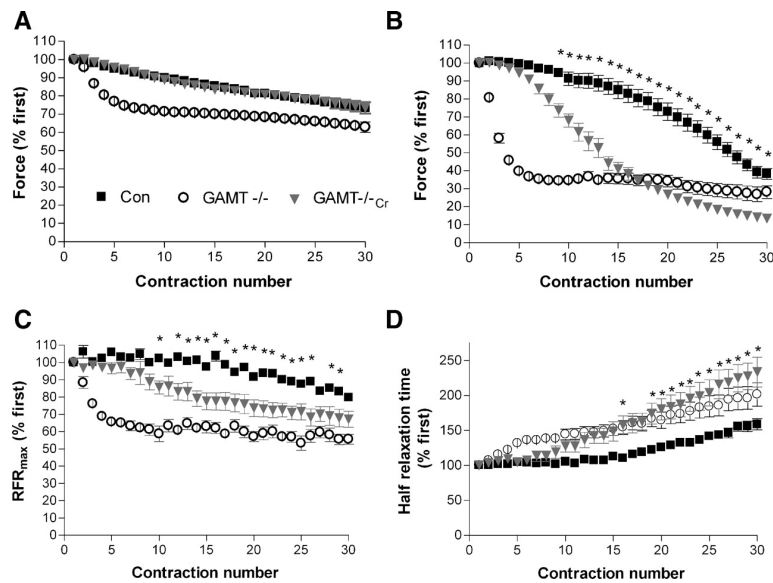


Figure 18: Creatine (Cr) supplementation for 2 days resulted in several changes in force characteristics of $GAMT^{-/-}$ mice. Characteristics are shown for Con, $GAMT^{-/-}$, and $GAMT^{-/-}_{Cr}$. During 30 repeated isometric contractions ($n = 10$, for $GAMT^{-/-}$ and Con, $n = 6$, for $GAMT^{-/-}_{Cr}$) force in $GAMT^{-/-}_{Cr}$ resembles Con behaviour (A), but this is not the case for the rate of force rise (C) and half-relaxation time (D). Finally, during 30 dynamic contractions (B); $n = 9$, for $GAMT^{-/-}$ and Con, $n = 5$ for $GAMT^{-/-}_{Cr}$), $GAMT^{-/-}$ mice with Cr supplementation displayed behaviour different from Con and $GAMT^{-/-}$ mice. Data are shown as means \pm SE, and $*P < 0.05$ indicates a significant difference between Con and $GAMT^{-/-}_{Cr}$ mice (adapted from 154).

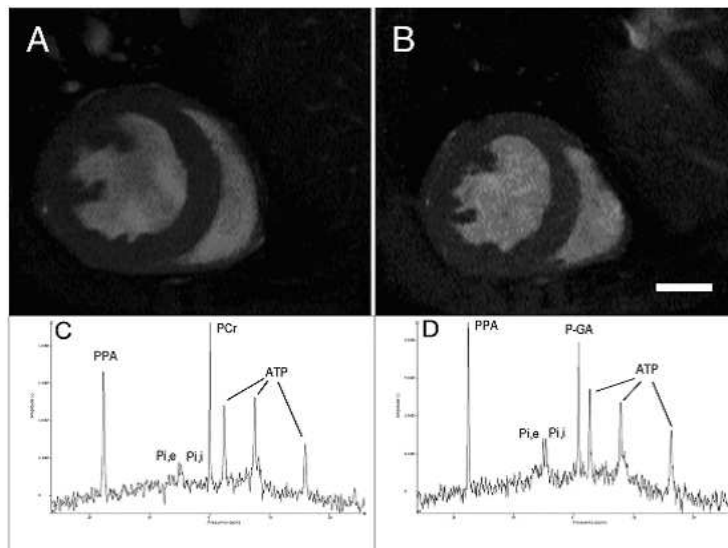


Figure 19: In vivo end-diastolic MR images from a WT (A) and a $GAMT^{-/-}$ (B) mouse. Bar=2 mm (applies to both panels). Note that the $GAMT^{-/-}$ heart is smaller. Typical ^{31}P -spectra of a heart from a WT (C) and a $GAMT^{-/-}$ (D) mouse. In WT hearts, PCr and 3 peaks for ATP are visible. In $GAMT^{-/-}$ hearts, ATP is visible, but no PCr could be detected. Instead, P-GAA appears at -0.5 ppm. In both spectra the phenylphosphonic acid (PPA) resonance originates from a PPA solution inside the intraventricular balloon (adapted from 143).

GAMT knockout model generation and phenotyping

3.3.3 Cardiac muscle

GAMT^{-/-} cardiac muscle has been analyzed in great detail by Ten Hove et al. (143). GAMT^{-/-} hearts showed profoundly altered cardiac energetics having undetectable myocardial PCr signals and P-GAA accumulation revealed by MRS (Fig19). Nevertheless, GAMT^{-/-} hearts did not display cardiac hypertrophy: neither myocyte cross-sectional areas nor classic markers for hypertrophy were abnormal. Also, hemodynamics for both systolic and diastolic function were unaffected as measured either invasively (left ventricular conductance catheter) or non-invasively (magnetic resonance imaging (MRI)) (143, Fig. 24).

However when GAMT^{-/-} hearts were acutely stressed by β -adrenergic ionotropic stimulation or ischemia/reperfusion they exhibited a markedly abnormal phenotype. During ionotropic stimulation with dobutamida, preload-recruitable stroke work (PRSW) failed to reach maximal levels of performance (Fig.20). Parallel ³¹P MRS measurement detected the usage of P-GAA as an energy storage compound in mutants. As mentioned before, this fact had been previously reported in MRS measurements performed in GAMT^{-/-} hindleg muscles and quantified to be kinetically lower than phosphorylation/dephosphorylation of Cr (103). Cardiac muscles are however richer in mitochondrial CK isoenzymes than muscle tissue, and cardiac mitochondrial CK isoenzymes have been reported not to phosphorylate GAA (171). It would be also interesting to address the kinetics of GAA phosphorylation in brain where the B-CK isoenzyme is the predominant form.

Ischemia/reperfusion practiced in isolated hearts by 10 minutes of total ischemia followed by 30 minutes of reperfusion showed that GAMT^{-/-} hearts recover partially to 36% of controls for systolic and diastolic function (143). Interestingly, Pi levels decreased rapidly in wildtype hearts during reperfusion but much more slowly in GAMT^{-/-} hearts, further indicating that P-GAA is not being as efficiently re-synthesized as PCr (143).

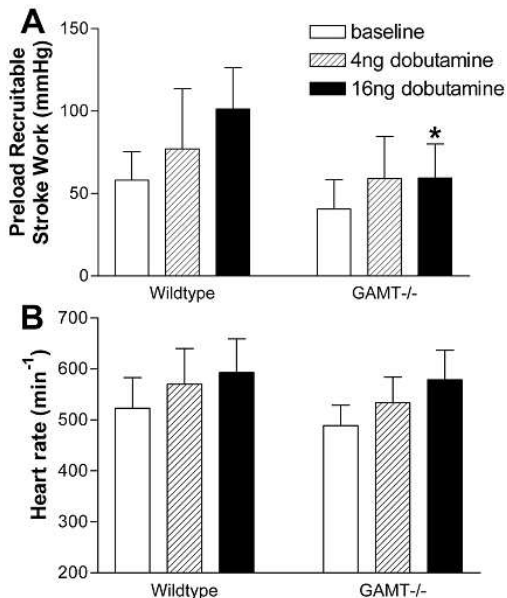


Figure 20: Reduced inotropic reserve in WT and GAMT^{-/-} mice. **(A)**, Preload recruitable stroke work (PRSW), a load-independent measurement of contractility, measured during inferior vena cava occlusion with an intraventricular conductance cannula in WT and GAMT^{-/-} mice. Measurements were taken at baseline and after infusion of 4 and 16 ng/g body wt per minute dobutamine. **P*=0.001 vs WT at same dose. **(B)**, Heart rate in the same mice immediately before inferior vena cava occlusion. Data are mean±SD (adapted from 143).

The data demonstrated that a fully functional CK/PCr system is not essential for cardiac function at low workloads but, when stressed by the mentioned means, hearts devoid of a properly functional CK/PCr/Cr system showed reduced inotropic reserve and aggravated injury after acute stress (143).

GAMT knockout model generation and phenotyping

3.3.4 Growth and body weight

The most obvious phenotype of $GAMT^{-/-}$ mice was a life-long reduction in body weight already apparent during the first weeks of life (Fig.21). The differences increased with age and were more pronounced in females than males. Importantly, length was not different between genotypes and thus the effect arose from smaller absolute mass of living tissues; nevertheless a 5% smaller tibial length was found suggesting a combination of growth retardation and lower body weight (143). Abdominal fat pads appeared reduced and whole-body chloroform extraction quantified that global fat content reached only 50% of controls (Fig.21 H).

Leptin, adiponectin and insulin levels were within normal ranges (Fig.22). It remains to be seen whether $GAMT^{-/-}$ mice display abnormalities in glucose homeostasis; that is, we do not yet know whether the mice display hyper or hypo-glycaemia or altered glucose tolerance. Since the pancreas is one of the main sites for Cr biosynthesis it might be anticipated that knockout of GAMT could affect glucose homeostasis as well. In this context GAA, and to a lower extent Arg and Cr, were seen to stimulate insulin secretion in the isolated perfused rat pancreas (144). The Cr/PCr system has been also implicated in the sensing of K_{ATP} channels to the intrinsic metabolic status of mitochondria, and the mechanism is particularly relevant in insulin secretion (143-148).

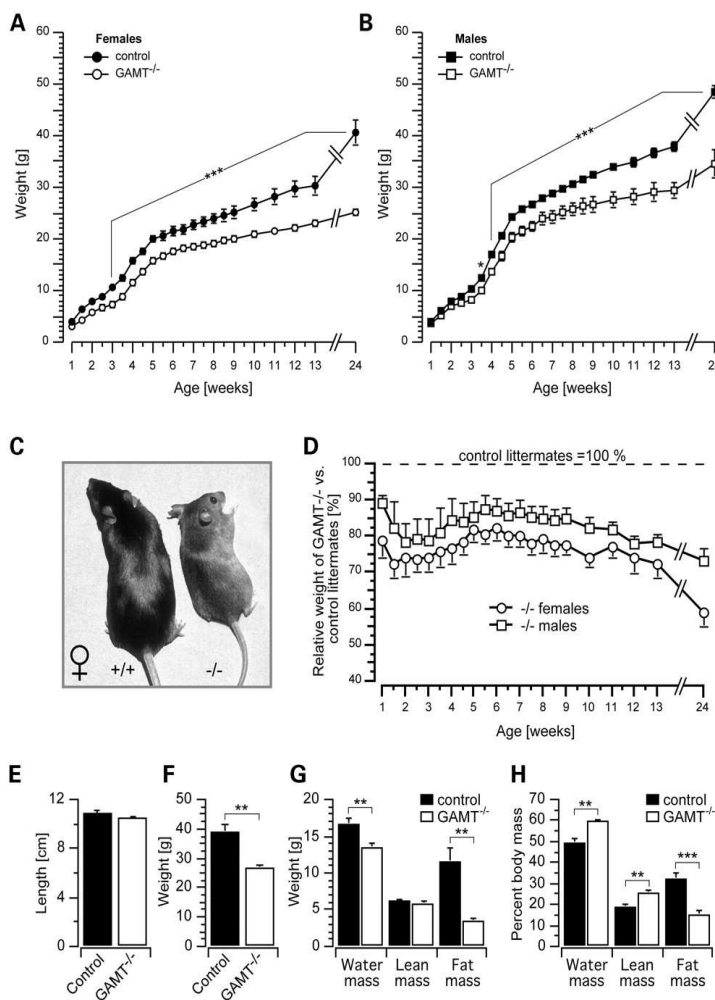


Figure 21: Reduced body weight and altered body composition in $GAMT^{-/-}$ mice. **(A)** Weight development of female control and $GAMT^{-/-}$ mice during a period of 6 months (control: $n=11$; $GAMT^{-/-}$: $n=11$). **(B)** Weight development of male control and $GAMT^{-/-}$ mice during a period of 6 months (control: $n=17$; $GAMT^{-/-}$: $n=14$). **(C)** Example of two female littermates housed together for 6 months in a mixed genotype group with *ad libitum* food supply. **(D)** Normalized weight development of female and male $GAMT^{-/-}$ mice. At each time point, the weight of $GAMT^{-/-}$ mice was normalized to the weight of control littermates of the same sex, which were housed in the same cage [numbers of mice as given in (A) and (B)]. Body length **(E)**, body weight **(F)** and absolute **(G)** or relative **(H)** quantification of body composition in female control and $GAMT^{-/-}$ mice (control: $n=10$; $GAMT^{-/-}$: $n=11$) aged 6–10 months. Significance levels: * $P<0.05$, ** $P<0.01$, *** $P<0.001$ (A, B: two-way repeated measurements ANOVA with Tukey's HSD post test; E–H: two-tailed heteroscedastic *t*-test). Absence of error bars indicates errors smaller than symbol size (adapted from 135)

GAMT knockout model generation and phenotyping

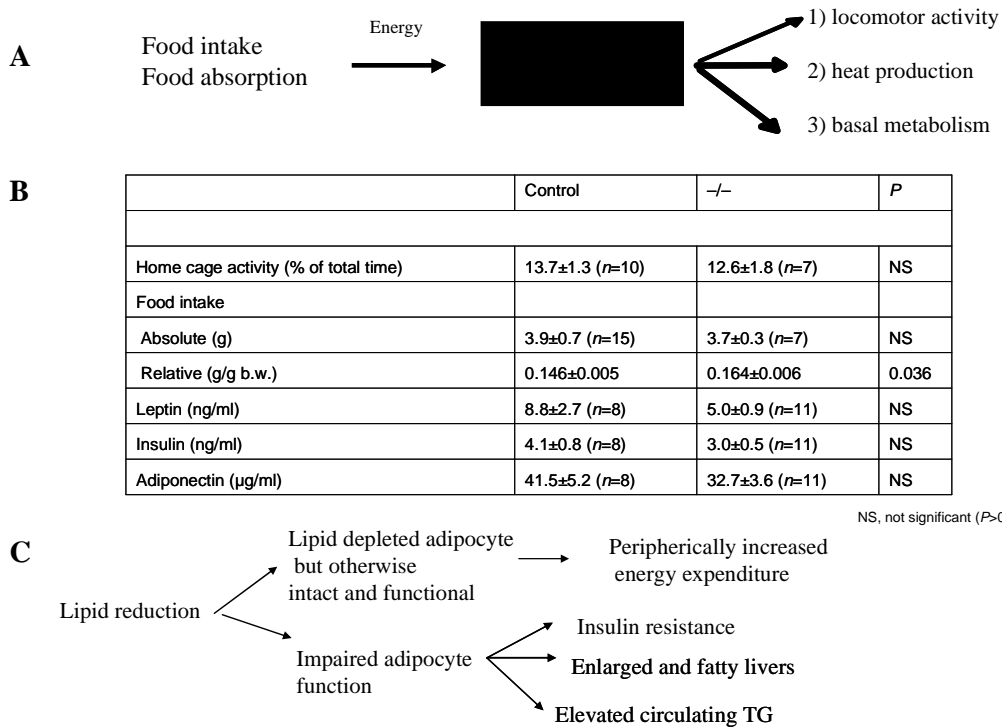


Figure 22: The metabolic phenotype of GAMT mice. (A) The black box indicates input and output of energy from an organism. As food intake and absorption, as well as locomotor activity were normal, increased heat production or increase basal metabolism remains as the two most likely hypotheses. (B) Cage activity, food assimilation and hormone levels of female GAMT^{-/-} and control mice. (C) Lower arrows follow the reasoning leading to the conclusion that adipose tissue function is not affected in GAMT mice, as insuline resistance, enlarged fatty livers or elevated circulating triglycerides (TG) are not seen in GAMT^{-/-} mice.

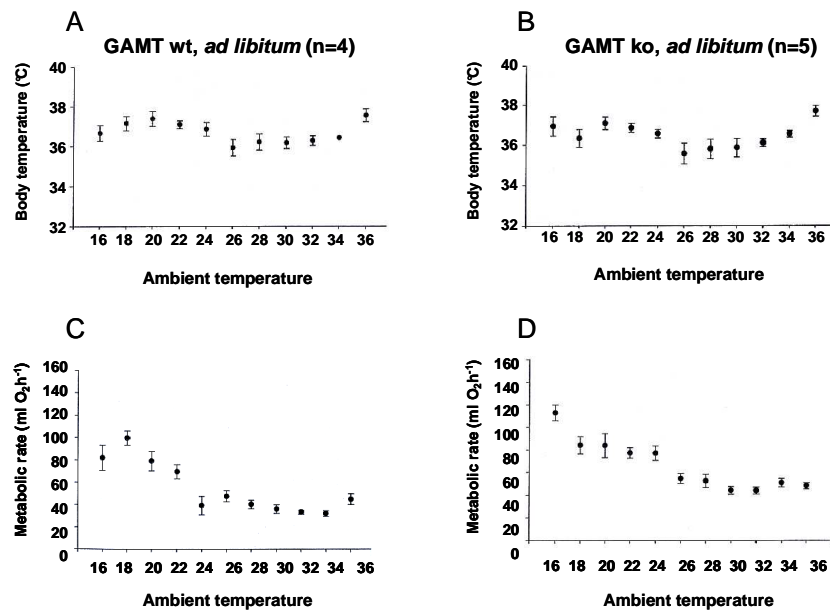


Figure 23: Body temperature (A) and (B) and metabolic rate (C) and (D) (measured as indirect O₂ consumption) at different environment temperatures (36 to 16 degrees). Note a sudden increase in oxigen consumption at 16 degrees while controls behaved conversely decreasing metabolic rates at the same temperature (data were generated by the German Mouse Clinic).

GAMT knockout model generation and phenotyping

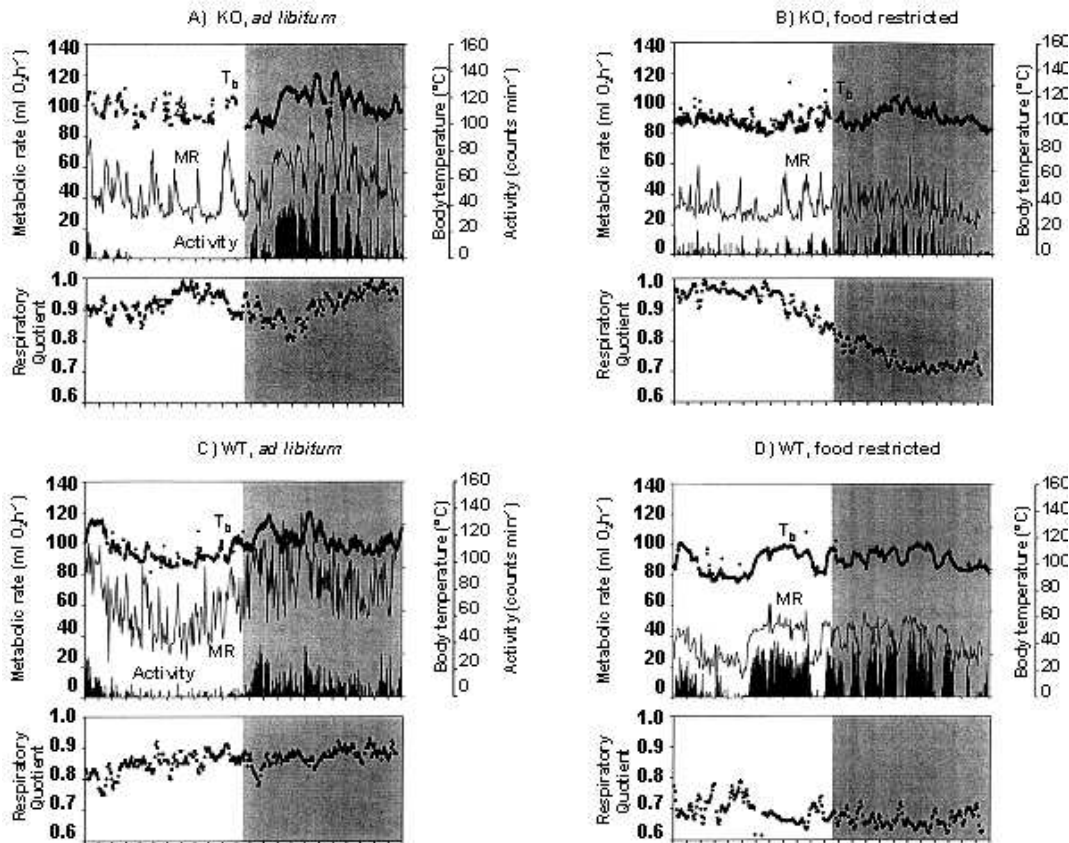


Figure 24: Respiratory quotient (RQ) under ad libitum and food restricted conditions during light/dark cycles. Body temperature and metabolic rate, as well as cage activity are also indicated. **A)** $GAMT^{-/-}$ ad libitum; **B)** $GAMT^{-/-}$ food restricted; **C)** WT ad libitum; **D)** WT food restricted. Note the differences in RQ under food restricted conditions of $GAMT^{-/-}$ mice (B), as the RQ is near 1, indicating higher carbohydrate burning and anaerobic metabolism, whereas RQ in the case of the controls is around 0.7 (D). (Data were generated by the German Mouse Clinic).

Locomotor activity revealed no differences between genotypes, and food intake was comparable as well as food intestine absorption (Fig.22). Indirect calorimetry as measured by O_2 consumption (149) revealed normal O_2 utilization, but higher metabolic activity when mutants were stressed at colder temperatures of 16 degrees was evident (Fig.23). This is an interesting observation considering that neonatal lethality of $GAMT^{-/-}$ littermates can be sometimes rescued by exposing the animals to red light; the data thus point to mild hypothermia perhaps due to unavailability of lipids to fuel endothermia. Increased O_2 consumption may also indicate hypoventilation-hypoxia under conditions of stressing metabolic demands such as cold exposure.

Nevertheless it can be preliminarily assumed that no signs of increased adaptive thermogenic or peripherally increased energy expenditure are involved in the reduced body weight of $GAMT^{-/-}$ mice. Thus no clues pointed to a decreased input (food intake-absorption) or increased output (locomotor activity, energy expenditure) of energy in the phenotype.

Respiratory quotient (RQ) ratio (VCO_2/VO_2), which indirectly evaluates metabolic fuel preference (fat vs. carbohydrates) (150,151) showed striking differences. When food restricted, $GAMT^{-/-}$ mice appeared to burn energy stores differently than controls (Fig.24). Mainly carbohydrates were used during both light and dark cycles, as the RQ was higher in mutants than controls. Higher RQ also indicates ongoing anaerobic metabolism. In agreement

GAMT knockout model generation and phenotyping

with this, glycogen stores were found reduced in a spatially restricted manner in livers of $GAMT^{-/-}$ mice, as shown by periodic acid schiff (PAS) staining (Fig.25). Periportal hepatocytes, mainly responsible for urea and glucose synthesis and expressing glutaminase, appeared particularly depleted of glycogen when compared to perivenous hepatocytes, expressing glutamine synthetase and responsible for ammonia delivery to the kidney in the form of glutamine (152). Liver-specific depletion of glycogen is also typical in anoxia and anaerobic metabolism (170). In addition, AGAT mRNA is elevated in heart failure and normalized after recovery (179), suggesting that the Cr biosynthesis pathway can be induced under ischemic conditions.

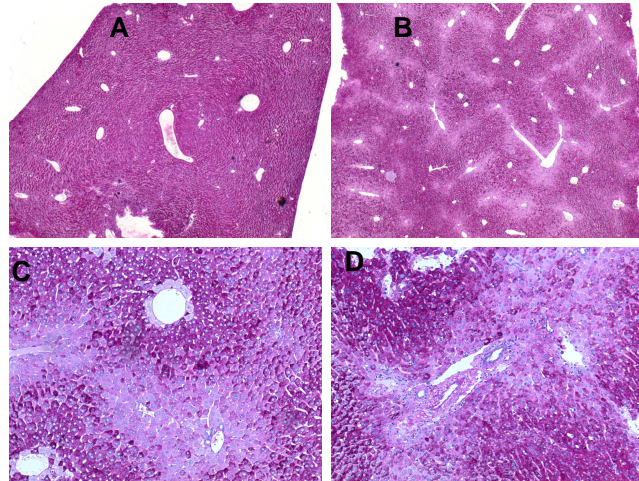


Figure 25: PAS staining of $GAMT^{-/-}$ and WT livers showed a decrease on glycogen stores spatially restricted to periportal hepatocytes. (A) WT liver (2.5X magnification) (B) $GAMT^{-/-}$ liver (2.5X magnification); (C) and (D) $GAMT^{-/-}$ livers detailed view (10X) of affected portal triads. The abnormalities were found in 3 out of 4 $GAMT^{-/-}$ animals investigated. Biochemically, periportal hepatocytes perform oxidative metabolism (TCA cycle and respiratory chain), glucose release (gluconeogenesis, glycogen synthesis from lactate, glycogen degradation to glucose), aminoacid and ammonia metabolism (amino acid uptake, amino acid conversion to glucose, amino acid deamination, glutamine deamination, ureagenesis from amino acid nitrogen and ureagenesis from gut ammonia), and lipid metabolism (fatty acid oxidation, cholesterol synthesis, bile formation, acetate conversion to acetyl-CoA). Perivenous hepatocytes on the other hand perform glucose uptake (glycolysis, glycogen synthesis from glucose, glycogen degradation to lactate), glutamine synthesis, and de novo lipogenesis, VLDL formation and secretion as well as acetate formation from acetyl-CoA.

3.3.5 Male and female fertility

In general, $GAMT^{-/-}$ mice were viable and required no specific precautions for survival and growth. However, analysis of $GAMT^{-/-}$ genotype frequency revealed an anomalously small number of $GAMT^{-/-}$ offspring ($GAMT^{+/+}$: 24.9%; $GAMT^{+/-}$: 60.6%; $GAMT^{-/-}$: 14.5%; $n=531$), presumably due to increased neonatal mortality. Also, when $GAMT^{-/-}$ male mice were prepared for breeding a decreased number of matings were successful, indicating a diminished male fertility.

3.3.5.1 Testicles

Semi-thin testicles sections (Fig.26) revealed that spermatogenesis was severely attenuated at the level of spermatid development: elongated spermatids were hardly present and mature spermatozoa were almost absent in the lumen of the seminiferous tubules, whose structure was highly unordered, showing a large number of resorption holes and a larger lumen. Multinucleated giant cells were frequently observed indicating increased phagocytic activity:

GAMT knockout model generation and phenotyping

their presence can be interpreted as a mechanism for removal of degenerated spermatids. Most likely, attenuation of the function of Sertoli cells in the seminiferous tubules interfered with maturation of spermatids, which only rarely reached the elongated stage or developed to mature spermatozoa.

The expression of GAMT transcripts is very high in Sertoli cells, and isolated cultures of this cell type synthesize GAA and Cr from Gly and Arg (138-140). In contrast, germ or interstitial cells do not express GAMT. Coupled with the high concentrations of Cr in seminal vesicles and seminal vesicle fluid and the fact that CrT is expressed in those cell types altogether support that Cr is transported from the blood in the seminal vesicles (141), a mechanism regulated by testosterone (142), while Cr is synthesized from GAA in Sertoli cells. The morphological abnormalities in $GAMT^{-/-}$ testicles further proved the role of Cr biosynthesis in sperm development and stressed the relevance of Cr biosynthesis in the nourishing of spermatozoa by Sertoli cells. The lack of Cr and/or GAA accumulation in seminal vesicles both might be responsible for the morphological alterations.

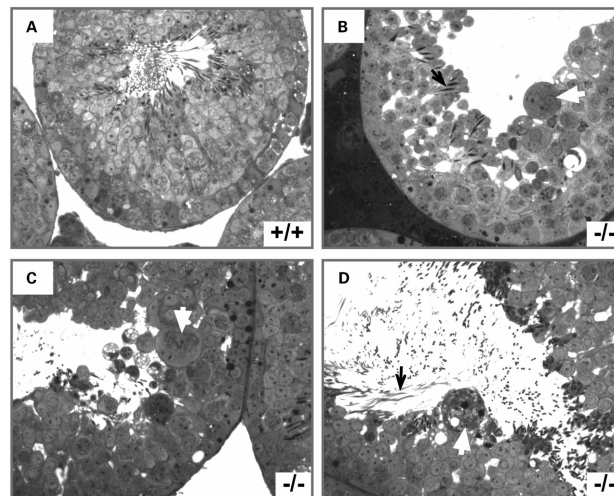


Figure 26: Reduced fertility in male $GAMT^{-/-}$ mice is associated with altered testis morphology. Representative illustrations of testis sections showing seminiferous tubules from control (A) and $GAMT^{-/-}$ mice (B–D). Spermatogenesis is severely affected in $GAMT$ -deficient mice, because elongated spermatids or spermatozoa are almost absent in large areas of the seminiferous tubules. In every section of the $GAMT^{-/-}$ testis tissue, several multinucleated giant cells were seen in seminiferous tubules (white arrows in B–D). In some regions, though, a few (B) or numerous elongated spermatids and spermatozoa (D) were observed (black arrows in B, D). Magnifications: A, B: 20x; C, D: 40x (adapted from 135).

3.3.5.2 Female fertility

A reduced number of successful matings was obtained when $GAMT^{-/-}$ females were prepared for breeding (6 successful matings out of 11; for comparison, 6 out of 6 matings were successful with $AGAT^{-/-}$ female mice) and decreased number of the littersizes was noted (87 mice were born from 11 matings of $GAMT^{-/-}$ females whereas 172 mice were born out of 6 matings with $AGAT^{-/-}$ females).

3. 4 MRS

In vivo proton 1H and phosphorous ^{31}P MRS spectroscopy is a non-invasive method instrumental in the diagnosis of CDS in humans because PCr signals in ^{31}P MR spectra are very prominent and their absence can not be overlooked; 1H spectra similarly displays a

GAMT knockout model generation and phenotyping

decreased Cr/PCr peak. Both have been applied to brain and muscles of $GAMT^{-/-}$ mice (153-156, Fig.27). The spectra presented with the characteristic PCr and Cr depletion as well as P-GAA accumulation found in human GAMT deficiency. The P-GAA signal, with much higher intensity in muscle than in brain, decreased when ischemia was applied to muscles and recovered after ischemia was released, indicating that P-GAA is being used by CK isoenzymes to phosphorylate ATP (153, 156); the flux between ATP and P-GAA was four times slower compared to ATP-PCr phosphorylation (0.034 ± 0.003 in mutants vs 0.117 ± 0.01 mM \cdot s in wild types (153).

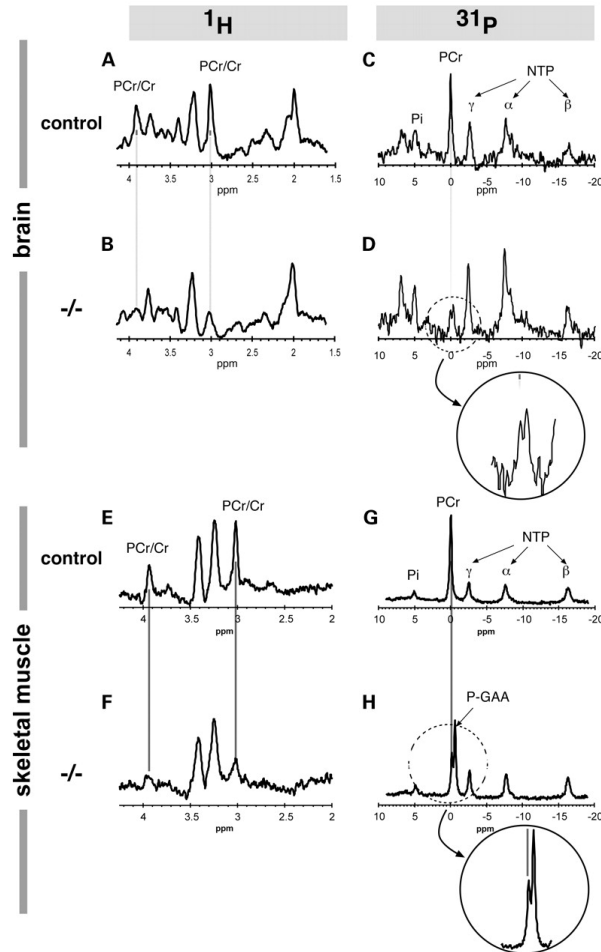


Figure 27: Localized *in vivo* ^1H and ^{31}P MRS in brain and skeletal muscle of $GAMT^{-/-}$ and control mice. Representative localized ^1H and ^{31}P MRS analyses of brain (A–D) and hindleg muscle (E–H) obtained from control or $GAMT^{-/-}$ mice. The left column shows localized ^1H MR spectra, whereas the right column shows localized ^{31}P MR spectra. Peak assignments: Pi, inorganic phosphate; Cr, creatine; PCr, creatine phosphate; P-GAA, guanidinoacetate phosphate. The resonances of nucleotide phosphates (e.g. ATP) are labeled with α , β and γ . Vertical scaling is arbitrary. The circles in (D) and (H) show a higher magnification of the double peak observed in knockout animals (adapted from 135).

In hindleg muscle relative inorganic phosphate (Pi) levels were increased before and after 25 minutes of ischemia, and the recovery rate of P-GAA after ischemia was decreased compared with that of PCr in wild-type mice, in all likelihood due to a reduced affinity of CK for P-GAA (153). Cr supplementation monitored during one month resulted in a rapid increase of Cr signal intensity in muscle until P-GAA signals disappeared, returning also Pi levels to normal values

4 AGAT Knockout model generation and phenotyping

4.1 Generation of AGAT deficient mice

The three AGAT patients reported so far carried a hemizygous non-sense mutation at amino acid tryptophan 149 leading to a stop codon (83). In order to disrupt the gene at a comparable site, we screened a 96-well formatted cosmid 129/Sv genomic library by PCR using oligonucleotides near exon 3, which encodes the respective amino acid tryptophan 149. A single cosmid genomic clone was isolated after two rounds of PCR and characterized by Southern blot (Fig.28) to contain exons 3-7 located in a clear 10kb band easy-to-purify from agarose gels, which was subcloned in pKO_scrambler 901(Fig.29). Two restriction sites singly present on the genomic subclone, *BsaAI* and *BstXI*, were used to engineer a targeting construct by subcloning a loxP sites flanked neomycin cassette, therefore removing splicing signals 3' downstream exon 3 and introducing a stop codon. Once the neomycin cassette was removed by backcrossing with Cre deleter mice (161), the endogenous translation of the AGAT mutant mRNA was expected to stop at exon 3, creating a frameshift mutation by lack of splicing signal to exon 4 (Fig.30).

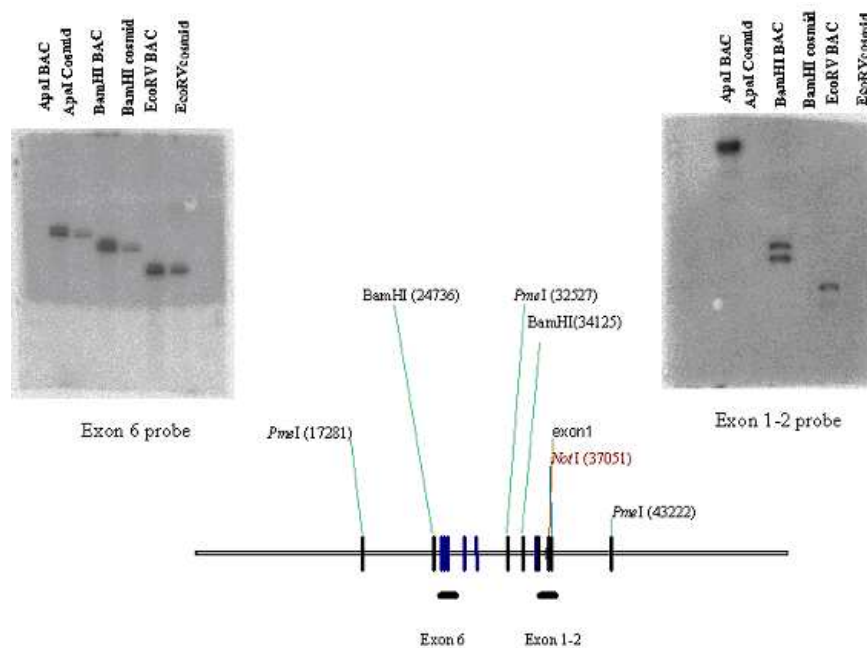


Figure 28: Mapping a cosmid genomic clone containing the AGAT genomic locus. *EcoRV*, *BamHI* and *ApaLI* digestions of a C57Bl/6 BAC, used as a control, and same digestions of the 129/Sv cosmid were blotted in two dimensions to obtain two replicas in nitrocellulose membranes. One of them was probed with a 300 bp probe containing exons 1 and 2, obtained with *BamHI-HincII* digestion and gel purification of AGAT cDNA, the second blot was probed with a smaller 200 bp probe containing exons 6-7 and 8, also retrieved by digestion of AGAT cDNA. As observed in the blots, the cosmid clone lacked the genomic region corresponding to exons 1-2, but contained and conserved the C57Bl/6 restriction sites arrangement. The 10kb *BamHI* band contains exon 3 and could be gel purified from *BamHI* digestions of the cosmid.

AGAT knockout model generation and phenotyping

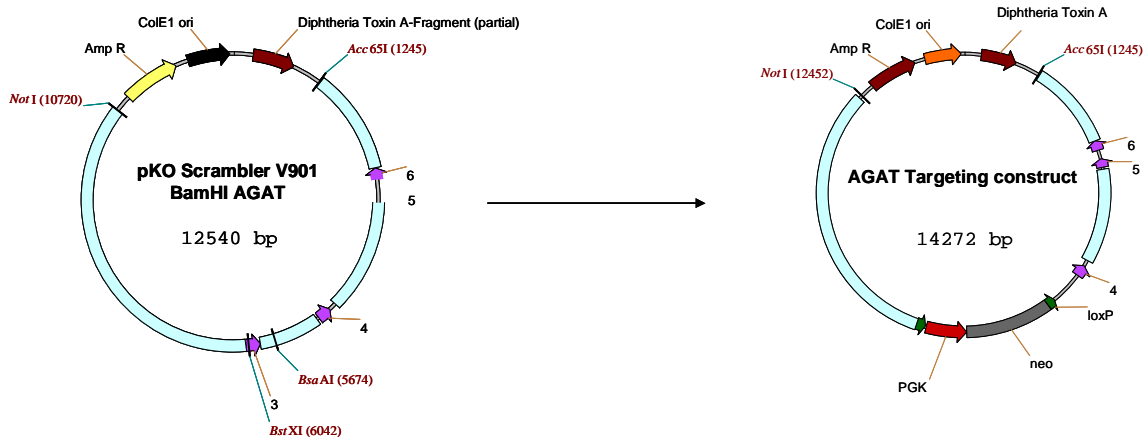


Figure 29: Subcloning of the 10 kb cosmid *BamHI* fragment in pKO-DTA, digested with *BamHI*, and subsequent subcloning of the neomycin cassette by further digestion with *BsaAI* (blunt) and *BstXI* (blunted with *Klenow*), both sites singly present on the genomic subclone. The linearized vector was ligated to a 1.7 kb neomycin cassette, retrieved by *AscI* digestion and blunted with *Klenow* from *AscI*-ploxPNEO.

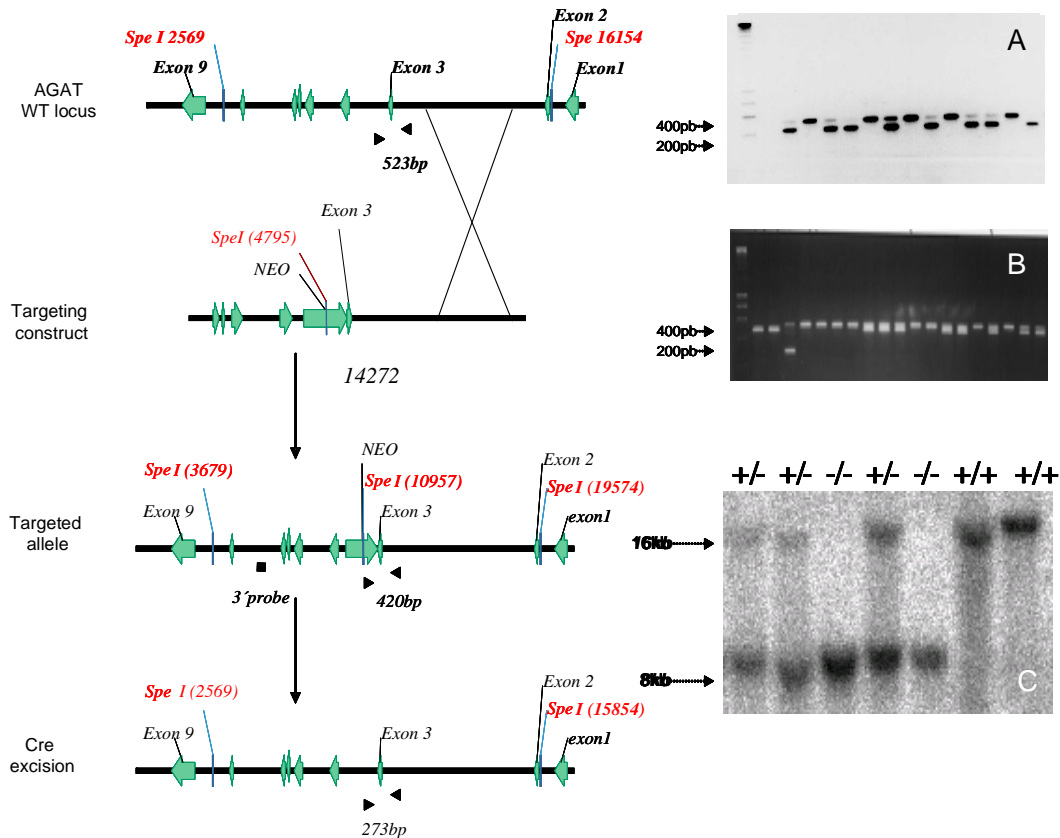


Figure 30: Schematic representation of the AGAT gene targeting strategy. Homologous recombination introduced an additional *SpeI* site present on the neomycin cassette, in addition to remove half of exon 3 and 250 bp of intron 4 and introduce a stop codon within exon 3. Positive clones were detected by Southern blot analysis (C), in which the wild type 16Kb fragment was digested in two smaller 8Kb fragments on genomic *SpeI* digestions upon correct homologous recombination of the construct. The 3' probe was 680 bp, generated by PCR amplification using a C57Bl/6 BAC as a template. The F1 offspring was screened by PCR using internal primers located external to exon 3 and internal to the neo cassette (A, B). The wild type band was 523bp and the mutant band 468bp. Upon neo excision just the two neo external primers were used for genotyping and the mutant band was 273bp (B) after excision because the original subcloning of the neo cassette removed 250 bp from the original locus.

AGAT knockout model generation and phenotyping

A 9% targeting efficiency was obtained and two clones were injected in C57Bl/6 blastocysts. Chimeric offspring (25 animals) showed high levels of chimerism. Two Chimeric males were mated to C57Bl/6 females and the brown offspring screened by Southern blot and PCR to detect germ-line transmission of the targeted allele (Fig.30A). Heterozygous founders were bred to homozygosity by intercrossing heterozygous animals.

4.2 AGAT^{-/-} mice phenotyping

4.2.1 MRS

In vivo proton ¹H and phosphorous ³¹P MR spectroscopy of AGAT^{-/-} muscle and brain confirmed the success of the knockout strategy at the biochemical level as the spectra showed the expected complete absence of Cr/PCr (Fig.31 A, B, C, D). All of the spectra of AGAT tissue showed a negligible Cr/PCr content, except for a ³¹P MR spectrum of skeletal muscle when the mutant mouse was housed with a control littermate (Fig.31D middle).

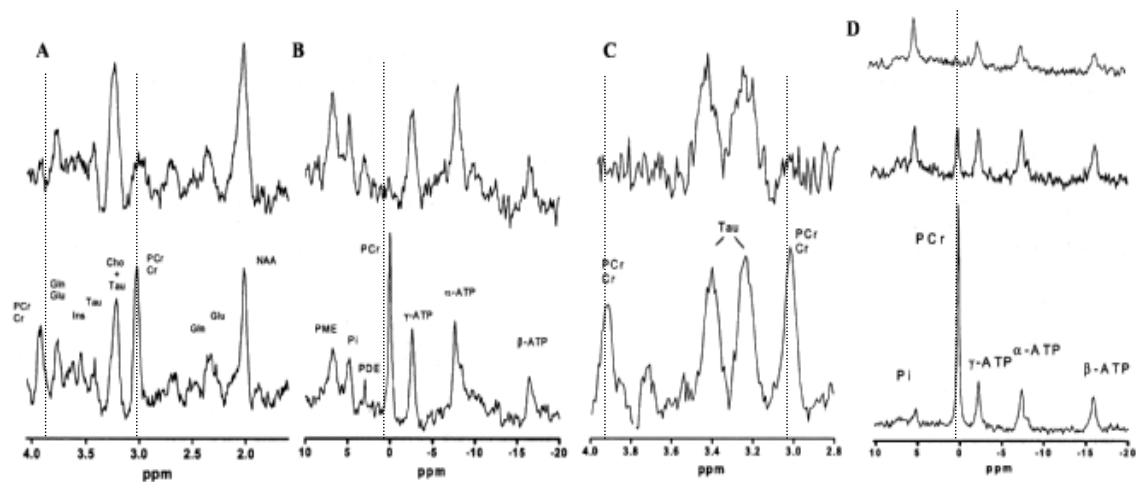


Figure 31: Brain ¹H-MR (A) and ³¹P-MR (B) spectra and muscle ¹H-MR (C) and ³¹P-MR (D) spectra of AGAT^{-/-} mice (upper) and controls (bottom). The muscle ³¹P-MR muscle spectra (D) were obtained from the same animal before (D middle) and after housing together with a control (D upper). Note the increased Pi peak but normal ATP levels (D upper). ¹H-MR muscle spectra (C) showed a complete absence of Cr/PCr, an increased signal to noise ratio and a splitting of the taurine peaks, indicative of increased effects of dipolar couplings caused by disturbances in muscle morphology and suggesting cytoarchitectural abnormalities (data obtained by Kan HE and Nabuurs C).

It was the first time that a MR spectrum showed a complete lack of high-energy related compounds (PCr/P-GAA); thus, the physiological impact of a truly non-existing Cr/PCr system could be studied in AGAT^{-/-} mice. Muscle ³¹P-MRS exhibited an abnormally elevated Pi/ γ -ATP signal (Fig.31D upper). Interestingly, the same animal had been previously housed together with control littermates. Due to coprophagia the spectra had a modest PCr peak and intermediate values regarding Pi and ATP levels (Fig.31D middle).

From the muscle ³¹P MR spectra we concluded that modest amounts of Cr were sufficient to keep ATP within normal levels, but not to maintain normal Pi concentrations as they were already markedly elevated (Fig.31D middle). Secondly, a complete absence of PCr further affected the increased signal in the Pi/ γ -ATP peaks. The data constitutes an *in vivo* evidence for a role of Cr/PCr in maintaining intracellular free Pi levels and thus represents an

AGAT knockout model generation and phenotyping

independent confirmation for a possible important role of guanidino compounds as intracellular Pi traps.

4.2.2 Skeletal muscle

Muscle ^1H MR spectra showed a complete absence of Cr/PCr, a reduction in the signal to noise ratio and a splitting of the taurine peaks (Fig. 31C), suggesting cytoarchitectural abnormalities, which were already apparent under light microscopy and further confirmed by electron microscopy (Fig.32 and 33). The Z banding arrangement at the sarcomere appeared deeply disorganized and circular holes of variable size were noted; interestingly the holes were fiber type specific (Fig.32C and D). Mitochondria also contained such holes (Fig.33F). Similar cytoarchitectural defects had been described in CK-M and MiCK double knockout mice and mitochondrial myopathies, where they were interpreted as lipid droplets and hypothesized to reflect an impaired capacity to utilize fatty acids as the substrate for oxidative ATP production (162). Accordingly, Sudan black staining of muscle sections, indicative of tissue lipid content, revealed muscle steatosis in $\text{AGAT}^{-/-}$ mice. We next wondered whether the abnormalities were reversible upon Cr-supplementation, which was the case (Fig.33B).

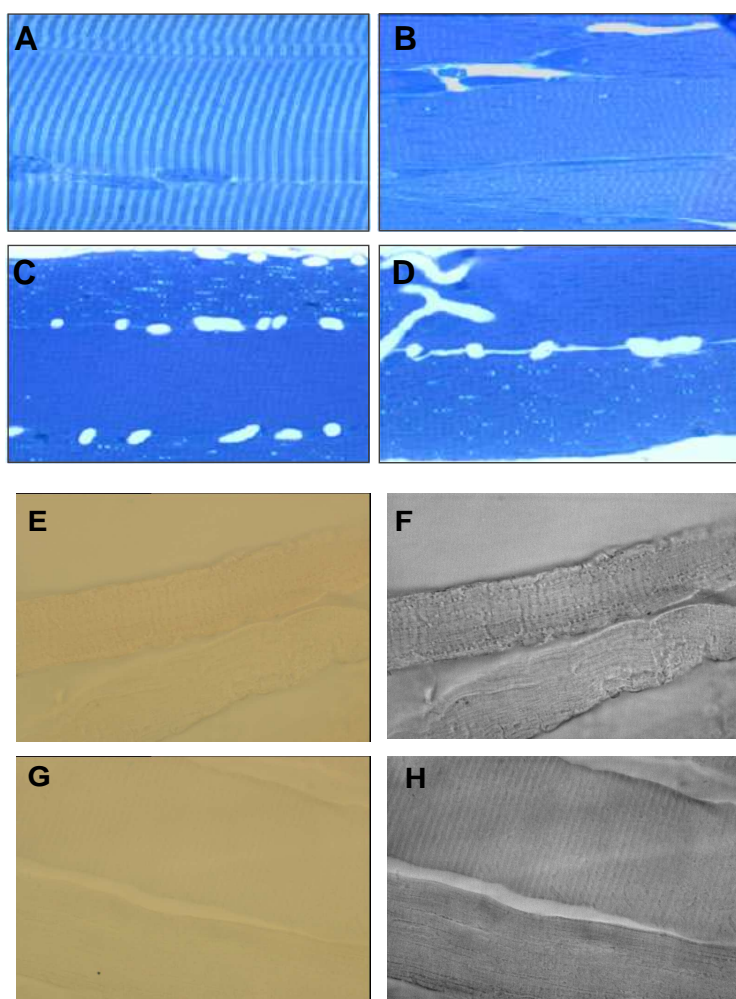


Figure 32: Hematoxylin-eosin staining and Sudan black staining of muscle sections under light microscopy revealed morphological muscle abnormalities and indicated that the nature of the holes was lipidic and fiber-type specific. From A to D: HE staining: (A) Control (n=3); (B-D) $\text{AGAT}^{-/-}$ mice (n=5). Note the increased number and diameter of blood vessel surrounding the affected fibers and the presence of holes within the sarcomeres (C) and (D). The Z banding was disturbed in affected fibers. (E and F) Sudan black staining of $\text{AGAT}^{-/-}$ mice (n=1) and control (n=1) (G and H) after 15 weeks DIO treatment (see below). Note the increased background staining of the knockouts compared to controls, indicative of muscle steatosis.

A note of caution when comparing the muscle phenotype of $\text{GAMT}^{-/-}$ and $\text{AGAT}^{-/-}$ mice should be discussed at this point. Although $\text{GAMT}^{-/-}$ muscle was reported not to have cytoarchitectural changes, unfortunately the animals were not kept under Cr free conditions

AGAT knockout model generation and phenotyping

most of the time and, thus, it is still possible that $GAMT^{-/-}$ muscle would present similar abnormalities missed in the first analysis just because the experiments were performed with coprophagia-rescued mice. Indeed, electron microscopy re-examination of $GAMT^{-/-}$ muscles disclosed the presence of holes also associated with mitochondria, but in fewer numbers and smaller size (Fig.34) with normal Z lattice structures and absent collagen-like fibers, suggesting that the muscle phenotype in $GAMT^{-/-}$ mice is not as pronounced as that of $AGAT^{-/-}$ mice.

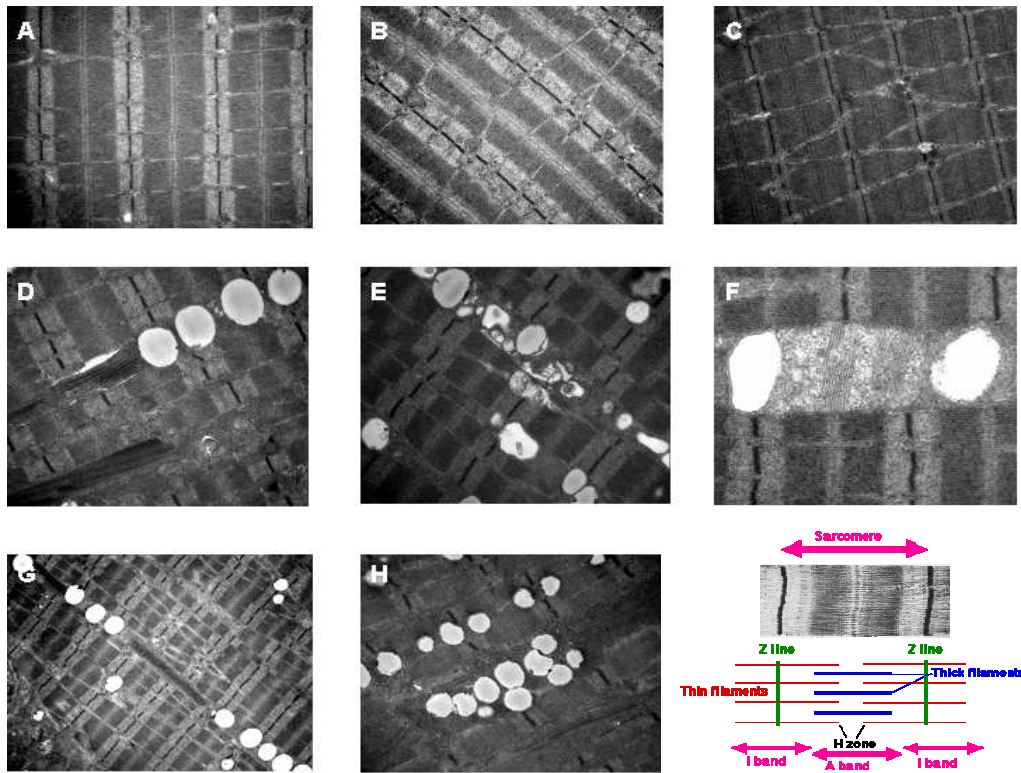


Figure 33: electronic microscopy of wildtype (n=3) (A and B), Cr-rescued $AGAT^{-/-}$ (n=2) (C), and $AGAT^{-/-}$ mice (n=5) (D-H) muscle showing ultrastructural changes. Holes of variable size were found associated with mitochondria and sometimes accompanied by collagen-like fibers. The abnormalities were rescued by Cr supplementation.

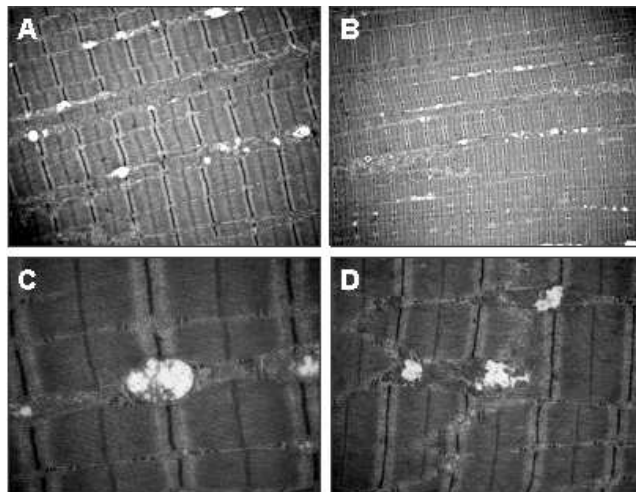


Fig 34: $GAMT^{-/-}$ muscle also presented similar changes but less severe in terms of number and size of the holes (A-D). Some cristernae resembling degenerated mitochondria were still present within such holes (C) and (D). The Z banding still appeared in normal register .

AGAT knockout model generation and phenotyping

4.2.3 Cardiac muscle

In hearts from AGAT^{-/-} mice, no Cr (HPLC) or PCr (³¹P MRS) could be detected (Fig.35). With both detection methods ATP values did not differ between groups. Inorganic phosphate levels, measured by calibrating ³¹P MRS data to the ATP concentration in control hearts measured with HPLC, were increased in AGAT^{-/-} hearts (see table in Fig.35). Intracellular pH did not differ between groups, nor did isovolumetric contractile function of isolated hearts. Interestingly, total CK activity was reduced in mutants due to a significant (30%) reduction in mitochondrial CK isoenzyme. Citrate synthase (CS) activity was not different between genotypes, indicating that mitochondria were not reduced in number in AGAT^{-/-} hearts.

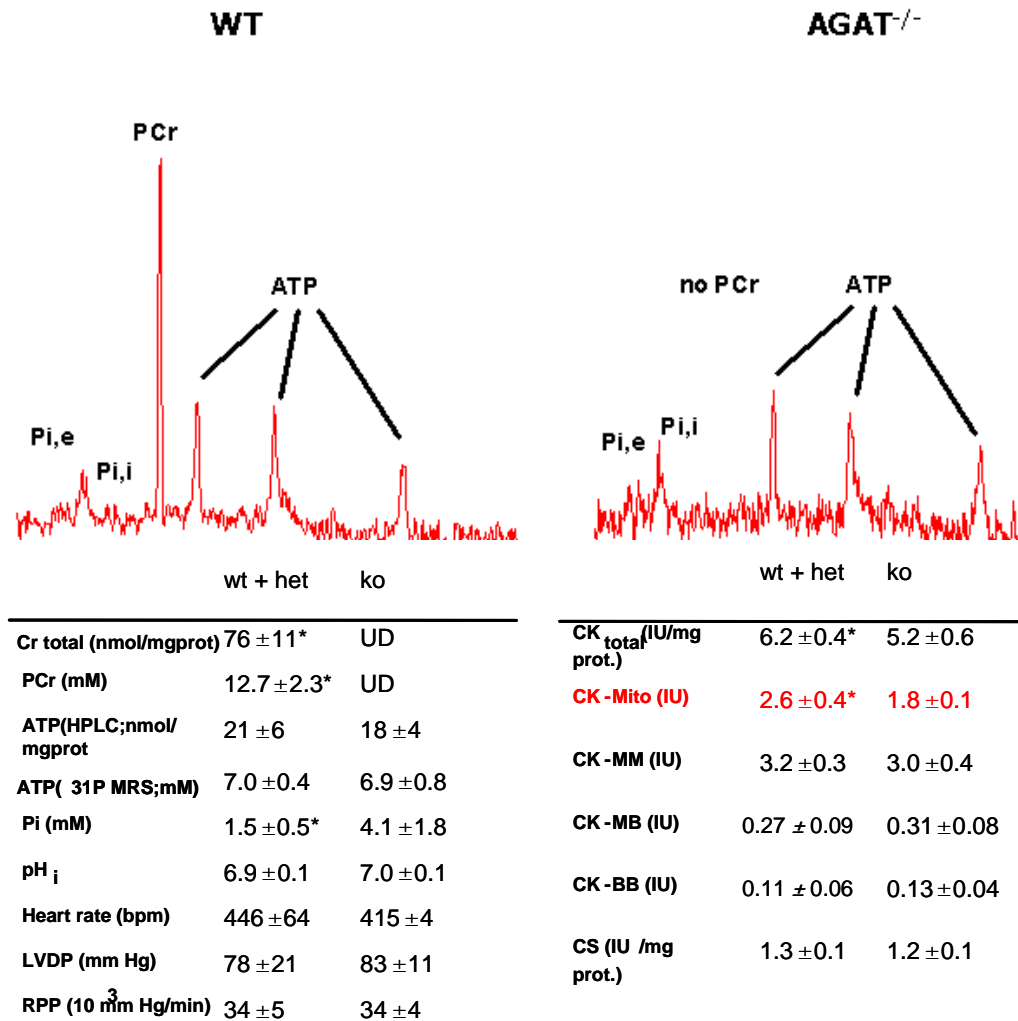


Figure 35: In hearts from AGAT^{-/-} mice, no phosphocreatine (HPLC or ³¹P MRS) could be detected. Pi levels were increased in mutants. Wet chemistry revealed decreased total CK activity due to a statistically significant specific decrease in mitochondrial CK isoenzyme activity (data obtained by Ten Hove M).

4.2.4 Body growth and creatine supplementation

AGAT^{-/-} mice showed normal Mendelian inheritance of the allele (AGAT^{+/+} 29%; AGAT^{+/-} 41%; AGAT^{-/-} 30% n=294). Homozygous mutant animals could be distinguished from the heterozygous or wild type littermates already after postnatal day 14 as they were markedly

AGAT knockout model generation and phenotyping

smaller (Fig.36). Therefore the phenotype developed soon and the animals were handicapped compared with their littermates during lactation and died more often.

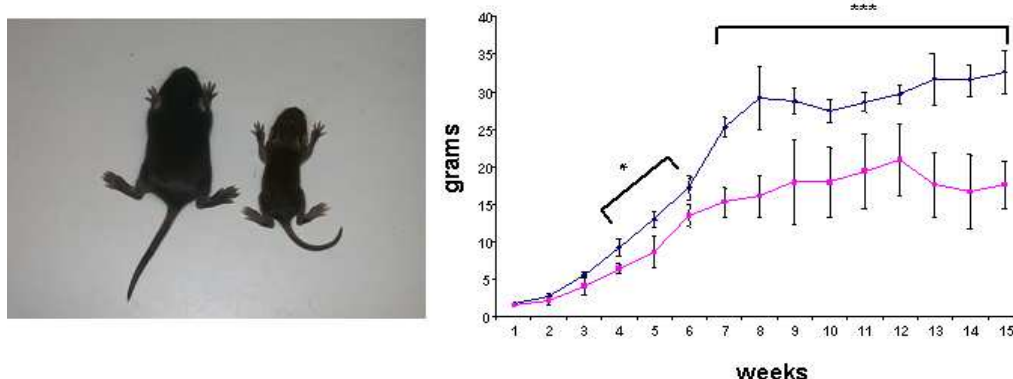
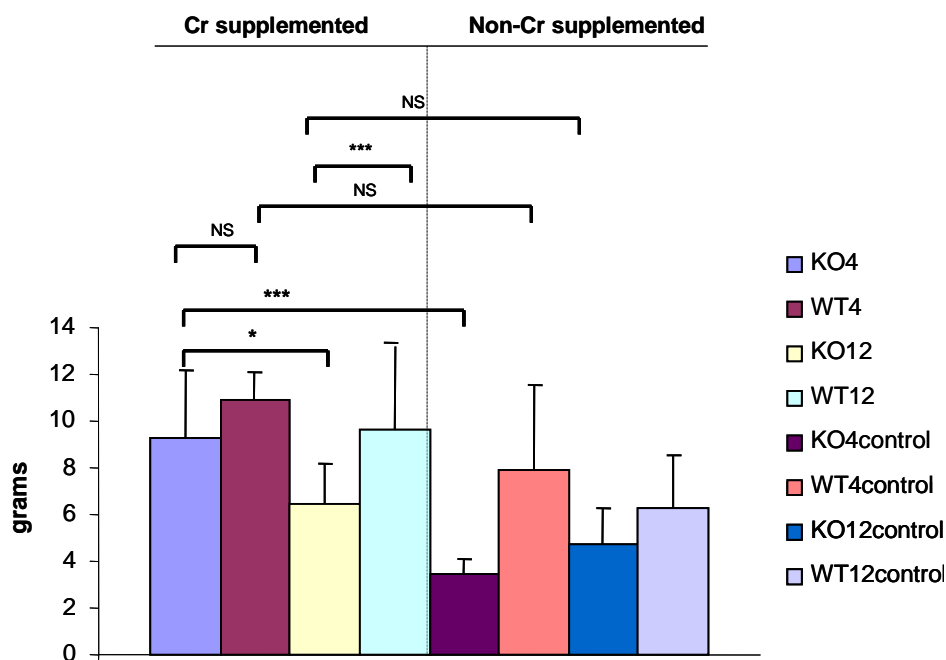


Figure 36: body weight development of AGAT^{-/-} mice and controls (male plus female) indicated that the differences in body weight were statistically significant already after the third week; data are given as mean±SD (n=423)

Female AGAT^{-/-} mice were fertile and bred with heterozygous males, because AGAT^{-/-} male mice were infertile (Fig.38). Therefore, besides the Cr produced by the heterozygous embryos of the offspring during pregnancy, development proceeded without Cr. The litter sizes were divided before the third week according to genotype to isolate AGAT^{-/-} mice as early as possible. Under those conditions of complete absence of Cr, AGAT^{-/-} mice failed to thrive after the fifth week and the body weight remained within 13-15 grams (Fig.36). Interestingly, although the muscle and testicle abnormalities could be rescued by Cr supplementation, the growth phenotype could not be completely ameliorated and strongly depended on the age at which Cr supplementation began (Fig.37). When measuring food intake, AGAT^{-/-} mice showed a tendency to eat more (Fig.39D). The presence of Cr in the food (5g Cr/Kg food) did not affect food intake.

Figure 37: body weight increase after 15 weeks Cr supplementation. Two groups of AGAT^{-/-} and controls were supplemented with Cr (5g/Kg food) starting at 4 (n=15) and 12 (n=11) weeks, and compared with littermates 4 (n=4) and 12 (n=7) weeks old fed in standard chow without Cr. When AGAT^{-/-} mice started supplementation at 4 weeks age they grew as much as the controls in Cr. However, when Cr supplementation started at 12 weeks the growth phenotype was not ameliorated (still statistically significant with age matched Cr supplemented controls and non significant with age matched non-supplemented AGAT^{-/-} mice). Data are given as mean±SD *P<0.05; ***P<0.001 NS: not significant.



AGAT knockout model generation and phenotyping

4.2.5 testicles

Hematoxylin-Eosin (HE) staining of AGAT^{-/-} male testicles displayed abnormalities similar to GAMT^{-/-} testicles, which were reversible upon Cr supplementation (Fig.38). Therefore, in another set of experiments AGAT^{-/-} males were rescued by Cr and successfully used for mating with female AGAT^{-/-}, thus obtaining a complete absence of Cr during development. Unexpectedly, rescuing AGAT^{-/-} males markedly improved the growth phenotype of the offspring (males reached a body weight of 23, 8 ± 1, 36 (n=3) and females 23, 15 ± 0, 94 (n=4); for comparison, aged matched AGAT^{-/-} mice weighted 17, 3 ± 3.5). An hypothesis to explain this unexpected finding relate to a role for Cr on prenatal/postnatal competition of the embryos for nutrients during pregnancy or lactation, from which creatine deficient mice would be curtailed compared to heterozygous littermates. If all mice of the offspring were knockouts the competition might not exist, thus explaining the improved body weight of the offspring. It remains to Cr substitute AGAT^{-/-} pregnant females at different time points during pregnancy and postnatal development to test this hypothesis, but it was surprising at first sight that rescuing AGAT^{-/-} males positively affected the growth phenotype of the offspring.

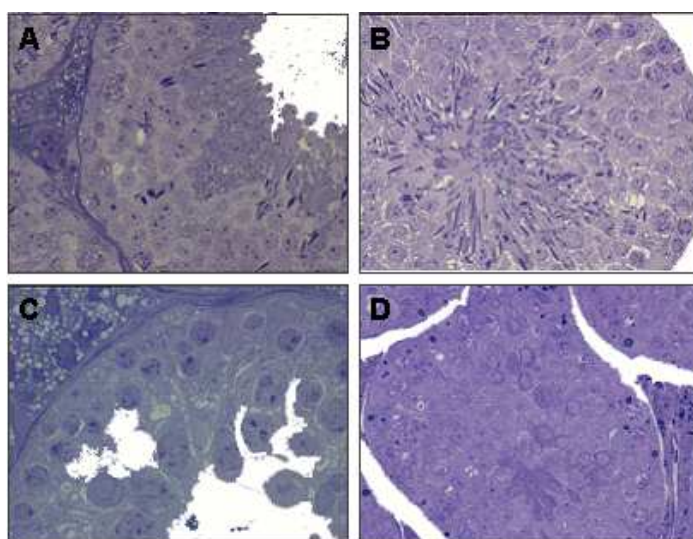


Figure 38: Hematoxylin-eosin staining of AGAT^{-/-} testicles showing a complete lack of spermatids in mutant animals (C-D) and impaired spermatogenesis, similar to the testis GAMT^{-/-} phenotype. Resorption holes were also present. The abnormalities were fully reversible with Cr (B, n=2) and the animals were fertile when fed on Cr food. (A) is a control.

4.2.6 Glucose and lipid homeostasis

To investigate lipid and glucose homeostasis, 10 to 12 weeks old mice were fed in atherogenic diets to achieve diet induced obesity (DIO). AGAT^{-/-} mice were resistant to DIO and did not precipitate full blown metabolic syndrome, as evidenced by a blunted increase in body weight (Fig.39), absent liver steatosis after 20 weeks DIO treatment (Fig.40) improved glucose tolerance after 15 weeks DIO treatment (Fig.41) and blunted increase in water consumption after 5 weeks treatment (Fig.39). Interestingly, AGAT^{-/-} mice even lost weight in atherogenic diets despite eating more than control mice (Fig.39D). To our knowledge, AGAT^{-/-} mice is the first example of a mouse model that responds with a decrease in body weight upon DIO treatment, being group 1B phospholipase A2 deficient mice the only, still less pronounced, similar instance (194). Given the full prevention of AGAT^{-/-} mice to DIO, the first possibility to rule out regarding the lipid phenotype of AGAT^{-/-} and GAMT^{-/-} mice is whether lipid digestion is itself impaired, as it was the case in 1B phospholipase A2 deficient mice. If so, some of the abnormalities in mice and humans could be explained as malabsorption problems. For example Cr might be needed for milk digestion during lactation.

AGAT knockout model generation and phenotyping

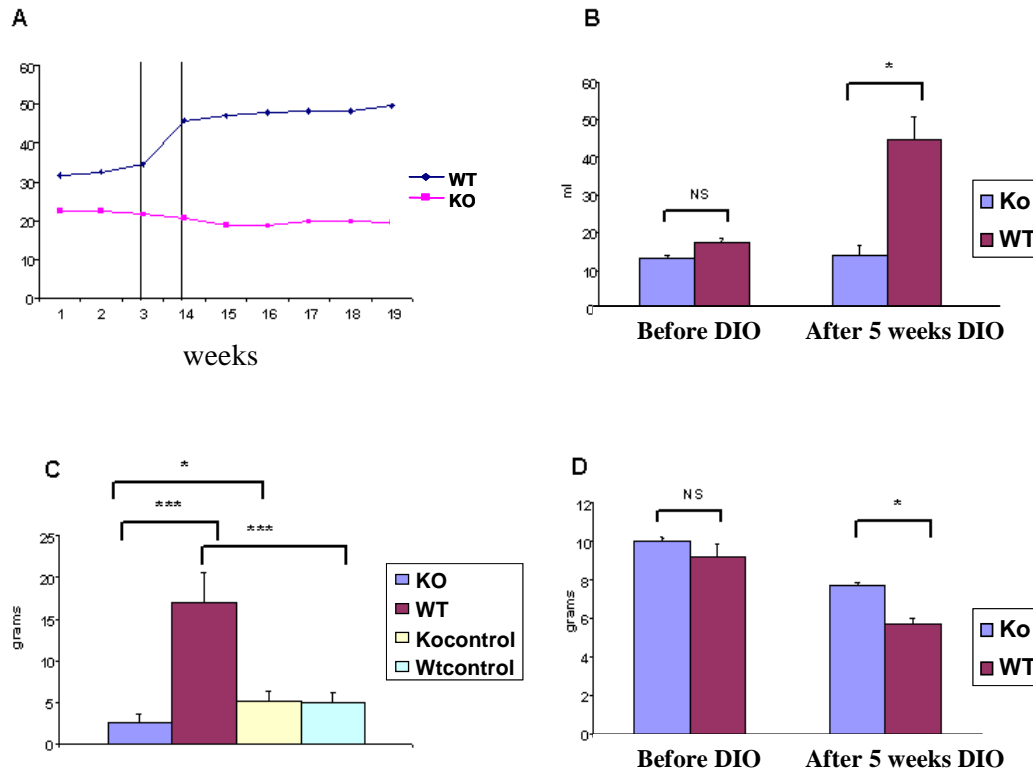


Figure 39: Body weight development and food-water consumption in atherogenic diets showed that $AGAT^{-/-}$ mice were resistant to diet induced obesity as noted by: **(A)** blunted increase on body weight ($n=3$ for each genotype), **(B)** blunted increase of water consumption ($n=4$ for each genotype) and blunted decrease of food consumption **(D)** $n=4$ for each genotype). Although $AGAT^{-/-}$ mice ate more, they even lost weight in atherogenic diets. Body weight increase quantification **(C)** showed that $AGAT^{-/-}$ mice in DIO ($n=7$) grew less than controls in DIO (WT $n=14$) and even less than $AGAT^{-/-}$ mutant controls ($AGAT^{-/-}$ mice fed in standard chow ($n=6$); WT controls fed in standard chow ($n=7$)) during the time of the experiment, suggesting that a deep metabolic/nutritional impairment underlies the phenotype. Food intake and water consumption **(B and D)** were measured during three days before and after 5 weeks DIO, and quantification of body weight increase **(C)** was calculated after 15 weeks DIO treatment. Data are given as mean \pm SD * $P<0.05$; *** $P<0.001$ NS: not significant.

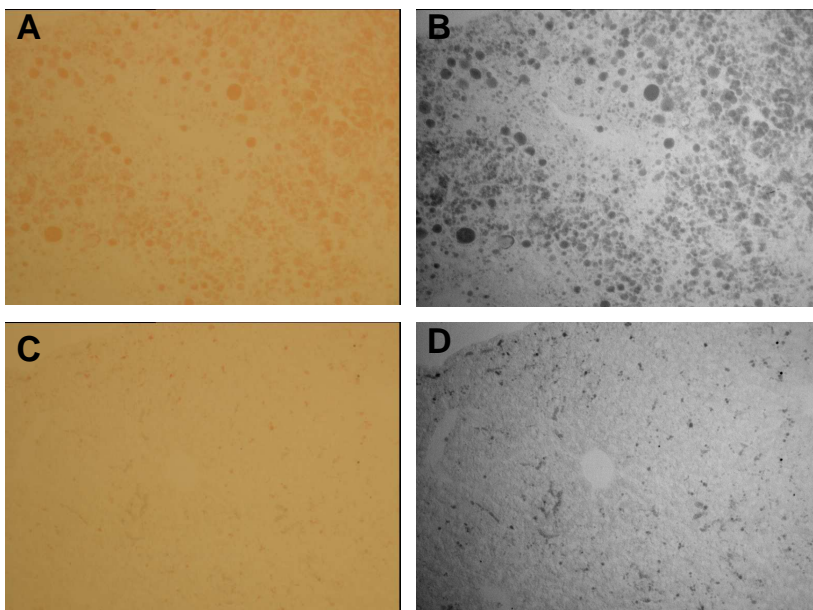


Fig 40: Liver Sudan black staining revealed that $AGAT^{-/-}$ mice did not develop liver steatosis typical of DIO treatment and concomitant metabolic syndrome. **(A)** and **(B)** control liver ($n=1$); **(C)** and **(D)** $AGAT^{-/-}$ liver ($n=1$).

AGAT knockout model generation and phenotyping

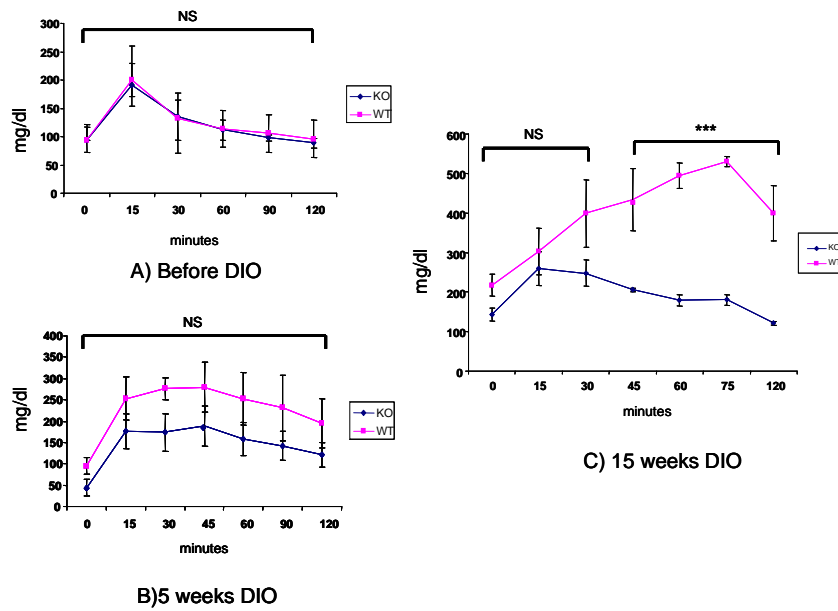


Figure 40: The glucose tolerance test revealed that $AGAT^{-/-}$ mice still have normal glucose tolerance after 5 (B) and 15 (C) weeks DIO treatment. Both genotypes had comparable glucose tolerance before DIO treatment started (A) (n=3 for each genotype). Data are given as mean \pm SEM. ***P<0.001

4.2.7 Bone

Tibiae of $AGAT^{-/-}$ mice weighed half of controls despite having comparable length, and were prone to breakage. As hematoxylin-eosin staining revealed normal bone morphology (Fig.41), reduced bone mass in $AGAT^{-/-}$ mice can be explained by decreased bone deposition and thus the possibility of osteogenesis imperfecta can be ruled out. Adult CrT patients presented similar symptoms (87).

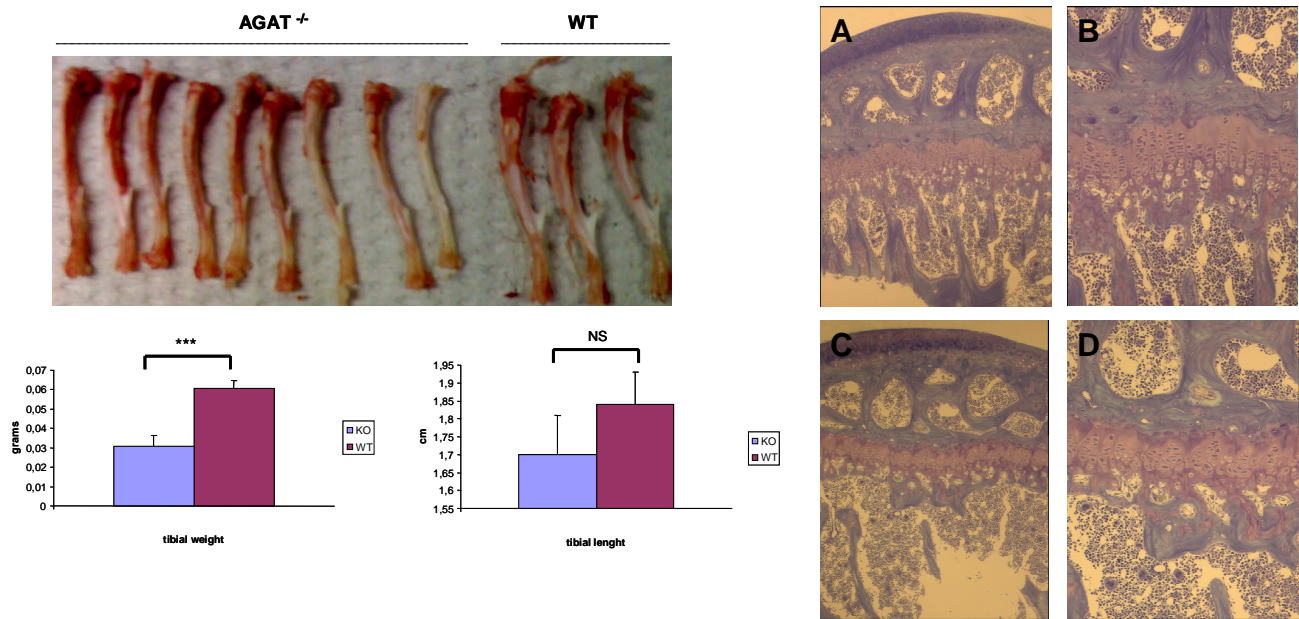


Figure 41: Tibial weight was different between age-matched $AGAT^{-/-}$ (n=9) and controls (n=6). $AGAT^{-/-}$ tibiae weighed half of the wild types, despite having approximately the same length, which was highly variable. Data are given as mean \pm SD ***P<0.001; NS: not significant. HE bone staining revealed no differences across genotypes. (A-B) control bone (n=1); (C-D) $AGAT^{-/-}$ bone (n=3).

5 Discussion

The first and most relevant question raised with the discovery of CDS is the absence of Cr/PCr signals in brain MR spectra in all of the CDS patients, a diagnostic clue common to the three diseases, because the answer to explain this fact revealed the importance and complexity of active transport of GAA and Cr within the brain as well as the intraorgan shuttle of Cr, which satisfactorily explain the absence of Cr/PCr in the spectra. It is the importance of the intraorgan shuttling phenomenon, as evidenced by the severe clinical phenotype of CDS patients, what raises a second question: why is it that strict separation of Cr-synthesizing and Cr-requiring cells exist, and does it apply not only in an interorgan but also in an intraorgan manner?

Another important finding from biochemical abnormalities of GAMT deficiency can be argued to answer this question, which is related to the Cr feedback repression mechanism as follows: AGAT upregulation was shown both at the protein level, with an AGAT antibody in Western blots of kidney GAMT^{-/-} tissues, and biochemically, by the prominent abnormalities in guanidino compounds present in GAMT^{-/-} brain homogenates and CSF fluid of GAMT human patients. Thus, under GAMT deficient conditions, AGAT is generating guanidino compounds out of essential substances like β -alanine (producing δ -GVA), GABA (producing GBA), δ AVA (producing β -GPA), α -K- δ -GVA (producing argA) by transamidation (Fig.13), elevating their concentrations up to one order of magnitude. Also GSA, produced by free radical assault on argininosuccinate leading to GSA and betain (102), is severely increased, as well as homoarginine. This fact, together with the large accumulation of GAA up to 142-fold indicates that Cr biosynthesis is deregulated, showing an uncontrolled activity when Cr is absent. Therefore we can learn how essential the Cr repressing feedback mechanism is for the Cr biosynthesis pathway in order not to divert the guanidino group into other important molecules. Also the accumulation of GAA and GBA in human and mouse SSADH deficiency is in line with this conclusion (134).

To answer the second question, AGAT catalytic unspecificity towards such important compounds like GABA on the one hand, and the proposed metabolic demands in terms of Arg, Gly and methylation substrates posed by the Cr-biosynthesis machinery on the other hand might be both reasons enough to keep Cr biosynthesis out of cells like muscle, neurons, germ cells, retina, or placenta. It would be thus necessary to consider the potential implications that an upregulated Cr biosynthesis in tissues other than where it is normally found, namely Cr-requiring tissues such as muscle, might have and how that relates to CDS pathophysiology. If this is important, it would predict a more severe phenotype in GAMT than in AGAT deficiencies, which is actually the case in the human diseases.

It is contradictory however that the the phenotype of AGAT^{-/-} mice seemed more pronounced than that of GAMT^{-/-} mice. To better understand the phenotypes of the mouse models, a number of considerations should be made at this point. By introducing a non-sense mutation in exon 3 of the AGAT genomic locus the complete Cr biosynthesis and transport pathways as well as the CK/PCr/Cr phosphorylating network have been disabled: thus, a total of seven proteins were rendered inactive. The resultant advantage is that, by keeping the animals in a restricted Cr diet and sorted by genotype to prevent coprophagia, subtle physiological functions of Cr show up. The inherent disadvantage is that it is conceptually difficult to distinguish whether a given aspect of the phenotype corresponds to the malfunctioning Cr biosynthesis pathway or Cr transport or the absent CK/PCr/Cr phosphorylating network. It can be also argued that the system is being pushed to a non-physiological level as human patients may easily obtain Cr from their food.

Discussion

Cr supplementation in $AGAT^{-/-}$ mice however represents a suitable strategy to delineate a feasible model and study what is indeed originating from a disabled CK/PCr/Cr system and thus a pure lack of PCr (namely those symptoms ameliorated with Cr and more severe in $AGAT^{-/-}$ than in $GAMT^{-/-}$ mice, as P-GAA should rescue in the latter case), or what is due to impaired function of the Cr biosynthesis system itself (those symptoms not rescued by Cr or absent in one of the knockouts). In turn, a dysfunction in the Cr biosynthesis can be due to pure inactivation ($AGAT$ knockout) or upregulation ($GAMT$ knockout): thus, non-Cr-rescued symptoms more pronounced in $GAMT^{-/-}$ mice can be inferred to originate from an upregulated system and those non-Cr-rescued symptoms worsen in $AGAT$ compared to $GAMT^{-/-}$ mice would be caused by a non-existent Cr biosynthesis. Alternatively, any phenotype not shared by both models could be interpreted as a malfunctioning Cr biosynthesis. Although the interpretation is not clear-cut at first sight, as non-Cr-rescued symptoms might also arise as a complication associated to the lack of CK/PCr/Cr in a given time of development, it is still possible to differentiate between both because in that case Cr supplementation should still be able to rescue in both models when supplemented during the relevant developmental stage. If, when doing so, just one of the models is rescued, then the complication can be interpreted as a dysfunction of the Cr biosynthesis system.

The testicles phenotype may be ascribed to lack of Cr/PCr because it can be completely rescued by Cr in both models. Therefore, the CK/PCr/Cr system is fully responsible. While Sertoli cells synthesize Cr from Gly and Arg, the CrT import synthesized Cr from Sertoli cells and blood for nourishing of germinal cells, and the process is essential for spermatogenesis.

The muscle phenotype can be also ascribed to a malfunctioning CK/PCr/Cr system as it is worst in $AGAT^{-/-}$ compared to $GAMT^{-/-}$ mice and fully reversed with Cr. Because the phenotype is less severe in $GAMT^{-/-}$ than in $AGAT^{-/-}$ mice, the former partially ameliorates the dysmorphology by GAA phosphorylation, but an $AGAT$ upregulated system and the subsequent accumulation of GAA in muscle do not seem to underly the phenotype. In this interpretation we are assuming that the origin of the abnormalities is one and the same for both models, as both manifested with holes within the sarcomere. However, if different reasons underly the dysmorphology (for example, reactive oxygen species generated by GAA in $GAMT$ mice could affect mitochondrial function, which would not be the case in the $AGAT^{-/-}$ model) then $AGAT$ upregulation and GAA accumulation would be important.

Two phenotypes could be ascribed to a faulty Cr biosynthesis. Concerning developmental complications, $GAMT^{-/-}$ animals died more often than $AGAT^{-/-}$ mice. In addition, $GAMT^{-/-}$ females were less proficient than $AGAT^{-/-}$ females when bred to heterozygous males, as the litter sizes were smaller and the matings less successful: thus both are particular features of $GAMT$ deficiency. On the other hand, the growing phenotype and the eventual failure to thrive could not be completely rescued in $AGAT^{-/-}$ mice and it was hardly dependent on the time at which Cr supplementation started. Hence, these phenotypes point to effects originating from a malfunctioning Cr biosynthesis system, at least during development-lactancy, because they could not be totally rescued by Cr or are distinctive of one of the deficiencies but not the other.

Perinatal death and female fertility complications in $GAMT^{-/-}$ mice could be associated with $AGAT$ upregulation and subsequent GAA accumulation because it is not seen in $AGAT^{-/-}$ mice. The fact that $AGAT$ mRNA is absent due to imprinting in placenta may point to a need for the mother to keep Cr biosynthesis inactive in this tissue to avoid competition for the energy by the embryo (32); thus $AGAT$ expression might escape the imprinting mechanism in placenta during pregnancy due to upregulation and cause the phenotype. The improved body weight of the $AGAT$ litter sizes when the complete offspring was mutant (as a

Discussion

result of breeding Cr rescued males and mutant females) argues in favour of a role for Cr in nutrients redistribution between the offspring and the mother.

The growth phenotype could be rather linked to an inactivated Cr biosynthesis during the neonatal period or absent CK/PCr/Cr in a given time of development, impairing a developmental process important for somatic growth which remains non-functioning during adulthood and not rescuable by Cr. An important role for Cr during prenatal/postnatal development can be inferred by the maximal AGAT expression in decidua and the maternofetal transport of Cr. It is obvious on the other hand that Cr is relevant during lactancy and postnatal development due to the prevention of the symptoms achieved when AGAT and GAMT patients were presymptomatically treated.

A role for Cr in digestion can be inferred by the following observations: first, AGAT expression is restricted to the acinar cells of the pancreas, draining into the intestine (175); additionally, periportal hepatocytes, first receiving enterohepatic circulation from postprandial absorption, were particularly depleted of glycogen in $GAMT^{-/-}$ mice. Secondly, Cr is found in the feces of animals kept on a Cr-free diet in considerable amounts, as seen in the spectra of animals housed in mixed genotypes, suggesting that Cr is secreted to the intestinal lumen from endogenous biosynthesis before targeting Cr-requiring tissues. Thirdly, Cr concentration and CrT mRNA expression is high in stomach parietal cells and brush border epithelial cells. Fourthly, although it cannot be considered a truly pathognomonic feature yet, adult CrT patients suffer gastric problems (87).

Cr/PCr might be needed for smooth muscle contraction and thus proper peristaltic movements for efficient digestion. Also, bile salt excretion is energetically costly and might need an extra energy supply in the form of PCr (176). Alternatively, Cr might be interacting with taurocholate, a bile salt containing taurine which is essential for lipid and vitamin absorption (177). In fact, taurocyamine, a quimeric molecule between taurine and Cr is detectable under uremic conditions (178) and it is a naturally occurring guanidino compound (Fig.1). The hypothesis would predict increased lipid levels in feces of $AGAT^{-/-}$ mice fed in atherogenic diets.

Regarding the bone phenotype, fat malabsorption problems also exhibit with metabolic defects of bones, secondary to reduced absorption of vitamins (vitamin D deficiency), and thus can cause bone disorders such as osteopenia or osteomalacia. Bone pain and pathological fractures may be observed (191). In fact, other adverse effects of malabsorption problems such as weight loss and increased caloric intake, as well as fatigue signs or muscle wasting may be present. Patients may also show loss of subcutaneous fat, motor weakness (pantothenic acid, vitamin D deficiency), peripheral neuropathy or ataxia and seizures (biotin) may be also present. Intriguingly, some symptoms of malabsorption overlap with AGAT, GAMT and CrT deficiencies in mice and humans.

Alternatively, the kidney and (to a lesser extent) the small intestine are the main organs maintaining Pi homeostasis and could eventually influence bone Pi content (163). It is tempting to speculate whether Cr biosynthesis modulates Pi homeostasis since first, the site for Cr biosynthesis in the kidney spatially overlaps with that of Pi resorption at the epithelial brush border of the proximal tubule of the kidney and both pathways are regulated by thyroid and growth hormone and activated by the same signaling pathway involving mTOR-SGK, and secondly, because intestinal Pi absorption also overlaps with Cr transport at the intestinal brush border epithelial cells and is also activated by the mentioned signaling pathway. If so, Cr biosynthesis might collaborate with the kidney-intestine for Pi resorption-absorption to provide CK-containing tissues with an intracellular trap for Pi retention when needed; in line with this hypothesis, Arg penetration into kidney mitochondria has been found to occur just in the presence of intracellular Pi (63). On the other hand, intestinal postprandial Pi absorption

Discussion

from dietary sources might well be coupled to the rate of Cr import at the intestine, as extracellular Cr stimulate Pi uptake in cultured cells (72).

Cr biosynthesis as a systemic regulator of Pi homeostasis would nicely complement the intracellular Pi trapping function if we consider the relevance of serum pH on Pi redistribution between intracellular/extracellular compartments (Fig.42, 163). Metabolic acidosis, in particular diabetic ketoacidosis, is a state in which the blood pH is low (under 7.35) due to increased production of protons or the inability of the body to form bicarbonate (HCO_3^-) in the kidney. The condition causes hyperphosphatemia and eventual phosphaturia (180), which we propose would trigger Cr synthesis for Pi internalization in tissues. Under diabetic ketoacidosis amino acid catabolism is enhanced in peripheral tissues like muscle, which eventually delivers nitrogen in the form of glutamine-alanine to the kidney and liver providing with an alternative energy source in the form of carbon skeletons for gluconeogenesis via anapleurosis; the amino groups liberated upon net glutamine-alanine breakdown might support the kidney and liver for Arg and Cr biosynthesis. In line with this hypothesis, Cr is increased in serum during starvation (181,182); metabolic acidosis enhance expression of NaPi-IIb, the isoform responsible for intestinal Pi absorption (185,186) and GAMT mice showed signs of anaerobic metabolism, which commonly precipitates acidosis. A caveat however of this view is the observed inhibition of Cr uptake by muscle under starving conditions (181), but it might be that muscle activates local Cr biosynthesis under these circumstances and thus Cr-synthesizing tissues deliver Cr to the blood to prepare peripheral tissues other than muscle for Cr uptake upon refeeding (see below), which would activate the mTOR system and the Cr transporter (183).

Acute respiratory alkalosis and metabolic alkalosis on the other hand induce hypophosphatemia as intracellular CO_2 decreases, causing intracellular pH to rise, a mechanism that stimulates the glycolytic pathway, specifically phosphofructokinase, the key rate-limiting enzyme of glycolysis, and enhance production of intracellular sugar phosphates, inducing intracellular Pi entry and ultimately decreasing serum Pi concentration (184). Whereas respiratory alkalosis enhances Pi uptake by muscle, the kidney responds by increasing Pi resorption and with refractoriness to the phosphaturic effect of parathyroid hormone (PTH) (187). Under these conditions Cr biosynthesis might be inhibited to allow intracellular Pi to exit the intracellular compartment and minimize muscle Pi overloading and exacerbated hypophosphatemia upon refeeding. Hypophosphatemia is also associated with other medical conditions of which hyperventilation is a feature, such as sepsis, heat stroke and hepatic coma as well as refeeding syndrome. The proposed mechanism of hypophosphatemia in these patients is increased insulin release that causes the mentioned intracellular shift in distribution of Pi. Enhanced synthesis of ATP, 2,3-diphosphoglycerate (DPG) and creatine kinase (CK) have been suggested to contribute to the hypophosphatemia associated with refeeding syndrome (185).

On these grounds, Cr synthesis would constitute a strategy connecting nitrogen detoxification with Pi homeostasis if Cr synthesis is triggered to achieve Pi internalization under hyperphosphatemia and acidic conditions, the biosynthesis fed by the ammonia generated during amino acid catabolism in muscle and subsequent delivery to the kidney-liver in the form of Gln-Ala, and inhibited under metabolic alkalosis and thus hypophosphatemia to allow Pi exit from intracellular compartments and minimize the impact of Pi internalization triggered by activated glycolysis and phosphofructokinase activation upon refeeding. Type II glycolytic fibers are best suited to act as a link between Cr biosynthesis, Pi homeostasis, glycolysis, oxidative-anaerobic and amino acid metabolism and collaborate with serum Cr and Pi concentrations, because they perform mainly anaerobic and glycolytic metabolism, have the highest and most fluctuating Cr concentrations as well as higher AMP deaminase

Discussion

activity and more active amino acid catabolism than fiber type I muscles (188). The model would predict increased concentrations of Pi in urine and stool of AGAT^{-/-} mice as well as acidic blood pH.

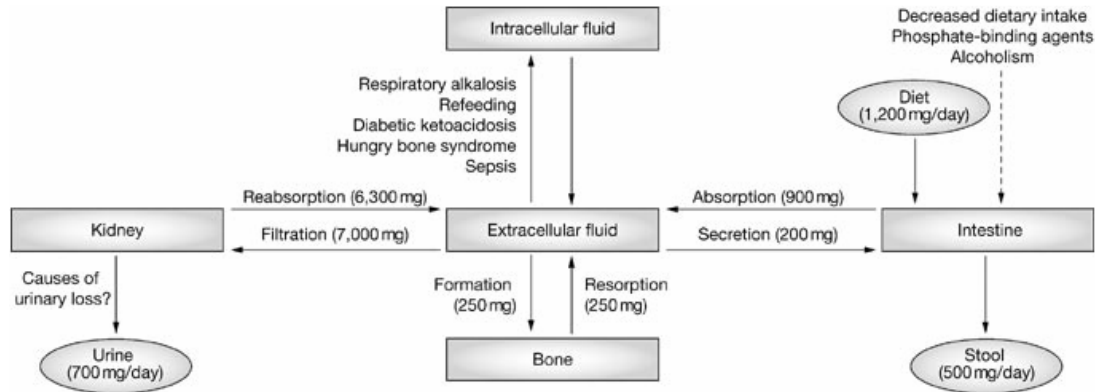


Figure 42: A role for Cr biosynthesis as a systemic regulator of phosphorous homeostasis. Approximately 1200 mg of phosphorous are daily absorbed at the level of the intestine from dietary sources. Cr, excreted from the liver and pancreas to the duodenum might act as a phosphate binding agent in collaboration with the CrT and CK expressed at high levels at intestinal epithelial cells. The kidney reabsorbs most of the filtered phosphorous at the proximal convoluted tubule of the nephron. As Cr biosynthesis is maximal at this physiological compartment, Cr production might be coupled with the phosphorous reabsorption process. Environmental and genetic factors causing hypophosphatemia are as follows: decreased intake (as an effect of phosphate-binding agents), redistribution (into the intracellular compartment in response to respiratory alkalosis) and increased excretion (in the urine) of phosphorus are the mechanisms underlying hypophosphatemia (adapted from 163).

Quantitative analysis of brain ¹H MRS showed a severe reduction in total Cr, elevated Pi/ γ -ATP and PME/ γ -ATP, accompanied with a significant elevation on tissue pH (Fig43, table right bottom). All other metabolite levels were similar except for a significant reduction in myo-inositol (Ins). Although not statistically significant, there was a trend toward increased levels of glutamine, also seen in the same spectra for GAMT^{-/-} mice (Fig.43). It is worth mentioning at this point the important role of the glutamine-glutamate cycle in brain. Glutamine is synthesized from glutamate in astrocytes, as glutamine synthetase is restricted to glial cells, after active glutamate import at glutamatergic synapses. Once uptaked glutamine is synthesized and exported to the neuron for its subsequent reconversion back to glutamate by phosphate dependent glutaminase. The cycle is recognized to be important for glutamate recycling and washing off from the synaptic cleft (172).

Increased Gln may indicate that Gln catabolism-anabolism or its transport is affected in AGAT^{-/-} and GAMT^{-/-} mice. PCr has been shown to promote glutamate uptake into synaptic vesicles (173), and thus the lack of PCr in neurons might slow glutamate filling of glutamate synaptic vesicles. Also, the lack of a Pi trapping system in neurons might decrease the activity of phosphate dependent glutaminase, as the enzyme is strongly activated by Pi concentrations (174). Of note is the coexistence in the same compartment of Cr-biosynthesis with glutamine synthetase, and of the CK/PCr/Cr system with phosphate dependent glutaminase. The arrangement is the opposite of muscle, with CK/PCr/Cr and glutamine synthetase, and kidney, with glutaminase and Cr biosynthesis. The reason for decreased Ins and increased brain pH is unknown at present, but increased glutamine concentrations could be responsible as glutamine is a basic amino acid.

Discussion

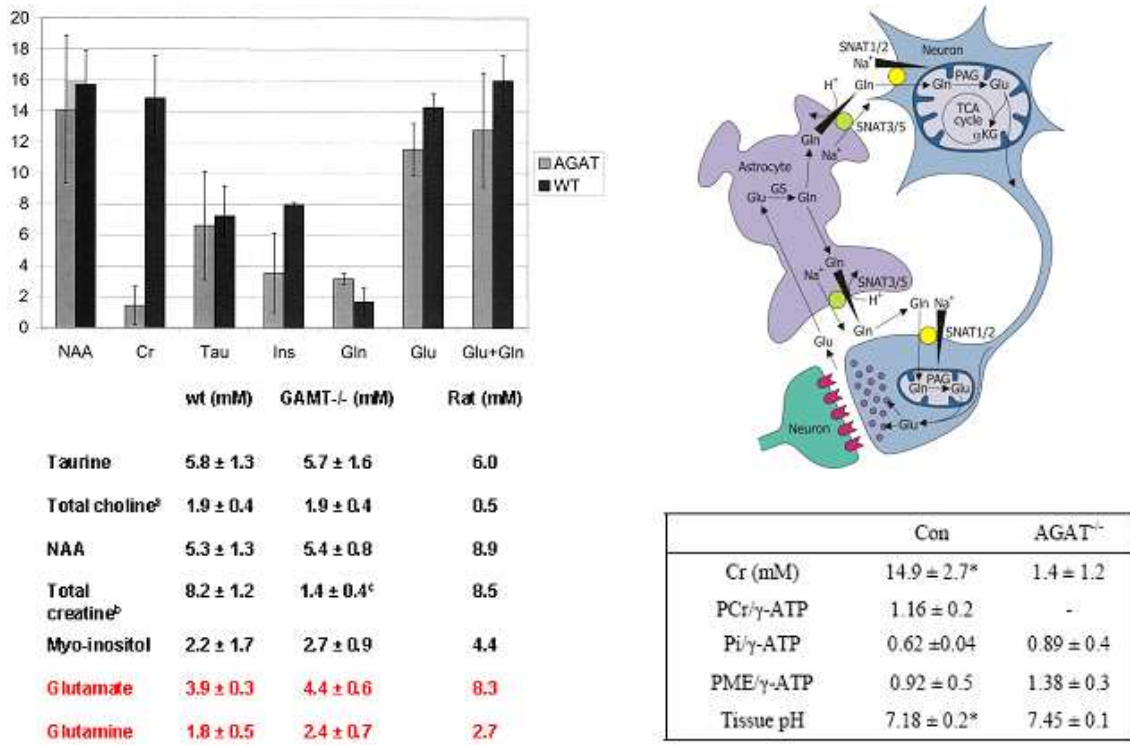


Figure 43: Quantitative analysis of brain metabolites calculated by ^1H MRS. Glutamine levels were increased in both knockout lines, but glutamate levels were increased in $\text{GAMT}^{-/-}$ mice and decreased in $\text{AGAT}^{-/-}$ mice. Note the decreased Ins levels, absent Cr/PCr, increased Pi/ γ -ATP and PME/ γ -ATP as well as statistically increased pH in brain of $\text{AGAT}^{-/-}$ mice (data obtained by Kan H and Nabuurs C).

Discussion

Summary

6 Summary

GAMT^{-/-} and AGAT^{-/-} deficient mice have been demonstrated to be valuable models for better understanding the pathophysiology underlying human creatine deficiency syndromes, as both recapitulated the human disorders at the biochemical and physiological levels; however, severe impairment of neurological functions such as seizures or dyskinetic movements were not observed. In addition, by comparing the phenotypes and treatment responses to Cr supplementation the models provided an excellent possibility to explore as yet unrecognized functions of Cr, which would be impossible to realize in humans patients because Cr would be easily obtained from the food during adulthood or from maternofetal transport during embryonic development. Although the phenotypes suggested a role for Cr during development, fertility, nutrition, skeletal and cardiac muscle metabolism and performance as well as somatic body growth, the specific mechanistic reasons are yet to be elucidated. By comparing the three human diseases, in particular by looking at GAMT differential symptomatology and treatment responses to lowering of GAA, we have learned that accumulation of reactive guanidino compounds clearly mediates a subset of the symptoms in GAMT deficiency such as therapy-refractory epileptic seizures and extrapyramidal movement disorder, and that AGAT upregulation underlies such pathognomonic feature. Finally, strong evidence indicated that Cr/PCr play important roles in brain function, muscle metabolism, spermatogenesis and proper development of the offspring, as the phenotypes could be rescued by Cr in mice and humans. The fact that some of the complications could not be completely ameliorated unless Cr supplementation started early enough, as it was the case with brain dysfunction in humans and somatic body growth in mice, suggested that Cr is important for the early establishment and proper prenatal/postnatal development of those organs responsible for brain function and somatic growth.

References

7- References

- 1) Chevreur 1832 cited in Rose WC: The metabolism of creatine and creatinine. *Annu Rev Biochem* 187, 1933.
- 2) Von Liebig J: Über die bestandteile der flüssigkeiten des fleisches. *Annu Chem Pharm* 52: 257, 1847
- 3) MORRISON JF. Arginine kinase and other invertebrate guanidino kinases. In: *The Enzymes* (3rd ed.), edited by P. D. Boyer. New York: Academic, 1973, p. 457-486
- 4) THOAI NV, AND ROBIN Y. Guanidine compounds and phosphagens. In: *Chemical Zoology*, edited by M. Florkin, and B. T. Scheer. New York: Academic, 1969, p. 163-203
- 5) Shalev-Alon G, Sukenik A, Livnah O, Schwarz R, Kaplan A. A novel gene encoding amidinotransferase in the cylindrospermopsin producing cyanobacterium *Aphanizomenon ovalisporum*. *FEMS Microbiol Lett.* 2002 Mar 19;209(1):87-91.
- 6) Hernandez-Guzman G, Alvarez-Morales A. Isolation and characterization of the gene coding for the amidinotransferase involved in the biosynthesis of phaseolotoxin in *Pseudomonas syringae* pv. *phaseolicola*. *Mol Plant Microbe Interact.* 2001 Apr;14(4):545-54.
- 7) Maladkar NK. Regulatory enzymes for the screening of streptomycin producing mutant strains of *Streptomyces griseus*. *Hindustan Antibiot Bull.* 1994 Feb-May;36(1-2):30-3.
- 8) Walker, J.B. (1979) Creatine: biosynthesis, regulation, and function. *Adv. Enzymol. Relat. Areas Mol. Biol.*, 50, 177-242.
- 9) GUTHMILLER P, VAN PILSUM JF, BOEN JR, AND MCGUIRE DM. Cloning and sequencing of rat kidney L-arginine:glycine amidinotransferase. Studies on the mechanism of regulation by growth hormone and creatine. *J Biol Chem* 269: 17556-17560, 1994
- 10) MCGUIRE DM, TORMANEN CD, SEGAL IS, AND VAN PILSUM JF. The effect of growth hormone and thyroxine on the amount of L-arginine:glycine amidinotransferase in kidneys of hypophysectomized rats. *J Biol Chem* 255: 1152-1159, 1980
- 11) Wyss M, Kaddurah-Daouk R. Creatine and creatinine metabolism. *Physiol Rev.* 2000 Jul; 80(3):1107-213. Review
- 12) DALY MM, AND SEIFTER S. Uptake of creatine by cultured cells. *Arch Biochem Biophys* 203: 317-324, 1980
- 13) PISANO JJ, ABRAHAM D, AND UDENFRIEND S. Biosynthesis and disposition of γ -guanidinobutyric acid in mammalian tissues. *Arch Biochem Biophys* 100: 323-329, 1963
- 14) Braissant O, Henry H, Villard AM, Speer O, Wallimann T, Bachmann C. Creatine synthesis and transport during rat embryogenesis: spatiotemporal expression of AGAT, GAMT and CT1. *BMC Dev Biol.* 2005 May 26;5:9.

References

- 15) BERLET HH, BONSMANN I, AND BIRRINGER H. Occurrence of free creatine, phosphocreatine and creatine phosphokinase in adipose tissue. *Biochim Biophys Acta* 437: 166-174, 1976
- 16) CHRISTENSEN M, HARTMUND T, AND GESSER H. Creatine kinase, energy-rich phosphates and energy metabolism in heart muscle of different vertebrates. *J Comp Physiol B Biochem Syst Environ Physiol* 164: 118-123, 1994
- 17) DELANGHE J, DE SLYPERE J-P, DE BUYZERE M, ROBBRECHT J, WIEME R, AND VERMEULEN A. Normal reference values for creatine, creatinine, and carnitine are lower in vegetarians. *Clin Chem* 35: 1802-1803, 1989
- 18) KUSHMERICK MJ, MOERLAND TS, AND WISEMAN RW. Mammalian skeletal muscle fibers distinguished by contents of phosphocreatine, ATP, and P_i. *Proc Natl Acad Sci USA* 89: 7521-7525, 1992
- 19) LEE HJ, FILLERS WS, AND IYENGAR MR. Phosphocreatine, an intracellular high-energy compound, is found in the extracellular fluid of the seminal vesicles in mice and rats. *Proc Natl Acad Sci USA* 85: 7265-7269, 1988
- 20) LOIKE JD, SOMES M, AND SILVERSTEIN SC. Creatine uptake, metabolism, and efflux in human monocytes and macrophages. *Am J Physiol Cell Physiol* 251: C128-C135, 1986
- 21) NAVON G, GOGOL E, AND WEISSENBERG R. Phosphorus-31 and proton NMR analysis of reproductive organs of male rats. *Arch Androl* 15: 153-157, 1985
- 22) WALLIMANN T, WEGMANN G, MOSER H, HUBER R, AND EPPENBERGER HM. High content of creatine kinase in chicken retina: compartmentalized localization of creatine kinase isoenzymes in photoreceptor cells. *Proc Natl Acad Sci USA* 83: 3816-3819, 1986
- 23) WINDISCHBAUER A, GRIESMACHER A, AND MÜLLER MM. In vitro effects of hypoxia and reoxygenation on human umbilical endothelial cells. *Eur J Clin Chem Clin Biochem* 32: 279-284, 1994
- 24) YANOKURA M, AND TSUKADA K. Decreased activities of glycine and guanidinoacetate methyltransferases and increased levels of creatine in tumor cells. *Biochem Biophys Res Commun* 104: 1464-1469, 1982
- 25) FITCH CD, AND SHIELDS RP. Creatine metabolism in skeletal muscle. I. Creatine movement across muscle membranes. *J Biol Chem* 241: 3611-3614, 1966
- 26) LOIKE JD, SOMES M, AND SILVERSTEIN SC. Creatine uptake, metabolism, and efflux in human monocytes and macrophages. *Am J Physiol Cell Physiol* 251: C128-C135, 1986
- 27) MÖLLER A, AND HAMPRECHT B. Creatine transport in cultured cells of rat and mouse brain. *J Neurochem* 52: 544-550, 1988
- 28) ODOOM JE, KEMP GJ, AND RADDA GK. The regulation of total creatine content in a myoblast cell line. *Mol Cell Biochem* 158: 179-188, 1996

References

- 29) SERAYDARIAN MW, ARTAZA L, AND ABBOTT BC. Creatine and the control of energy metabolism in cardiac and skeletal muscle cells in culture. *J Mol Cell Cardiol* 6: 405-413, 1974
- 30) GONZALEZ AM, AND UHL GR. "Choline/orphan V8-2-1/creatine transporter" mRNA is expressed in nervous, renal and gastrointestinal systems. *Mol Brain Res* 23: 266-270, 1994
- 31) VAN PILSUM JF, OLSEN B, TAYLOR D, ROZYCKI T, AND PIERCE JC. Transaminase activities, in vitro, of tissues from various mammals and from rats fed protein-free, creatine-supplemented and normal diets. *Arch Biochem Biophys* 100: 520-524, 1963
- 32) Sandell LL, Guan XJ, Ingram R, Tilghman SM. Gcm, a creatine synthesis enzyme, is imprinted in mouse placenta. *Proc Natl Acad Sci U S A*. 2003 Apr 15;100(8):4622-7
- 33) DAVIS BM, MILLER RK, BRENT RL, AND KOSZALKA TR. Materno-fetal transport of creatine in the rat. *Biol Neonate* 33: 43-54, 1978
- 34) CONWAY MA, AND CLARK JF. *Creatine and Creatine Phosphate: Scientific and Clinical Perspectives*. Orlando, FL: Academic, 1996
- 35) SAKS VA, BOBKOV YG, AND STRUMIA EDS E. *Creatine Phosphate: Biochemistry, Pharmacology and Clinical Efficiency*. Torino, Italy: Edizioni Minerva Medica, 1987
- 36) SAKS VA, VENTURA-CLAPIER R, LEVERVE X, RIGOLET M, AND ROSSI A, Eds. Bioenergetics of the cell: quantitative aspects. *Mol Cell Biochem* 184: 1-460, 1998
- 37) Ellington WR. Evolution and physiological roles of phosphagen systems. *Annu Rev Physiol*. 2001;63:289-325. Review.
- 38) Askenasy N, Koretsky AP. Transgenic livers expressing mitochondrial and cytosolic CK: mitochondrial CK modulates free ADP levels. *Am J Physiol Cell Physiol*. 2002 Feb;282(2):C338-46.
- 39) Brosnan MJ, Chen LH, Wheeler CE, Van Dyke TA, Koretsky AP. Phosphocreatine protects ATP from a fructose load in transgenic mouse liver expressing creatine kinase. *Am J Physiol*. 1991 Jun; 260(6 Pt 1):C1191-200.
- 40) Miller K, Halow J, Koretsky AP. Phosphocreatine protects transgenic mouse liver expressing creatine kinase from hypoxia and ischemia. *Am J Physiol*. 1993 Dec;265(6 Pt 1):C1544-51.
- 41) Owen OE, Kalhan SC, Hanson RW. The key role of anaplerosis and cataplerosis for citric acid cycle function. *J Biol Chem*. 2002 Aug 23;277(34):30409-12.. Review
- 42) WALLIMANN T, WYSS M, BRDICZKA D, NICOLAY K, AND EPPENBERGER HM. Intracellular compartmentation, structure and function of creatine kinase isoenzymes in tissues with high and fluctuating energy demands: the "phosphocreatine circuit" for cellular energy homeostasis. *Biochem J* 281: 21-40, 1992

References

- 43)Griffiths JR. 1981. A fresh look at glycogenolysis in skeletal muscle. *Biosci. Rep.* 1: 595–610
- 44)VAN PILSUM JF, McGUIRE DM, AND MILLER CA. The antagonistic action of creatine and growth hormone on the expression of the gene for rat kidney L-arginine:glycine amidinotransferase. In: *Guanidino Compounds in Biology and Medicine*, edited by P. P. De Deyn, B. Marescau, V. Stalon, and I. A. Qureshi. London: Libbey, 1992, p. 147-151
- 45)Morris SM Jr. Enzymes of arginine metabolism. *J Nutr.* 2004 Oct;134(10 Suppl):2743S-2747S; discussion 2765S-2767S. Review
- 46)Morris SM Jr. Arginine: beyond protein. *Am J Clin Nutr.* 2006 Feb;83(2):508S-512S. Review.
- 47) Wu G, Morris SM Jr. Arginine metabolism: nitric oxide and beyond. *Biochem J.* 1998 Nov 15;336 (Pt 1):1-17. Review.
- 48) Sobrevia L, Nadal A, Yudilevich DL, Mann GE. Activation of L-arginine transport (system y+) and nitric oxide synthase by elevated glucose and insulin in human endothelial cells. *J Physiol.* 1996 Feb 1;490 (Pt 3):775-81.
- 49) Castillo L, Beaumier L, Ajami AM, Young VR. Whole body nitric oxide synthesis in healthy men determined from [¹⁵N]arginine-to-[¹⁵N]citrulline labeling. *Proc Natl Acad Sci U S A.* 1996; 93: 11460–11465
- 50) Takeda M, Kiyatake I, Koide H, Jung KY, Endou H. Biosynthesis of guanidinoacetic acid in isolated renal tubules. *Eur J Clin Chem Clin Biochem.* 1992 Jun;30(6):325-31
- 51) GROSS MD, SIMON AM, JENNY RJ, GRAY ED, McGUIRE DM, AND VAN PILSUM JF. Multiple forms of rat kidney L-arginine:glycine amidinotransferase. *J Nutr* 118: 1403-1409, 1988
- 52) GUTHMILLER P, VAN PILSUM JF, BOEN JR, AND McGUIRE DM. Cloning and sequencing of rat kidney L-arginine:glycine amidinotransferase. Studies on the mechanism of regulation by growth hormone and creatine. *J Biol Chem* 269: 17556-17560, 1994
- 53) McGUIRE DM, GROSS MD, ELDE RP, AND VAN PILSUM JF. Localization of L-arginine-glycine amidinotransferase protein in rat tissues by immunofluorescence microscopy. *J Histochem Cytochem* 34: 429-435, 1986
- 54) VAN PILSUM JF, McGUIRE DM, AND MILLER CA. The antagonistic action of creatine and growth hormone on the expression of the gene for rat kidney L-arginine:glycine amidinotransferase. In: *Guanidino Compounds in Biology and Medicine*, edited by P. P. De Deyn, B. Marescau, V. Stalon, and I. A. Qureshi. London: Libbey, 1992, p. 147-151
- 55) TAKEDA M, KIYATAKE I, KOIDE H, JUNG KY, AND ENDOU H. Biosynthesis of guanidinoacetic acid in isolated renal tubules. *Eur J Clin Chem Clin Biochem* 30: 325-331, 1992
- 56) MUDD SH, EBERT MH, AND SCRIVER CR. Labile methyl group balances in the human: the role of sarcosine. *Metabolism* 29: 707-720, 1980

References

- 57) Walkey CJ, Donohue LR, Bronson R, Agellon LB, Vance DE. Disruption of the murine gene encoding phosphatidylethanolamine N-methyltransferase. *Proc Natl Acad Sci U S A*. 1997 Nov 25;94(24):12880-5.
- 58) Stead LM, Brosnan JT, Brosnan ME, Vance DE, Jacobs RL. It time to reevaluate methyl balance in humans? *Am J Clin Nutr*. 2006 Jan;83(1):5-10.
- 59) Stead LM, Au KP, Jacobs RL, Brosnan ME, Brosnan JT. Methylation demand and homocysteine metabolism: effects of dietary provision of creatine and guanidinoacetate. *Am J Physiol Endocrinol Metab*. 2001 Nov;281(5):E1095-100.
- 60) Loscalzo J. Adverse effects of supplemental L-arginine in atherosclerosis: consequences of methylation stress in a complex catabolism? *Arterioscler Thromb Vasc Biol*. 2003 Jan 1;23(1):3-5
- 61) Chen J, Kuhlencordt P, Urano F, Ichinose H, Astern J, Huang PL. Effects of chronic treatment with L-arginine on atherosclerosis in apoE knockout and apoE/inducible NO synthase double-knockout mice. *Arterioscler Thromb Vasc Biol*. 2003 Jan 1;23(1):97-103
- 62) Handy DE, Scolaro J, Chen J, Huang P, Loscalzo J. L-arginine increases plasma homocysteine in apoE^{-/-}/iNOS^{-/-} double knockout mice. *Cell Mol Biol (Noisy-le-grand)*. 2004 Dec;50(8):903-9.
- 63) GRAZI E, MAGRI E, AND BALBONI G. On the control of arginine metabolism in chicken kidney and liver. *Eur J Biochem* 60: 431-436, 1975
- 64) KIM GS, CHEVLI KD, AND FITCH CD. Fasting modulates creatine entry into skeletal muscle in the mouse. *Experientia* 39: 1360-1362, 1983
- 65) HANDLOGTEN ME, AND KILBERG MS. Induction and decay of amino acid transport in the liver. *J Biol Chem* 259: 3519-3525, 1984
- 66) GREEN AL, HULTMAN E, MacDONALD IA, SEWELL DA, AND GREENHAFF PL. Carbohydrate ingestion augments skeletal muscle creatine accumulation during creatine supplementation in humans. *Am J Physiol Endocrinol Metab* 271: E821-E826, 1996
- 67) GREEN AL, SIMPSON EJ, LITTLEWOOD JJ, MacDONALD IA, AND GREENHAFF PL. Carbohydrate ingestion augments creatine retention during creatine feeding in humans. *Acta Physiol Scand* 158: 195-202, 1996
- 68) STEENGE GR, LAMBOURNE J, CASEY A, MacDONALD IA, AND GREENHAFF PL. Stimulatory effect of insulin on creatine accumulation in human skeletal muscle. *Am J Physiol Endocrinol Metab* 275: E974-E979, 1998
- 69) Shojaiefard M, Christie DL, Lang F. Stimulation of the creatine transporter SLC6A8 by the protein kinases SGK1 and SGK3. *Biochem Biophys Res Commun*. 2005 Sep 2;334(3):742-6.
- 70) Shojaiefard M, Christie DL, Lang F. Stimulation of the creatine transporter SLC6A8 by the protein kinase mTOR. *Biochem Biophys Res Commun*. 2006 Mar 24;341(4):945-9.

References

- 71) Shojaiefard M, Lang F. Stimulation of the intestinal phosphate transporter SLC34A2 by the protein kinase mTOR. *Biochem Biophys Res Commun*. 2006 Jul 14;345(4):1611-4.
- 72) POLGREEN KE, KEMP GJ, AND RADDA GK. Modulation of inorganic phosphate uptake into a mouse myoblast cell line by extracellular creatine. *Biochem Soc Trans* 21: 440S, 1993
- 73) NASH SR, GIROS B, KINGSMORE SF, ROCHELLE JM, SUTER ST, GREGOR P, SELDIN MF, AND CARON MG. Cloning, pharmacological characterization, and genomic localization of the human creatine transporter. *Receptors Channels* 2: 165-174, 1994
- 74) SORA I, RICHMAN J, SANTORO G, WEI H, WANG Y, VANDERAH T, HORVATH R, NGUYEN M, WAITE S, ROESKE WR, AND YAMAMURA HI. The cloning and expression of a human creatine transporter. *Biochem Biophys Res Commun* 204: 419-427, 1994
- 75) GUIMBAL C, AND KILIMANN MW. A Na⁺-dependent creatine transporter in rabbit brain, muscle, heart, and kidney. cDNA cloning and functional expression. *J Biol Chem* 268: 8418-8421, 1993
- 76) FITCH CD, SHIELDS RP, PAYNE WF, AND DACUS JM. Creatine metabolism in skeletal muscle. III. Specificity of the creatine entry process. *J Biol Chem* 243: 2024-2027, 1968
- 77) Stockler S, Holzbach U, Hanefeld F, Marquardt I, Helms G, Requart M, Hanicke W, Frahm J. Creatine deficiency in the brain: a new, treatable inborn error of metabolism. *Pediatr Res*. 1994 Sep;36(3):409-13
- 78) Stockler S, Isbrandt D, Hanefeld F, Schmidt B, von Figura K. Guanidinoacetate methyltransferase deficiency: the first inborn error of creatine metabolism in man. *Am J Hum Genet*. 1996 May;58(5):914-22.
- 79) von Figura, K., Hanefeld, F., Isbrandt, D. and Stöckler-Ipsiroglu, S. 2001 Guanidinoacetate methyltransferase deficiency. In Scriver, C.R., Beaudet, A.L., Sly, W.S. and Valle, D. (eds), *The Metabolic and Molecular Bases of Inherited Disease.*, McGraw-Hill, New York, Vol. II, pp. 1897–1908
- 80) Cecil KM, Salomons GS, Ball WS Jr, Wong B, Chuck G, Verhoeven NM, Jakobs C, DeGrauw TJ. Irreversible brain creatine deficiency with elevated serum and urine creatine: a creatine transporter defect? *Ann Neurol*. 2001 Mar;49(3):401-4
- 81) Salomons GS, van Dooren SJ, Verhoeven NM, Cecil KM, Ball WS, Degrauw TJ, Jakobs C. X-linked creatine-transporter gene (SLC6A8) defect: a new creatine-deficiency syndrome. *Am J Hum Genet*. 2001 Jun;68(6):1497-500.
- 82) Bianchi MC, Tosetti M, Fornai F, Alessandrì MG, Cipriani P, De Vito G, Canapicchi R (2000) Reversible brain creatine deficiency in two sisters with normal blood creatine level. *Ann Neurol* 47:511-513
- 83) Item CB, Stockler-Ipsiroglu S, Stromberger C, Muhl A, Alessandri MG, Bianchi MC, Tosetti M, Fornai F, Cioni G. Arginine:glycine amidinotransferase deficiency: the third inborn error of creatine metabolism in humans. *Am J Hum Genet*. 2001 Nov;69(5):1127-33

References

- 84) Schulze A. Creatine deficiency syndromes. *Mol Cell Biochem.* 2003 Feb; 244(1-2):143-50.
- 85) Sykut-Cegielska J, Gradowska W, Mercimek-Mahmutoglu S, Stockler-Ipsiroglu S. Biochemical and clinical characteristics of creatine deficiency syndromes. *Acta Biochim Pol.* 2004;51(4):875-82. Review.
- 86) Lion-Francois L, Cheillan D, Pitelet G, Acquaviva-Bourdain C, Bussy G, Cotton F, Guibaud L, Gerard D, Rivier C, Vianey-Saban C, Jakobs C, Salomons GS, des Portes V. High frequency of creatine deficiency syndromes in patients with unexplained mental retardation. *Neurology.* 2006 Nov 14;67(9):1713-4.
- 87) Kleefstra T, Rosenberg EH, Salomons GS, Stroink H, van Bokhoven H, Hamel BC, de Vries BB. Progressive intestinal, neurological and psychiatric problems in two adult males with cerebral creatine deficiency caused by an SLC6A8 mutation. *Clin Genet.* 2005 Oct;68(4):379-81.
- 88) Stromberger C, Bodamer OA, Stockler-Ipsiroglu S. Clinical characteristics and diagnostic clues in inborn errors of creatine metabolism. *J Inher Metab Dis.* 2003;26(2-3):299-308
- 89) Arias A, Ormazabal A, Moreno J, Gonzalez B, Vilaseca MA, Garcia-Villoria J, Pampols T, Briones P, Artuch R, Ribes A. Methods for the diagnosis of creatine deficiency syndromes: a comparative study. *J Neurosci Methods.* 2006 Sep 30;156(1-2):305-9.
- 90) Stockler S, Hanefeld F, Frahm J. Creatine replacement therapy in guanidinoacetate methyltransferase deficiency, a novel inborn error of metabolism. *Lancet.* 1996 Sep 21;348(9030):789-90
- 91) Ohtsuki S, Tachikawa M, Takanaga H, Shimizu H, Watanabe M, Hosoya K, Terasaki T. The blood-brain barrier creatine transporter is a major pathway for supplying creatine to the brain. *J Cereb Blood Flow Metab*
- 92) Tachikawa M, Fukaya M, Terasaki T, Ohtsuki S, Watanabe M. Distinct cellular expressions of creatine synthetic enzyme GAMT and creatine kinases uCK-Mi and CK-B suggest a novel neuron-glia relationship for brain energy homeostasis. *Eur J Neurosci.* 2004 Jul;20(1):144-60
- 93) Virgintino D, Monaghan P, Robertson D, Errede M, Bertossi M, Ambrosi G, Roncali L. An immunohistochemical and morphometric study on astrocytes and microvasculature in the human cerebral cortex. *Histochem J.* 1997 Sep;29(9):655-60
- 94) Schulze A, Ebinger F, Rating D, Mayatepek E. Improving treatment of guanidinoacetate methyltransferase deficiency: reduction of guanidinoacetic acid in body fluids by arginine restriction and ornithine supplementation. *Mol Genet Metab.* 2001 Dec;74(4):413-9.
- 95) Schulze A, Bachert P, Schlemmer H, Harting I, Polster T, Salomons GS, Verhoeven NM, Jakobs C, Fowler B, Hoffmann GF, Mayatepek E. Lack of creatine in muscle and brain in an adult with GAMT deficiency. *Ann Neurol.* 2003 Feb;53(2):248-51.

References

- 96) Valle, D. and Simell, O. (1995) in *The Metabolic and Molecular Bases of Inherited Disease* (Scriver, C. R., Beaudet, A. L., Sly, W. S. and Valle, D., eds.), pp. 1147–1185, McGraw-Hill Inc., New York
- 97) Feillet F, Leonard JV. Alternative pathway therapy for urea cycle disorders. *J Inherit Metab Dis.* 1998;21 Suppl 1:101-11. Review
- 98) de Sanctis L, Bonetti G, Bruno M, De Luca F, Bisceglia L, Palacin M, Dianzani I, Ponzzone A. Cystinuria phenotyping by oral lysine and arginine loading. *Clin Nephrol.* 2001 Dec;56(6):467-74.
- 99) Battini R, Alessandri MG, Leuzzi V, Moro F, Tosetti M, Bianchi MC, Cioni G. Arginine:glycine amidinotransferase (AGAT) deficiency in a newborn: early treatment can prevent phenotypic expression of the disease. *J Pediatr.* 2006 Jun;148(6):828-30.
- 100) Schulze A, Hoffmann GF, Bachert P, Kirsch S, Salomons GS, Verhoeven NM, Mayatepek E. Presymptomatic treatment of neonatal guanidinoacetate methyltransferase deficiency. *Neurology.* 2006 Aug 22;67(4):719-21.
- 101) van Deursen J, Heerschap A, Oerlemans F, Ruitenbeek W, Jap P, ter Laak H, Wieringa B. Skeletal muscles of mice deficient in muscle creatine kinase lack burst activity. *Cell.* 1993 Aug 27;74(4):621-31.
- 102) Steeghs K, Peters W, Bruckwilder M, Croes H, Van Alewijk D, Wieringa B. Mouse ubiquitous mitochondrial creatine kinase: gene organization and consequences from inactivation in mouse embryonic stem cells. *DNA Cell Biol.* 1995 Jun;14(6):539-53.
- 103) Steeghs K, Oerlemans F, Wieringa B. Mice deficient in ubiquitous mitochondrial creatine kinase are viable and fertile. *Biochim Biophys Acta.* 1995 Jun 30;1230(3):130-
- 104) Watchko JF, Daood MJ, Wieringa B, Koretsky AP. Myofibrillar or mitochondrial creatine kinase deficiency alone does not impair mouse diaphragm isotonic function. *J Appl Physiol.* 2000 Mar;88(3):973-80.
- 105) Jost CR, Van Der Zee CE, In 't Zandt HJ, Oerlemans F, Verheij M, Streijger F, Fransen J, Heerschap A, Cools AR, Wieringa B. Creatine kinase B-driven energy transfer in the brain is important for habituation and spatial learning behaviour, mossy fibre field size and determination of seizure susceptibility. *Eur J Neurosci.* 2002 May;15(10):1692-706.
- 106) Yamamichi H, Kasakura S, Ohkawa J, Yamamori S, Iwasaki R. [Acute myocardial infarction without elevation of CK activity: analysis of CK-MM protein and gene of CK-MM] *Rinsho Byori.* 1995 Jan;43(1):26-33.
- 107) Yamamichi H, Kasakura S, Yamamori S, Iwasaki R, Jikimoto T, Kanagawa S, Ohkawa J, Kumagai S, Koshihara M. Creatine kinase gene mutation in a patient with muscle creatine kinase deficiency. *Clin Chem.* 2001 Nov;47(11):1967-73.
- 108) Mori A. Biochemistry and neurotoxicology of guanidino compounds. History and recent advances. *Pavlov J Biol Sci.* 1987 Jul-Sep;22(3):85-94. Review

References

- 109) De Deyn PP, Macdonald RL. Guanidino compounds that are increased in cerebrospinal fluid and brain of uremic patients inhibit GABA and glycine responses on mouse neurons in cell culture. *Ann Neurol.* 1990 Nov;28(5):627-33.
- 110) De Deyn PP, Marescau B, Macdonald RL. Guanidino compounds that are increased in hyperargininemia inhibit GABA and glycine responses on mouse neurons in cell culture. *Epilepsy Res.* 1991 Mar;8(2):134-41.
- 111) D'Hooge R, De Deyn PP, Van de Vijver G, Antoons G, Raes A, Van Bogaert PP. Uraemic guanidino compounds inhibit gamma-aminobutyric acid-evoked whole cell currents in mouse spinal cord neurones. *Neurosci Lett.* 1999 Apr 16;265(2):83-6.
- 112) Neu A, Neuhoff H, Trube G, Fehr S, Ullrich K, Roeper J, Isbrandt D. Activation of GABA(A) receptors by guanidinoacetate: a novel pathophysiological mechanism. *Neurobiol Dis.* 2002 Nov;11(2):298-307.
- 113) D'Hooge R, Pei YQ, Marescau B, De Deyn PP. Convulsive action and toxicity of uremic guanidino compounds: behavioral assessment and relation to brain concentration in adult mice. *J Neurol Sci.* 1992 Oct;112(1-2):96-105
- 114) Zugno AI, Franzon R, Chiarani F, Bavaresco CS, Wannmacher CM, Wajner M, Wyse AT. Evaluation of the mechanism underlying the inhibitory effect of guanidinoacetate on brain Na⁺, K⁺-ATPase activity. *Int J Dev Neurosci.* 2004 Jun;22(4):191-6.
- 115) Ohtsuki S, Tachikawa M, Takanaga H, Shimizu H, Watanabe M, Hosoya K, Terasaki T. The blood-brain barrier creatine transporter is a major pathway for supplying creatine to the brain. *J Cereb Blood Flow Metab*
- 116) Mori A, Kohno M, Masumizu T, Noda Y, Packer L. Guanidino compounds generate reactive oxygen species. *Biochem Mol Biol Int.* 1996 Sep;40(1):135-43.
- 117) McGilvery RW, Murray TW. 1974. Calculated equilibria of phosphocreatine and adenosine phosphates during the utilization of high energy phosphate by muscle. *J. Biol. Chem.* 249:5845-50
- 118) Meyer RA, Kushmerick MJ, Brown TR. 1982. Application of ³¹P-NMR spectroscopy to the study of striated skeletal muscle metabolism. *Am. J. Physiol. Cell Physiol.* 242:C1-C11
- 119) Kammermeier H. 1987. Why do cells need phosphocreatine and a phosphocreatine shuttle? *J. Mol. Cell. Cardiol.* 19:115-1
- 120) Kammermeier H. 1993. Meaning of energetic parameters. *Basic Res. Cardiol.* 88:380-84
- 121) Kammermeier H, Schmidt P, Jungling E. 1982. Free energy change of ATP-hydrolysis: a causal factor of early hypoxic failure of the myocardium. *J. Mol. Cell. Cardiol.* 14:267-77
- 122) Meyer RA, Sweeney HL, Kushmerick MJ. 1984 A simple analysis of the "phosphocreatine shuttle." *Am. J. Physiol. Cell Physiol.* 246:C365-C77

References

- 123) Sweeney HL. 1994. The importance of the creatine kinase reaction: the concept of metabolic capacitance. *Med. Sci. Sports Exerc.* 26:30–36
- 124) Bessman SP, Carpenter CL. 1985. The creatine-creatine phosphate energy shuttle. *Annu. Rev. Biochem.* 54:831–62
- 125) Bessman SP, Geiger PJ. 1981. Transport of energy in muscle: the phosphorylcreatine shuttle. *Science* 211:448–52
- 126) Wyss M, Smeitink J, Wevers RA, Wallimann T. 1992. Mitochondrial creatine kinase: a key enzyme of aerobic energy metabolism. *Biochim. Biophys. Acta* 1102:119–66
- 127) Wallimann T, Schnyder T, Schlegel J, Wyss M, Wegmann G, et al. 1989. *Subcellular compartmentation of creatine kinase isoenzymes, regulation of CK and octameric structure of mitochondrial CK: important aspects of the phosphoryl-creatine circuit.* In *Muscle Energetics*, ed. RJ Paul, G Elzinga, K Yamada, 1pp. 59–176. New York: Liss. 627 pp
- 128) Wallimann T, Eppenberger HM. 1990. The subcellular compartmentation of creatine kinase isoenzymes as precondition for proposed phosphoryl-creatine circuit. In *Isozymes: Structure, Function and Use in Biology and Medicine*, ed. Z-I Ogita, CL Markert, pp. 87789. New York: Wiley-Liss. 973 pp
- 129) Aliev MK, Saks VA. 1997. Compartmentalized energy transfer in cardiomyocytes: use of mathematical modelling for analysis of in vivo regulation of respiration. *Biophys. J.* 73:428–
- 130) Rosa RB, Schuck PF, de Assis DR, Latini A, Dalcin KB, Ribeiro CA, da C Ferreira G, Maria RC, Leipnitz G, Perry ML, Filho CS, Wyse AT, Wannmacher CM, Wajner M. Inhibition of energy metabolism by 2-methylacetoacetate and 2-methyl-3-hydroxybutyrate in cerebral cortex of developing rats. *J Inherit Metab Dis.* 2005;28(4):501-15.
- 131) Fleck RM, Rodrigues Junior V, Giacomazzi J, Parissoto D, Dutra-Filho CS, de Souza Wyse AT, Wajner M, Wannmacher CM. Cysteamine prevents and reverses the inhibition of creatine kinase activity caused by cystine in rat brain cortex. *Neurochem Int.* 2005 Apr;46(5):391-7.
- 132) Reis de Assis D, Maria Rde C, Borba Rosa R, Schuck PF, Ribeiro CA, da Costa Ferreira G, Dutra-Filho CS, Terezinha de Souza Wyse A, Duval Wannmacher CM, Santos Perry ML, Wajner M. Inhibition of energy metabolism in cerebral cortex of young rats by the mediumchain fatty acids accumulating in MCAD deficiency. *Brain Res.* 2004 Dec 24;1030(1):141-51.
- 133) Bodamer OA, Sahoo T, Beaudet AL, O'Brien WE, Bottiglieri T, Stockler-Ipsiroglu S, Wagner C, Scaglia F. Creatine metabolism in combined methylmalonic aciduria and homocystinuria. *Ann Neurol.* 2005 Apr;57(4):557-60
- 134) Jansen EE, Verhoeven NM, Jakobs C, Schulze A, Senephansiri H, Gupta M, Snead OC, Gibson KM. Increased guanidino species in murine and human succinate semialdehyde dehydrogenase (SSADH) deficiency. *Biochim Biophys Acta.* 2006 Apr;1762(4):494-8.

References

- 135) Schmidt A, Marescau B, Boehm EA, Renema WK, Peco R, Das A, Steinfeld R, Chan S, Wallis J, Davidoff M, Ullrich K, Waldschutz R, Heerschap A, De Deyn PP, Neubauer S, Isbrandt D. Severely altered guanidino compound levels, disturbed body weight homeostasis and impaired fertility in a mouse model of guanidinoacetate N-methyltransferase (GAMT) deficiency. *Hum Mol Genet.* 2004 May 1;13(9):905-21
- 136) Torremans A, Marescau B, Possemiers I, Van Dam D, D'Hooge R, Isbrandt D, De Deyn PP. Biochemical and behavioural phenotyping of a mouse model for GAMT deficiency. *J Neurol Sci.* 2005 Apr 15;231(1-2):49-55.
- 137) Stockler S, Marescau B, De Deyn PP, Trijbels JM, Hanefeld F. Guanidino compounds in guanidinoacetate methyltransferase deficiency, a new inborn error of creatine synthesis. *Metabolism.* 1997 Oct;46(10):1189-93.
- 138) Lee H, Ogawa H, Fujioka M, Gerton GL. Guanidinoacetate methyltransferase in the mouse: extensive expression in Sertoli cells of testis and in microvilli of caput epididymis. *Biol Reprod.* 1994 Jan;50(1):152-62.
- 139) Lee, H., Kim, J.H., Chae, Y.J., Ogawa, H., Lee, M.H. and Gerton, G.L. (1998) Creatine synthesis and transport systems in the male rat reproductive tract. *Biol. Reprod.*, 58, 1437–1444
- 140) Lee H, Kim JH, Chae YJ, Ogawa H, Lee MH, Gerton GL. Creatine synthesis and transport systems in the male rat reproductive tract. *Biol Reprod.* 1998 Jun;58(6):1437-44.
- 141) Lee H, Gong CL, Wu S, Iyengar MR. Accumulation of phosphocreatine and creatine in the cells and fluid of mouse seminal vesicles is regulated by testosterone. *Biol Reprod.* 1991 Mar;44(3):540-5
- 142) Moore NP, Gray TJ, Timbrell JA. Creatine metabolism in the seminiferous epithelium of rats. I. Creatine synthesis by isolated and cultured cells. *J Reprod Fertil.* 1998 Mar;112(2):325-30.
- 143) ten Hove M, Lygate CA, Fischer A, Schneider JE, Sang AE, Hulbert K, Sebag-Montefiore L, Watkins H, Clarke K, Isbrandt D, Wallis J, Neubauer S. Reduced inotropic reserve and increased susceptibility to cardiac ischemia/reperfusion injury in phosphocreatine-deficient guanidinoacetate-N-methyltransferase-knockout mice. *Circulation.* 2005 May 17;111(19):2477-85.
- 144) ALSEVER RN, GEORG RH, AND SUSSMAN KE. Stimulation of insulin secretion by guanidinoacetic acid and other guanidine derivatives. *Endocrinology* 86: 332-336, 1970
- 145) Carrasco AJ, Dzeja PP, Alekseev AE, Pucar D, Zingman LV, Abraham MR, Hodgson D, Bienengraeber M, Puceat M, Janssen E, Wieringa B, Terzic A. Adenylate kinase phosphotransfer communicates cellular energetic signals to ATP-sensitive potassium channels. *Proc Natl Acad Sci U S A.* 2001 Jun 19;98(13):7623-8. Epub 2001 Jun 5.
- 146) Dzeja PP, Terzic A. Phosphotransfer reactions in the regulation of ATP-sensitive K⁺ channels. *FASEB J.* 1998 May;12(7):523-9. Review.

References

- 147) Abraham MR, Selivanov VA, Hodgson DM, Pucar D, Zingman LV, Wieringa B, Dzeja PP, Alekseev AE, Terzic A. Coupling of cell energetics with membrane metabolic sensing. Integrative signaling through creatine kinase phosphotransfer disrupted by M-CK gene knock-out. *J Biol Chem.* 2002 Jul 5;277(27):24427-34
- 148) Selivanov VA, Alekseev AE, Hodgson DM, Dzeja PP, Terzic A. Nucleotide-gated KATP channels integrated with creatine and adenylate kinases: amplification, tuning and sensing of energetic signals in the compartmentalized cellular environment. *Mol Cell Biochem.* 2004 Jan-Feb;256-257(1-2):243-56.
- 149) Mc Lean JA, Tobin G. 1987. Animal and human Calorimetry. Cambridge: cambridge univ. Press.338pp.
- 150) Jequier E, Felber JP. Indirect calorimetry. *Baillieres Clin Endocrinol Metab.* 1987 Nov;1(4):911-35. Review
- 151) Livesey G, Elia M. Estimation of energy expenditure, net carbohydrate utilization, and net fat oxidation and synthesis by indirect calorimetry: evaluation of errors with special reference to the detailed composition of fuels. *Am J Clin Nutr.* 1988 Apr;47(4):608-28. Review.
- 152) Haussinger D. Hepatic glutamine metabolism. *Beitr Infusionther Klin Ernahr.* 1987;17:144-57. Review
- 153) Kan HE, Renema WK, Isbrandt D, Heerschap A. Phosphorylated guanidinoacetate partly compensates for the lack of phosphocreatine in skeletal muscle of mice lacking guanidinoacetate methyltransferase. *J Physiol.* 2004 Oct 1;560(Pt 1):219-29
- 154) Kan HE, Buse-Pot TE, Peco R, Isbrandt D, Heerschap A, de Haan A. Lower force and impaired performance during high-intensity electrical stimulation in skeletal muscle of GAMT-deficient knockout mice. *Am J Physiol Cell Physiol.* 2005 Jul;289(1):C113-9
- 155) ten Hove M, Lygate CA, Fischer A, Schneider JE, Sang AE, Hulbert K, Sebag-Montefiore L, Watkins H, Clarke K, Isbrandt D, Wallis J, Neubauer S. Reduced inotropic reserve and increased susceptibility to cardiac ischemia/reperfusion injury in phosphocreatine-deficient guanidinoacetate-N-methyltransferase-knockout mice. *Circulation.* 2005 May 17;111(19):2477-85.
- 156) Renema WK, Schmidt A, van Asten JJ, Oerlemans F, Ullrich K, Wieringa B, Isbrandt D, Heerschap A. MR spectroscopy of muscle and brain in guanidinoacetate methyltransferase (GAMT)-deficient mice: validation of an animal model to study creatine deficiency. *Magn Reson Med.* 2003 Nov;50(5):936-43.
- 157) Watanabe Y., Shindo S. & Mori M. (1985) Developmental changes in guanidino compound levels in mouse organs. Mori M. Cohen B. D. Lowenthal A. eds. Guanidines 1985:49-58 Plenum Press New York, NY
- 158) de Jonge WJ, Marescau B, D'Hooge R, De Deyn PP, Hallemeesch MM, Deutz NE, Ruijter JM, Lamers WH. Overexpression of arginase alters circulating and tissue amino acids and guanidino compounds and affects neuromotor behavior in mice. *J Nutr.* 2001 Oct;131(10):2732-40.

References

- 159) de Jonge WJ, Hallemeesch MM, Kwikkers KL, Ruijter JM, de Gier-de Vries C, van Roon MA, Meijer AJ, Marescau B, de Deyn PP, Deutz NE, Lamers WH. Overexpression of arginase I in enterocytes of transgenic mice elicits a selective arginine deficiency and affects skin, muscle, and lymphoid development. *Am J Clin Nutr.* 2002 Jul;76(1):128-40.
- 160) Murer H, Hernando N, Forster L, Biber J. Molecular mechanisms in proximal tubular and small intestinal phosphate reabsorption (plenary lecture). *Mol Membr Biol.* 2001 Jan-Mar;18(1):3-11. Review.
- 161) Schwenk, F., Baron, U., and Rajewsky, K. (1995): A *cre*-transgenic mouse strain for the ubiquitous deletion of *loxP*-flanked gene segments including deletion in germ cells. *Nucleic Acids Res.* 23, 5080-5081
- 162) Steeghs K, Benders A, Oerlemans F, de Haan A, Heerschap A, Ruitenbeek W, Jost C, van Deursen J, Perryman B, Pette D, Bruckwilder M, Koudijs J, Jap P, Veerkamp J, Wieringa B. Altered Ca²⁺ responses in muscles with combined mitochondrial and cytosolic creatine kinase deficiencies. *Cell.* 1997 Apr 4;89(1):93-103.
- 163) Amanzadeh J, Reilly RF Jr. Hypophosphatemia: an evidence-based approach to its clinical consequences and management. *Nat Clin Pract Nephrol.* 2006 Mar;2(3):136-48. Review.
- 164) Bogusky RT, Lowenstein LM, Lowenstein JM. The purine nucleotide cycle. A pathway for ammonia production in the rat kidney. *J Clin Invest.* 1976 Aug;58(2):326-35.
- 165) Swain JL, Hines JJ, Sabina RL, Harbury OL, Holmes EW. Disruption of the purine nucleotide cycle by inhibition of adenylosuccinate lyase produces skeletal muscle dysfunction. *J Clin Invest.* 1984 Oct;74(4):1422-7.
- 166) Flanagan WF, Holmes EW, Sabina RL, Swain JL. Importance of purine nucleotide cycle to energy production in skeletal muscle. *Am J Physiol.* 1986 Nov;251(5 Pt 1):C795-802.
- 167) Schultz V, Lowenstein JM. Purine nucleotide cycle. Evidence for the occurrence of the cycle in brain. *J Biol Chem.* 1976 Jan 25;251(2):485-92.
- 168) Yudkoff M, Nissim I, Pleasure D. [¹⁵N]aspartate metabolism in cultured astrocytes. Studies with gas chromatography-mass spectrometry. *Biochem J.* 1987 Jan 1;241(1):193-201.
- 169) Dringen R, Verleysdonk S, Hamprecht B, Willker W, Leibfritz D, Brand A. Metabolism of glycine in primary astroglial cells: synthesis of creatine, serine, and glutathione. *J Neurochem.* 1998 Feb;70(2):835-40.
- 170) Sharma RJ, Rodrigues LM, Whitton PD, Hems DA. Control mechanisms in the acceleration of hepatic glycogen degradation during hypoxia. *Biochim Biophys Acta.* 1980 Jul 3;630(3):414-24.
- 171) Boehm EA, Radda GK, Tomlin H, Clark JF. The utilisation of creatine and its analogues by cytosolic and mitochondrial creatine kinase. *Biochim Biophys Acta.* 1996 Jun 13;1274(3):119-28.

References

- 172) Westergaard N, Sonnewald U, Schousboe A. Metabolic trafficking between neurons and astrocytes: the glutamate/glutamine cycle revisited. *Dev Neurosci*. 1995;17(4):203-11. Review
- 173) Westergaard N, Sonnewald U, Schousboe A. Metabolic trafficking between neurons and astrocytes: the glutamate/glutamine cycle revisited. *Dev Neurosci*. 1995;17(4):203-11. Review
- 174) Masson J, Darmon M, Conjard A, Chuhma N, Ropert N, Thoby-Brisson M, Foutz AS, Parrot S, Miller GM, Jorisch R, Polan J, Hamon M, Hen R, Rayport S. Mice lacking brain/kidney phosphate-activated glutaminase have impaired glutamatergic synaptic transmission, altered breathing, disorganized goal-directed behavior and die shortly after birth. *J Neurosci*. 2006 Apr 26;26(17):4660-71.
- 175) Sorenson RL, Stout LE, Brelje TC, Van Pilsum JF, McGuire DM. Evidence for the role of pancreatic acinar cells in the production of ornithine and guanidinoacetic acid by L-arginine:glycine amidinotransferase. *Pancreas*. 1995 May;10(4):389-94.
- 176) Kullak-Ublick GA, Stieger B, Meier PJ. Enterohepatic bile salt transporters in normal physiology and liver disease. *Gastroenterology*. 2004 Jan;126(1):322-42. Review.
- 177) Trauner M, Boyer JL. Related Articles, Bile salt transporters: molecular characterization, function, and regulation. *Physiol Rev*. 2003 Apr;83(2):633-71. Review.
- 178) Tanaka A, Takahashi Y, Mizokuchi M, Shimada N, Koide H. Plasma, urinary, and erythrocyte concentrations of guanidino compounds in patients with chronic renal failure. *Ren Fail*. 1999 Sep;21(5):499-514.
- 179) Cullen ME, Yuen AH, Felkin LE, Smolenski RT, Hall JL, Grindle S, Miller LW, Birks EJ, Yacoub MH, Barton PJ. Myocardial expression of the arginine:glycine amidinotransferase gene is elevated in heart failure and normalized after recovery: potential implications for local creatine synthesis. *Circulation*. 2006 Jul 4;114(1 Suppl):I16-20.
- 180) Palmese S, Pezza M, De Robertis E. Hypophosphatemia and metabolic acidosis. *Minerva Anesthesiol*. 2005 May;71(5):237-42.
- 181) FITCH CD, HSU C, AND DINNING JS. The mechanism of kidney transaminidase reduction in vitamin E-deficient rabbits. *J Biol Chem* 236: 490-492, 1961
- 182) KIM GS, CHEVLI KD, AND FITCH CD. Fasting modulates creatine entry into skeletal muscle in the mouse. *Experientia* 39: 1360-1362, 1983
- 183) Wang X, Proud CG. The mTOR pathway in the control of protein synthesis. *Physiology (Bethesda)*. 2006 Oct;21:362-9. Review.

References

- 184) Favus MJ (2002) Intestinal absorption of calcium, magnesium, and phosphorus. In Disorders of Bone and Mineral Metabolism, 48–73 (Eds Coe FL and Favus MJ) Philadelphia: Lippincott Williams and Wilkins
- 185) Xu H *et al.* (2001) Regulation of the human sodium-phosphate cotransporter NaP_i-IIb gene promoter by epidermal growth factor. *Am J Physiol Cell Physiol* 280: C628–C636
- 186) Xu H *et al.* (2003) Regulation of intestinal NaP_i-IIb cotransporter gene expression by estrogen. *Am J Physiol Gastrointest Liver Physiol* 285: G1317–G1324
- 187) Hoppe A *et al.* (1982) Effect of respiratory alkalosis on renal phosphate excretion. *Am J Physiol* 243: F471–F475
- 188) SIPILÄ I, SIMELL O, RAPOLA J, SAINIO K, AND TUUTERI L. Gyrate atrophy of the choroid and retina with hyperornithinemia: tubular aggregates and type 2 fiber atrophy in muscle. *Neurology* 29: 996-1005, 1979
- 189) SIPILÄ I, SIMELL O, AND ARJOMAA P. Gyrate atrophy of the choroid and retina with hyperornithinemia. Deficient formation of guanidinoacetic acid from arginine. *J Clin Invest* 66: 684-687, 1980
- 190) VANNAS-SULONEN K, SIPILÄ I, VANNAS A, SIMELL O, AND RAPOLA J. Gyrate atrophy of the choroid and retina. A five-year follow-up of creatine supplementation. *Ophthalmology* 92: 1719-1727, 1985
- 191) Forsmark CE. Chronic pancreatitis and malabsorption. *Am J Gastroenterol.* 2004 Jul;99(7):1355-7.
- 192) Wang T, Lawler AM, Steel G, Sipila I, Milam AH, Valle D. Mice lacking ornithine-delta-aminotransferase have paradoxical neonatal hypoornithinaemia and retinal degeneration. *Nat Genet.* 1995 Oct;11(2):185-90.
- 193) Yu H, Iyer RK, Kern RM, Rodriguez WI, Grody WW, Cederbaum SD. Expression of arginase isozymes in mouse brain. *J Neurosci Res.* 2001 Nov 1;66(3):406-22.
- 194) Huggins KW, Boileau AC, Hui DY. Protection against diet-induced obesity and obesity-related insulin resistance in Group 1B PLA2-deficient mice. *Am J Physiol Endocrinol Metab.* 2002 Nov;283(5):E994-E1001.

Acknowledgments

The most important person for this work was Dirk Isbrandt for he took my hand when I was 23 years old, a time at which I had not seen a pipette or a mouse in all my life nor heard a word about physiology, and now, in my late twenties, he leaves me transformed in a scientist in mouse genetics and physiology. He first sequenced the GAMT mutation in human patients in 1996, disclosed the GABA_A partial agonism of GAA to explain GAMT pathophysiology and funded and coordinated the generation of GAMT and AGAT deficient models at his laboratory. I am most thankful to Irm Hermans-Borgmeyer and Tina Koppelman at the transgenic facility of the ZMNH, who assisted with the ES cells gene targeting and generation of AGAT mice, particularly for their counselling and patience when things did not work. We are indebted to Kan HE for her analysis of GAMT muscle and brain MRS, carried out in conjunction with Renema W, and her analysis of GAMT muscle performance, as well as MRS of AGAT mice, done in conjunction with Nabuurs C. We are also very much grateful to Ten Hove M, who carried out the MRS analysis, performance and wet chemistry of GAMT and AGAT hearts. Special thanks are also dedicated to Schweizer M who pursued light and electron microscopy of GAMT and AGAT muscle as well as testicles light microscopy. We would also like to thank Torremans M, for his performed biochemical and behavioural analysis of GAMT mice. Particularly important for this work was Schmidt A, who generated GAMT mice. Prof O Pongs was also essential as he provided financial support and interesting discussions. Boehm U offered most valuable personal support and feedback when my soul got lost. Schillemeit S helped a lot with GAMT genotyping and assisted my understanding on the culture of this country for five and a half years. Voss H and Kurzawa A, provided invaluable help at the animal facility. Finally, I would like to thank Fernandez Fernandez E because she was always and will be always there to help when things go wrong. To my mice, because they were the substrate and sufferers of this investigation and thus were the most important factor of all, I would like to say: see you soon (on the other life) and sorry for all I did to you guys. To everybody, including my parents (who besides having and educating me during 28 years, provided with strong human and financial support during this period) to my colleagues at the Institut für Neurale Signalverarbeitung, to my friends and of course, my mice, thanks to all, you will be always in my heart.

